



morphotonics

# Large Scale Overlay

A study into accuracies in roll-to-plate  
nanoimprint lithography

R.A.W. Neelen



# Large scale overlay

A study into accuracies in roll-to-plate  
nanoimprint lithography

by

R.A.W. Neelen

to obtain the degree of Master of Science  
at the Delft University of Technology,  
to be defended publicly on **13-07-2021**

Student number: 4451074  
Project duration: September, 2020 – July, 2021  
Thesis committee: Dr. Ir. R.A.J. van Ostayen, TU Delft, supervisor  
Ir. J. Snieder, TU Delft daily supervisor  
Ir. J. Spronck, Independent member  
drs. A. Willems, Morphotonics daily supervisor

*This thesis is confidential and cannot be made public until July 13, 2023.*

An electronic version of this thesis is available at <http://repository.tudelft.nl/>.



# Preface

This thesis was written for the completion of the Master Mechanical Engineering at the Faculty of 3ME of the Delft University of Technology. The thesis project is carried out during a graduation internship at the company Morphotonics based in Veldhoven the Netherlands. The objective is to research overlay in roll-to-plate nanoimprint lithography, for which I was able to use the clean room facilities and machinery of Morphotonics.

I would like to express my thanks to my supervisors: Dr. Ir. R.A.J. van Ostayen and Ir. J. Snieder from the Delft University of Technology, and drs. A. Willems from Morphotonics for their assistance throughout this thesis project. I sincerely enjoyed my collaboration with my supervisors and the feedback I received during our weekly meetings were of great value to the results presented in this thesis. In addition, I would like to thank Morphotonics as a company for the opportunity to use their machines and materials throughout this project. Furthermore, the engineers of Morphotonics were very helpful and enabled me to use the tooling present in their clean room facilities. Therefore, I would like to thank all the employees of Morphotonics for their amazing support and assistance, which enabled me to obtain the results presented in this thesis.

*Rob Neelen  
Delft, June 30, 2021*



# Abstract

Roll-to-Plate (R2P) nanoimprint lithography (NIL) is a fabrication process with the potential for low-cost high-volume fabrication of micro- and nano-patterns on large areas. As a result, R2P is regarded as a promising production process for micro- and nano-scale features which exceed the conventional wafer sizes. In addition, the process has the potential to scale up the production of wafer based textures at a low costs, which would make the implementation of nano-features in products more accessible. To compete with alternative imprint techniques, R2P NIL must meet requirements set by the industry for position accuracy and system repeatability.

In this thesis, a study is performed on the positioning of micron- and nano-sized features in a two-dimensional plane in collaboration with Morphotonics, a company based in Veldhoven the Netherlands. The metrology of overlay from the semi-conductor industry is applied to NIL, to quantify the relative displacement and deformations of a given nano-pattern. Experimental results, obtained in a preliminary phase of the project, characterized the current overlay performance of machines available at Morphotonics. From the test results, a positioning error of the complete nano-pattern was found, in combination with a complex deformation which affected the relative distance of the imprinted features. For imprints within a single batch the accuracy of the nano-pattern was measured to be accurate within  $< 30[\mu m]$ , whilst for samples between batches an accuracy of  $< 160[\mu m]$  was observed. Based on the characterization of overlay in R2P NIL, various potential error sources are considered which could lead to the observed deformation pattern. Based on the coherence in magnitude and direction of error components, an interest in deformations of the flexible mould is developed.

Concepts from roll-to-roll (R2R) production processes are used, to quantify the deformation observed in experiments. In R2R processes, deformation of a thin elastic material (web) is quantified by applying a beam model to the web. Using the beam model, the deformation of a web segment, constrained by two rollers, could be quantified in both quasi-static and dynamic conditions. The models based on literature of lateral web dynamics, combined with experimental results obtained at Morphotonics, have given insight in the behaviour of the elastic mould during the imprint process. The models describe the transverse motion of the web on a roller surface and the deformation of the web in between two consecutive rollers in a dynamic system.

Verification of the model was performed on the machines of Morphotonics, which is a complete system will multiple imperfections introduced to the web. Therefore, it was critical to use verification in which a larger disturbance was added to the existing system in order to retrieve a significant and measurable difference. As a result, the interpretation of experimental results were challenging and the results obtained from the measurement did not exactly match the expectation based on model results. However, the transverse motion of the elastic mould over the rollers was clearly observed in the measurement, including a repeatable deformation pattern of the imprints as a result of a forced disturbance exposed to the system. Both of which, were expected to be observed based on the modelled expectations. Nevertheless, the exact error magnitude did not meet the expectations and only a rough relation between model and experimental results was found.

In spite of the verification results not perfectly matching the model, the theory applied in this thesis has given insight in the lateral dynamic behaviour and accompanying deformations for an elastic mould in R2P NIL. The model identified critical parameters which affect the dynamic response of a web when exposed to disturbances, as well as the deformation in a web segment. A parameter study with a logarithmic sensitivity analysis was used to compare the impact of system parameters on the deformation in the web. From the study a large sensitivity for the web dimensions was found, as a large length web ratio had a positive effect on the deformations, whilst longer web spans will show a larger transverse displacement as a result of a disturbance.

In conclusion, from the observations and gathered knowledge of this thesis, the performance of overlay

in large scale roll-to-plate nanoimprint lithography has been characterized. Measurements on overlay in the current line of machines at Morphotonics led to a deeper understanding of the critical aspects in R2P NIL. Deformation of the elastic mould was related to a coherent deformation profile in the imprints, which was roughly verified by experimental results. Combining all the results gathered in this thesis several considerations for future concepts are presented which will be critical to achieving a high overlay accuracy in large scale overlay.



# Nomenclature

## List of Abbreviations

3ME	Faculty of Mechanical Engineering
NIL	Nano-Imprint-Lithography
P2P	Plate-to-Plate imprinting
R2P	Roll-to-Plate imprinting
R2R	Roll-to-Roll imprinting
SCIL	Substrate conformal imprint lithography
TUD	Technische Universiteit Delft

## List of Symbols

$\gamma$	angle of the roller axis
$\kappa$	inverse shear coefficient for a Timoshenko beam
$\phi$	bending angle of the web
$\psi$	shear angle of the web
$\rho$	density
${}_0$	subscript indicating value of variable at $x = 0$
$_L$	subscript indicating value of variable at $x = L$
$a$	a parameter describing the effect of shear deformation in the web according to $1 + \frac{nT}{AG}$
$C_i$	constant coefficients for a differential equation, depending on $[K, L, \frac{nT}{AG}]$
$E$	elastic modulus
$G$	shear modulus
$g_i$	functions dependent on $[K, L, \frac{nT}{AG}]$ used to simplify algebraic notations. The functions are constant for given derivations.
$h$	web material thickness
$h_i$	functions dependent on $[K, L, \frac{nT}{AG}]$ used to simplify algebraic notations. The functions are constant for given derivations.
$I$	area moment of inertia
$K$	a constant of a partial differential equations, according to $K^2 = \frac{T}{EIa}$
$L$	span length
$M$	bending moment in the web
$n$	shear coefficient for a Timoshenko beam, equal to $n = 1.2$ for a rectangular cross-section

---

$Q$	shear force in the web
$T$	Tension
$t$	time
$\nu$	Poisson's ratio
$v_0$	web velocity in machine direction
$w$	web material width
$x$	displacement along length of the web
$y$	lateral position of the web
$y_0$	lateral web displacement at the upstream roller $x = 0$
$y_L$	lateral web displacement at the downstream roller $x = L$
$z$	lateral displacement of roller relative to the ground

# Contents

<b>1</b>	<b>Introduction</b>	<b>1</b>
1.1	Nano-imprint lithography . . . . .	1
1.2	Roller based imprinting . . . . .	2
1.3	Applications for roller-based imprinting . . . . .	3
1.4	Project description . . . . .	4
<b>2</b>	<b>Background Theory</b>	<b>7</b>
2.1	Precision vs. Accuracy . . . . .	7
2.2	Overlay . . . . .	8
2.3	Handling of thin materials . . . . .	9
<b>3</b>	<b>Analysis of system at hand</b>	<b>11</b>
3.1	Top-level design of Morphotonics . . . . .	11
3.2	Quantifying errors in overlay . . . . .	14
3.2.1	Imprint repeatability . . . . .	14
3.2.2	Machine to machine repeatability . . . . .	15
3.3	Problem analysis . . . . .	16
3.4	Problem definition and outline . . . . .	17
<b>4</b>	<b>Modelling of a web as a beam</b>	<b>19</b>
4.1	Introduction to web guiding . . . . .	19
4.2	Discussion on previous research . . . . .	20
4.2.1	Shear in the Timoshenko beam model . . . . .	20
4.3	Quasi-static beam model . . . . .	21
4.3.1	Boundary conditions . . . . .	21
4.4	Dynamics of a web . . . . .	22
4.4.1	Normal entry rule . . . . .	22
4.4.2	Derivation of the lateral acceleration . . . . .	23
4.4.3	Overview of assumptions . . . . .	23
4.5	Planar deformation of the web . . . . .	24
4.6	Conclusion . . . . .	25
<b>5</b>	<b>Implementation of lateral web dynamics</b>	<b>27</b>
5.1	Model description . . . . .	27
5.1.1	Building a multi-span system . . . . .	29
5.2	Validation of models . . . . .	29
5.2.1	Replicating Browns model . . . . .	30
5.3	Case study . . . . .	32
5.3.1	Sine input . . . . .	32
5.3.2	Roller misalignment . . . . .	33
5.3.3	Eccentricity . . . . .	33
5.4	Mapping of web deformation . . . . .	34
5.4.1	Main deformation components . . . . .	35
<b>6</b>	<b>Verification</b>	<b>37</b>
6.1	Verification method . . . . .	37
6.2	Expectations based on model results . . . . .	38
6.3	Results . . . . .	39
6.3.1	Visual comparison of imprint deformation . . . . .	42
6.4	Discussion and conclusion of results . . . . .	42

<b>7</b>	<b>Parameter study</b>	<b>45</b>
7.1	Logarithmic sensitivities . . . . .	45
7.2	Model parameters . . . . .	46
7.3	Results . . . . .	47
7.3.1	Sensitivity analysis on angular misalignment . . . . .	47
7.3.2	Sensitivity analysis on lateral displacement . . . . .	48
7.4	Conclusions to parameter study . . . . .	49
<b>8</b>	<b>Suggestions and design considerations</b>	<b>51</b>
8.1	Critical degrees of freedom . . . . .	51
8.1.1	Degrees of freedom in Morphotonics' concept . . . . .	52
8.1.2	Tolerances on alignment . . . . .	53
8.2	Web dimensions . . . . .	53
<b>9</b>	<b>Discussion of the results</b>	<b>55</b>
9.1	Discussion . . . . .	55
<b>10</b>	<b>Conclusions</b>	<b>57</b>
<b>11</b>	<b>Recommendations</b>	<b>59</b>
<b>A</b>	<b>Measurement of overlay</b>	<b>61</b>
A.1	Test description . . . . .	61
A.2	Test objectives . . . . .	61
A.3	Overview of performed tests . . . . .	62
A.4	Test setup and methods . . . . .	63
A.4.1	Test equipment . . . . .	63
A.4.2	XYZ stage . . . . .	63
A.4.3	Image processing . . . . .	64
A.4.4	Software . . . . .	64
A.4.5	Image processing . . . . .	65
A.5	Analysis of Overlay . . . . .	65
A.5.1	Rigid alignment . . . . .	65
A.5.2	Affine transformations . . . . .	66
A.5.3	Polynomial transformations . . . . .	67
A.6	Test results . . . . .	68
A.6.1	Inter-Imprint comparison . . . . .	68
A.6.2	Stamp material comparison . . . . .	70
A.6.3	Machine comparison . . . . .	70
A.6.4	Imprint pressure . . . . .	71
<b>B</b>	<b>Derivations in beam theory</b>	<b>73</b>
B.1	Coefficients derived for the static web shape . . . . .	73
B.2	Derivation of boundary conditions . . . . .	73
B.2.1	Boundary conditions . . . . .	74
B.3	Deriving the lateral acceleration / Modified Sievers method . . . . .	76
B.3.1	Additional derivations for strain . . . . .	77
B.3.2	Validation of derived equations . . . . .	78
<b>C</b>	<b>Lateral web dynamics</b>	<b>81</b>
C.1	Case study using an Euler-Bernoulli beam model . . . . .	81
C.1.1	Sine input . . . . .	81
C.1.2	Roller misalignment . . . . .	82
C.1.3	Eccentricity . . . . .	82
<b>D</b>	<b>Sensitivity Analysis</b>	<b>83</b>
D.1	Input conditions . . . . .	83
D.2	Parameter sweep . . . . .	85
D.2.1	Angular misalignment . . . . .	85
D.2.2	Lateral displacement . . . . .	86

---

D.3	Convergence . . . . .	87
<b>E</b>	<b>Out-of-plane web deformations</b>	<b>89</b>
E.1	Trough formation . . . . .	90
E.2	Disturbances which induce web troughs . . . . .	91
E.3	Trough formation by roller misalignment . . . . .	91
E.4	Trough formation by roller taper . . . . .	92
E.5	Wrinkle formation . . . . .	93
E.6	Relevance of out-of-plane deformations. . . . .	94
E.7	Tension Dynamics . . . . .	94
E.7.1	External effects on web tension . . . . .	95



# Introduction

In this thesis report, an analysis of overlay accuracy in roll-to-plate nano-imprint lithography will be presented. Nanoimprinting is a fabrication method which produces micro- and nanostructures using a low-cost and high throughput replication process. This thesis project is a collaboration with Morphotonics, a company based in Veldhoven Netherlands. The roll-to-plate technique of Morphotonics is a method for roller based nano-imprint lithography. The production process has the potential to fabricate nano-textures on extremely large surfaces of over one square meter. In this thesis, the errors involved in the positioning of nano-features on large surfaces will be researched, with the goal of reaching a micron-scale overlay accuracy in roll-to-plate nanoimprinting. Based on the study to inaccuracies in overlay, improvements to the imprint process and machine design will be proposed.

The facilities of Morphotonics will be used to quantify the errors leading to overlay inaccuracies in the R2P imprint process. An analysis to the machine design and production process of Morphotonics, in combination with experimental results, will give insight in the errors relevant to R2P NIL. Presumably, multiple sources contribute to the overlay inaccuracies and not all errors can be mitigated within the limitations of the current setup. However, the focus of this project is to break down the error components systematically, from which improvements to the imprint process and machine design can be proposed. The conclusions of this project will contribute to the field of nano-imprint lithography and alternative roller based imprint techniques, and the results can be used to achieve high overlay accuracies in the production of nano-textures on large areas.

## 1.1. Nano-imprint lithography

Nanoimprint lithography (NIL) is a technique for producing micron- or nano-scale features and patterns, based on mechanical deformation of a resist. Compared to alternative techniques, such as: photo-lithography, electron beam lithography and scanning probe lithography, the NIL process does not directly produce a texture in a material. Rather, the fabrication process utilizes a mould to transfer a pattern onto a desired surface in a replication process. The mould, embedded with the inverse geometry, can be used consecutively in a long life-cycle of replication steps. Therefore, the NIL production process is suitable for large scale and high throughput production at low costs, compared to more conventional production processes [50] [44]. In addition, the replicating step enables the production of nano-patterns on surfaces larger than the conventional silicon wafers with a limited radius of 300[mm]. The increase in imprint area makes nanoimprint lithography highly suitable to a new range of applications and supports the innovation of new products.

The concept of NIL was first presented, by Stephen Chou [41], who used a plate-to-plate (P2P) method to replicate wafer sized patterns. An inverse nano-structure would be produced on a silicon wafer, using electron beam lithography. The silicon structure, referred to as the mould, is placed on top of the substrate with a layer of viscous resist. By uniformly pressing the mould into the resist, the deformation of the resist results in an inverse replication of the geometry. The resist would be cured using UV-light

or heat to solidify the replicated texture. Replication from a single silicon wafer posed an alternative process to the costly electron beam lithography.

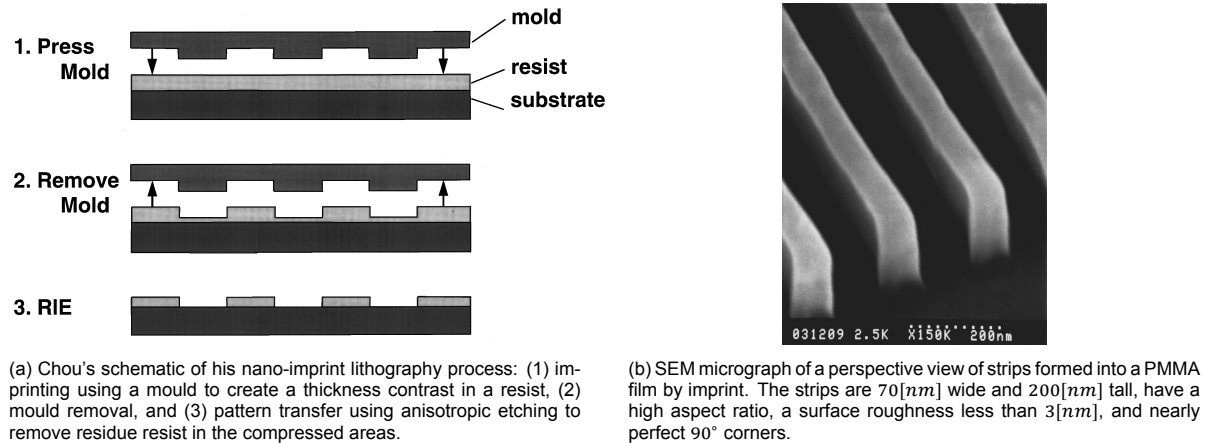


Figure 1.1: The first results in the field of NIL produced by Stephen Y. Chou [41].

The P2P production proved repeatable and accurate on wafer scale imprints, and various advances have been made in the field of nano-imprint lithography due to P2P fabrication. The process could even be applied on a larger scale by relocating the mould on the substrate in a step and repeat process. However, the process also had its limitations, as introduced by B. Kwon and Jong H. Kim [23]. In their paper, Kwon and Jong emphasize the physical limits of imprint techniques using mechanical pressure. Due to geometrical or material imperfections in both the mould or substrate, defects would occur in the imprint process, as can be seen in 1.2. These physical defects are geometrical errors resulting in a limitation on the maximum achievable imprint size, and proved to be inherent to the production process itself.

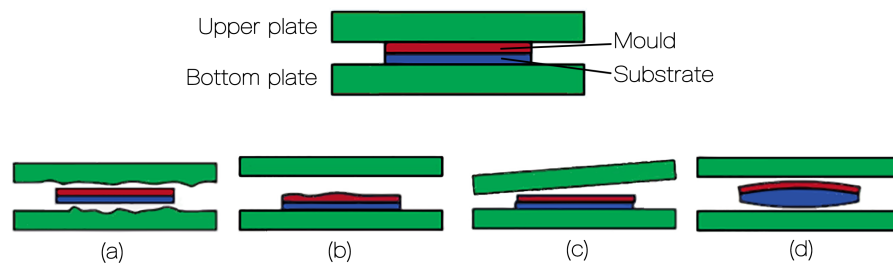


Figure 1.2: A schematic diagram of the solid parallel-plate mechanical press nano-imprint method and potential drawbacks: (a) failure due to surface imperfections, (b) failure due to uneven mould/substrate backside, (c) failure due to non-parallelism, and (d) failure due to curved sample surfaces. [23]

The limitations of P2P imprinting, combined with an interest in soft materials, initiated the development of substrate conformal imprint lithography (SCIL). Specific concepts for SCIL are roller-based imprint techniques, such as roll-to-roll (R2R) and roll-to-plate (R2P), which have the potential to overcome the limitations found in P2P NIL. As a result, the roller-based imprint techniques are able to achieve larger imprint areas, suitable to high volume production. As such, both R2R and R2P are regarded as promising concepts for the large-area manufacturing of micro- or nano-scale patterns, both with their own application and characteristics [25].

## 1.2. Roller based imprinting

The reduced contact area of roller based imprint techniques, in combination with the elasticity of the roller material, can compensate the roughness and imperfections in the imprint process. Both R2R and R2P apply pressure using a roller and utilize flexible materials, such as foils, as a mould to transfer a nano-structure to a substrate. In figure 1.3 an early development concept of a R2P application is visu-



alized, in which a stamp with nano-texture is pressed onto a substrate using a roller. On a conceptual level, a lot of variations of the same process have been developed in which the texture can be placed on the elastic stamp or on the roller. Still, all variations use the same fundamental concept of a roller based imprint technique with elastic materials to transfer a nano-pattern.

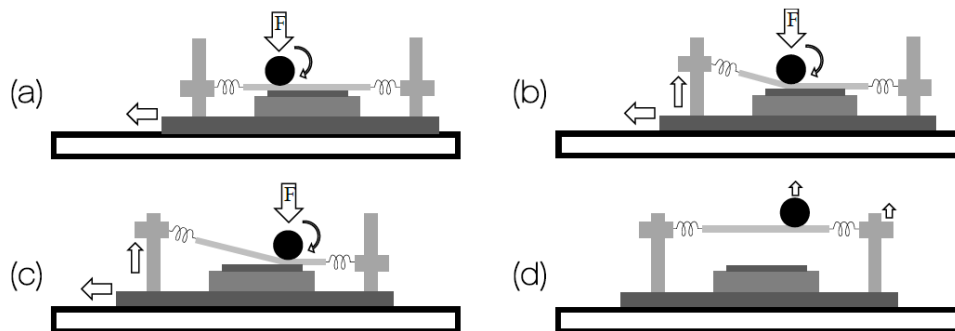


Figure 1.3: Schematic of a roller based imprint process for flat substrates. In (a) the roller is used to apply pressure to the stamp. In (b) and (c) the roller moves over the stamp and delaminates at the same time. In (d) the stamp has fully delaminated and the imprint process is completed. [47]

Morphotonics is one of the companies implementing roll-to-plate nanoimprint lithography to produce micron- or nano-textures on extremely large areas. In the case of Morphotonics a maximum imprint area of over a square meter is considered. Due to the significant scaling of imprint dimensions, the imperfections found in existing nanoimprint applications proved to be more challenging, as most error components tend to scale with the imprint size.

The use of elastic materials and scaling of the imprint dimensions are part of the challenges faced in large-scale overlay, as will be addressed elaborately in this thesis. Generally, soft materials are more susceptible to dimensional effects, such as strain or thermal expansion. Still, literature describing the development of NIL often neglect the distortions of features on larger dimensions. Rather, they refer to the resolution of the nano-features as a definition of imprint accuracy, which is not the same as overlay. Likely, most applications design their nano-structures on small scales to prevent dimensional distortions during imprinting, as the dimensional effects can not yet be compensated on a micron-level accuracy. The lack of documentation on large-scale overlay in literature, emphasizes the challenges foreseen in the early development of NIL.

### 1.3. Applications for roller-based imprinting

Due to the potential of R2P NIL, as a high volume and low-cost production process, the fabrication of micron- and nano-features would become more accessible and cost-efficient. As a result, high-volume NIL would enable the development and innovation of various applications in a range of industries. The applications considered, using NIL imprint techniques, are data storage, nano-electronics, optics, bio-sensors, flexible electronics and displays as seen in figure 1.4 [1, 47, 36, 8, 29, 2, 44, 50, 13, 14, 2]. Most of these applications require imprint areas exceeding the conventional wafer size. With the introduction of NIL, new fields can utilize the production of nano-sized patterns on a large scale, which would otherwise be constrained by the standards and production costs of conventional imprint techniques.

The exact requirement on overlay accuracy is dependent on the application. However, in essence NIL is capable of replicating features on a  $10[nm]$  resolution at a high throughput and low costs, as stated by Chou [41]. Still, the techniques require additional development to realize most of these applications at a high throughput. Especially applications which require a high overlay accuracy on a large-scale, such as the OLED or high quality display applications, pose additional challenges in terms of repeatability and resolution [31, 42].

Literature on results of P2P production processes report sub- $10[nm]$  overlay tolerances, which would support Chou's statement on the theoretical performance of NIL [21, 31]. However, the P2P imprint process utilizes small imprint areas for the reasons discussed in section 1.1. Similar results have not

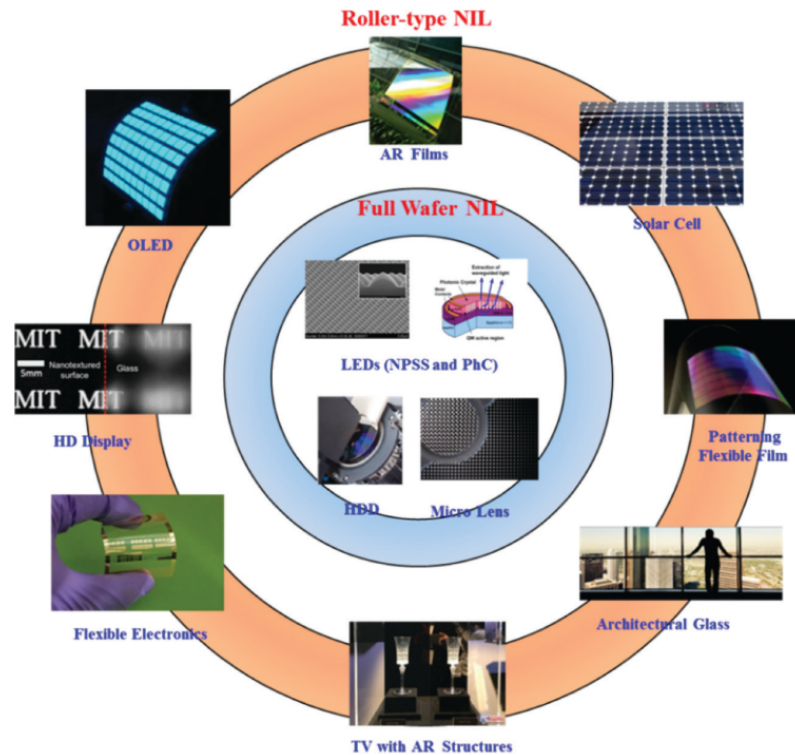


Figure 1.4: An overview of applications for nano-structures produced by wafer sized plate-to-plate imprinting and roller based nano-imprint lithography [25]. The applications considered for roller-based NIL exceeds the existing market for wafer based fabrication processes.

been reported for conformal imprint techniques such as R2R or R2P.

The transition of P2P imprinting, using silicon moulds with a maximum 200 or 300mm imprint area, to soft imprinting with an elastic stamp on large areas is proven to be challenging. The difference between the imprint techniques is not well documented, as the research of both field is clearly separated. However, based on the knowledge obtained in this thesis it is assumed that the use of elastic moulds, larger imprint areas, and alternative materials introduced additional error sources which are not present in P2P applications. For P2P the nano-pattern is transferred from one silicon-like material to another on a small imprint area, whereas for soft imprinting the transfer of patterns require alternative materials with a different thermal and mechanical behaviour. These challenges will be encountered throughout this thesis project.

## 1.4. Project description

As of today, roll-to-plate nanoimprinting can not compete with the accuracies set by conventional wafer based production processes applied in the semi-conductor industry. Also, within the field of nanoimprint lithography, R2P is a relatively undeveloped concept compared to P2P or R2P. Still, the knowledge and methods applied in other fabrication processes and fields of research, can be applied to R2P in order to catch up the deficit in performance. This thesis focuses on the inaccuracies found in roll-to-plate imprinting, based on experience from other disciplines and user experience from the machines at Morphotonics in Veldhoven.

In chapter 3, two phases of the project will be addressed. First, the concept of Morphotonics will be introduced and analysed for possible error sources in their machine design and imprint process. From the analysis, a first understanding of the system will be developed, in which critical components and aspects of the imprint process will be identified. Then, a prediction for the behaviour of errors in the imprints will be developed, which will be used in the interpretation of experimental data.

Second, the analysis of the system at Morphotonics will be compared to two experiments performed in a preliminary phase of the project. The prediction of error behaviour will be used to relate observations to specific aspects of the imprint process. The result of the analysis is a quantification of overlay performance and an initial understanding of dominant errors in overlay.

Notably, at the start of this project, I have made the assumption that a part of the error in overlay is related to the alignment between components in the system. I believe these type of positioning problems can be solved by existing solutions available on the market, which would partly solve the inaccuracies in existing systems. However, the remaining errors are much more complex in nature and are a result of fundamental choices made in the design of R2P imprint processes. Especially, the use of elastic materials as a mould is challenging, due to the alteration in (thermal-) mechanical behaviour. Therefore, the fundamental choice to select flexible materials as a mould in NIL will be a critical point of interest in order to obtain a higher degree of overlay accuracy.

From the results of this thesis, a new perspective to large-scale overlay in R2P imprinting is obtained. The observed distortions in overlay will be related to machine or process parameters, and the knowledge can be used in the design of future concepts and machines.

Now that the reader has been introduced to the scope of the project, chapter 2 will provide more background information on the theory that is applied in this thesis. In chapter 3, an analysis of the system available at Morphotonics will be performed, from which a problem definition and project outline will be defined. The remaining chapters of this thesis will research a specific aspect of overlay inaccuracies in R2P NIL in more detail. Aspects which are not covered in this thesis, but have been observed or discussed throughout this thesis, will be proposed as recommendations for future research in chapter 11.



# 2

## Background Theory

Before diving into the topic of this thesis, some background information will be presented which will be of assistance in the coming chapters. The knowledge from literature applied in this thesis will also be summarized in this chapter, and for more detailed support material references will be made to the appendix or papers.

As this report focuses on overlay in nano-imprint lithography applications, the definition of overlay will be discussed as well as the terminology to describe or quantify accuracy in positioning systems. With an understanding of how errors are identified and how errors in imprint applications are quantified, the systems available to us can be analysed.

Next, a small introduction to theory applied in this thesis will be given. As the systems of Morphotonics use a roller based imprint technique, with additional roller transport of an elastic and thin material (web), a similarity was found to web handling applications. The field of web handling focusses on the transport of thin materials over a system of rollers and quantifies the dynamic behaviour during transport. This theory can be applied to the concepts discussed in this thesis and can help in the analysis of errors in roller based NIL.

### 2.1. Precision vs. Accuracy

Errors observed in mechanical positioning systems can be identified as different types of errors, each with alternative solutions and methods to deal with the error. A good understanding of the errors present in a system is critical to predict and improve machine performance.

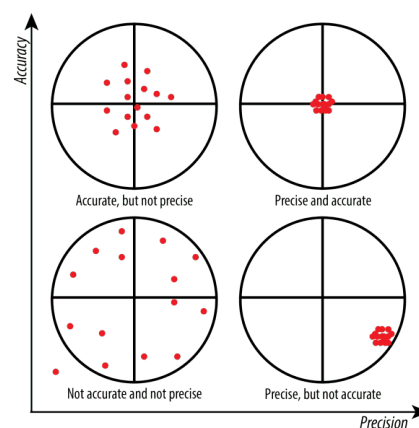


Figure 2.1: Four combinations of accuracy and precision which can be observed in mechanical systems [33]

The most fundamental identification of errors in mechatronic systems is the distinction between accu-

racy and precision [38]. Accuracy is defined as the ability to tell the "true" value of a position. In practice, accuracy is seen as the representation of systematic errors in a system which result in a deviation from the "true" value. Precision on the other hand, also referred to as repeatability, is the ability to repeatedly obtain the same measured value from a system. Repeatability or precision are often considered to be the most important parameter of a system, as it indicates to what extent the performance of an existing system can be optimized. In figure 2.1 the physical interpretation of accuracy and precision is visualized by four distinctive cases with varying accuracy and precision levels.

From a statistical analysis of errors in mechanical systems, the accuracy and repeatability can be derived. The accuracy is related to systematic errors, whereas the repeatability errors are observed as random errors. Ideally, a system is repeatable, and the systematic errors can be compensated for in a calibration or alignment step to end up with both an accurate and repeatable system. In practice, the non-repeatable errors are more complex to mitigate and often require alterations to the system to remove specific error components.

Note, that the non-repeatable errors are considered to be random. However, within a given system the non-repeatable errors can show a systematic behaviour, which can simply not be compensated with the current specifications of that system. In this thesis, an analysis will be performed to the non-repeatable errors in R2P imprinting, in order to mitigate the random behaviour. A possible outcome, is that an existing system is limited in its current design, and conceptual- or component-level improvements are required to mitigate error components.

## 2.2. Overlay

The term overlay is derived from the semi-conductor industry, in which multiple layers of nano-patterns are stacked vertically to build an electronic circuit. Overlay is defined as the positioning accuracy of a printed pattern on top of an existing layer, measured on any point of the two-dimensional object [18]. For a single point, the error component is determined by comparing the location of the point to the intended position. For a grid of multiple points, the same error components can be determined to form a two-dimensional grid of vectors. The visualization of overlay errors in a planar object using vectors is a common representation in the semi-conductor industry, and will also be used in this thesis.

The concept of overlay has transferred from the semi-conductor industry to NIL applications, as the definitions and methods also apply to quantification of accuracies in NIL fabrication [14, 8, 51, 35, 36]. However, the term overlay in NIL does not relate the accuracy of an imprinted layer to its neighbouring layers. Rather, overlay quantifies the accuracy to which a pattern design has been reproduced on a substrate surface. Distortions in NIL overlay will be related to imperfections in the replication process of a nano-texture from a mould to the end-product.

In this thesis, overlay will be applied from two different perspectives. First, the overlay accuracy of an object, or series of objects, can be analysed by comparing the imprint position of a point to its reference position. For a grid of points, statistical analysis is used to quantify the behaviour of errors over multiple points, in which commonly a Gaussian distribution is assumed with a mean  $|\mu|$  and variation  $3\sigma$ . Second, the vector field is analysed for its vector magnitude and direction, in order to find an underlying pattern and improve the accuracy of the imprint process. The underlying relation can potentially be

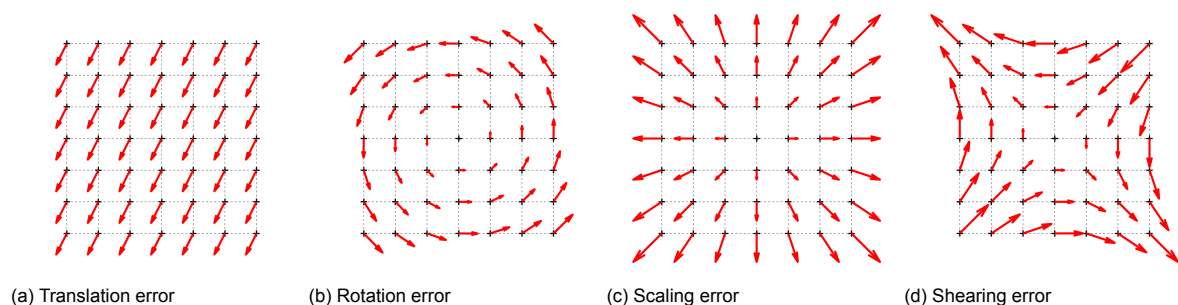


Figure 2.2: Decoupled error components found in overlay.

linked to a specific error or defect in the fabrication process. Decoupling of the error components will assist in isolating specific errors. Examples of error components are: translations, rotation, linear scaling, shearing or higher-order distortions. Analysis of the underlying patterns is performed with the sole objective of reducing the errors, and thus achieving a better overlay performance. Examples of specific error components in a vector field are visualized in figure 2.2.

The two approaches, considered above, are applied to NIL in this thesis. However, the methods by which overlay is quantified from experimental results, will differ from the standards applied in the semiconductor industry. The Gaussian distribution is suitable for statistical analysis of a large set of measurements, and is applied directly to the measurement data. However, in chapter 3 the first experimental results of this thesis will be presented, in which only two datasets will be compared with additional post-process steps to isolate error components. The limited number of measurements, combined with the post-processed data, make a Gaussian distribution not suitable for the applications considered in this thesis. Rather, an average and maximum absolute error will be considered. The average error will be representable for the mean value considered in the Gaussian distribution, and the maximum error is more realistic compared to the  $3\sigma$  due to a limited number of measurements.

In the post-process steps, applied to all measurements in this thesis, two different problems will be identified: alignment and deformation of the object. A translation and rotation error represent misalignment between the substrate and mould, whilst higher order transformations represent deformation of the nano-texture during the imprint process. These higher-order terms can represent warping, shear deformation or non-linear scaling. Each specific error component will require solutions unique to the type of deformation. An example of error decoupling is given in figure 2.3, in which an exemplary vector field is decoupled for translation and rotation to observe the residual error. Similar methods will be applied in this thesis, to decouple errors caused by alignment or by deformation of the object.

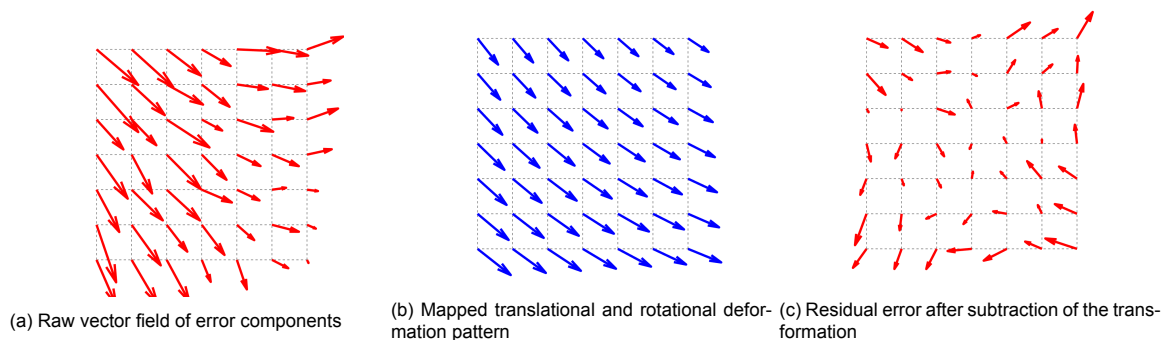


Figure 2.3: Decoupling of error components in a 2D grid of vectors.

So, in chapter 3 measurements on overlay in R2P NIL will be presented, and the error components will be decoupled as introduced in this section. The methods applied in the post-process steps are elaborated in the appendix A.5, according to transformations on two-dimensional objects [13, 14].

## 2.3. Handling of thin materials

The substrate conform imprint methods presented in chapter 1, commonly apply a roller based imprint process combined with flexible mould designs. Consequently, the contact line between the mould (stamp) and substrate moves gradually over the surface to apply local pressure. The concepts to perform such a fabrication method usually involve a motion of the roller or the flexible stamp, in a dynamic process.

In this thesis, a relation is found between the flexible materials moving over a roller and the web handling industry. A web is defined as a thin continuous material transported over a set of rollers, which has been applied in many industries for the past decades, such as: sheet metal production, foil transport, textile production and paper printing [37]. The industry of web handling has been researched extensively and knowledge on the dynamic behaviour of a web has been analysed from various perspectives. In practice, the focus of web handling is to maintain a uniform and flat web shape during transport,

in which imperfections and distortions can not impact the quality of the product. Fundamentally, the SCIL imprint process considered in this thesis is similar compared to the web handling applications, as in NIL imperfections and distortions to the elastic mould should be minimized to create a repeatable imprint process. Therefore, the knowledge and theory from web handling industries could potentially be applied to NIL.

In the field of web handling, various phenomena have been studied in order to control the deformation or imperfections of the web. From literature the following main topics have been defined:

**Lateral web dynamics**

The lateral web dynamics describes the transverse motion of a moving web, as a result of imperfections in a system of rollers. Lateral dynamic models have been developed to predict the progression of errors over time in a system of rollers and quantify the effect of disturbances or misalignment from rollers. Beam theory is applied to model the web as a beam and quantify the dynamic behaviour. [37, 43, 24, 7, 6, 49, 48, 10]

**Out-of-plane deformation**

A deformation of the web, visible as troughs or wrinkles, which result from geometrical imperfections in the handling of a web. The out-of-plane deformations are a sign of improper handling of a material resulting in compressive stresses, as well as actual defect which can affect the product quality. [11, 3, 12]

**Tension dynamics**

The transport velocity and tension along the transport direction can vary over time due to the dynamics of components in a system of rollers. In tension dynamics both passive systems and active systems to control web tension are modelled to maintain a desired reference value for velocity or tension [28, 17, 5, 27]. An small study is presented in appendix E.7

**Non-cylindrical rollers**

The roller geometry can determine the behaviour of a web over a series of rollers, as well as the pressure over the contact line. Several geometrical errors are considered, such as: eccentricity, taper, crowned rollers etc. [16, 5]



(a) Web distortions due to non-cylindrical roller profiles. In this case, bending of the roller axle is considered.

(b) Web distortions due to misalignment in rollers, resulting in an out-of-plane deformation of the web.

Figure 2.4: A visualization of defects in web handling during transport [15].

In the coming chapter, the theory from web handling will be used to define a modelling approach for deformation of the elastic mould used in R2P NIL. From a literature study, several potential defects or disturbances to webs have been found, which will be related to NIL applications. Out of the topics introduced in this section, the lateral web dynamics is seen as the most relevant discipline due to the concepts and models applied in literature describing the dynamic behaviour of a web. In the coming chapters, these concepts will be applied to quantify deformations of elastic moulds in R2P resulting from machine imperfections. The remaining topics have been useful to gain insight in the behaviour of elastic materials in roller transport, but will not play a significant role in the remainder of this thesis.



# 3

## Analysis of system at hand

This chapter will introduce the machine and production process of Morphotonics, used to perform measurements on large-scale overlay. The high-level design of the machine will be discussed, as well as the steps performed during R2P NIL fabrication. For both the design and production process, an analysis on possible error sources will be performed to gain insight in the introduction of errors which lead to overlay inaccuracies.

From a high-level understanding of the R2P production process, the overlay performance of Morphotonics can be quantified using the facilities available in their clean room. The observations on overlay accuracy will be used to relate errors to potential error sources. For this analysis, two exemplary measurements will be presented in section 3.2 to quantify various error components. Over the course of this thesis project multiple tests have been performed under various conditions and the complete documentation of the methods and test results will be discussed in greater detail in appendix A.

### 3.1. Top-level design of Morphotonics

For automated roll-to-plate NIL production, Morphotonics has developed the NIL1100 to transfer a nano-texture from a flexible mould to a substrate at a high throughput rate. For this thesis the NIL1100 has been used to produce samples and the design of the NIL1100 will be used to analyse the roll-to-plate imprint process.

In the production process of a sample, the substrate goes through several processing steps in order to transfer a texture with good resolutions and adhesion to a substrate. In the production cycle, the following steps can be identified:

1. Preparation of the substrate at the start of the imprint process.
2. Dispense the resist on the substrate using the Coater1100 by Morphotonics.
3. Transportation of the substrate to the feed-in table of the NIL1100.
4. Alignment of the substrate at the start of the imprint process to set the initial position.
5. Imprinting using the NIL1100 in which the nano-texture is transferred from mould to substrate and the elastic mould is detached from the substrate simultaneously.

The process steps described above are performed in an in-line production process, as visualized in figure 3.1. From the given process steps, only the alignment of the substrate (4) and the imprint process (5) can be identified as critical steps to overlay. The remaining steps are chemical processes which are assumed to have no significant effect on overlay accuracy.



Figure 3.1: The roll-to-plate NIL production line present at Morphotronics, including: (1) the Coater1100, (2) the transport and feed-in table of the NIL1100, (3) the NIL1100 imprint module, and (4) the feed-out table.

This thesis will focus on the Portis NIL1100 imprint module. In figure 3.2, a side-view of the NIL1100 is shown. In the figure, the imprint process is illustrated for a substrate with a UV-curable resist layer. The first contact point between the stamp and substrate deforms the resist with the imprint roller to transfer the nano-texture from the mould to the substrate. Next, the deformed resist, laminated between a stamp and substrate, is cured using UV-light. In the final step, the stamp is gradually detached from the cured nano-texture in a delamination step. When the full surface area has been imprinted with the desired nano-pattern, the substrates exits the NIL1100 at the feed-out table and the flexible mould returns to its starting position in a cyclic motion.

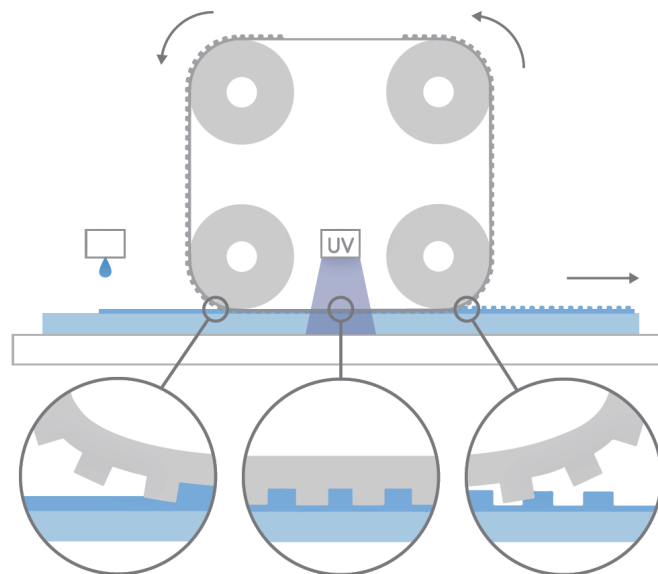


Figure 3.2: A schematic side-view of the Portis1100, an automated roll-to-plate line designed by Morphotronics [30]. Three imprint steps are shown for the imprint process: (1) Lamination of stamp and substrate with a resist in between, (2) curing of the viscous resist by UV light and (3) delamination of the stamp from the substrate. In the illustration the substrate, stamp, one imprint roller, one delamination roller and two transport rollers guiding the stamp are visible.

From the process illustrated in figure 3.2 several key characteristics to the design and imprint process can be identified:

- First, the stamp is transported over a series of rollers up until the imprint roller where the stamp is laminated onto a substrate with resist in between. From literature, the guidance of a thin web over a series of rollers can cause imperfections to the material or show undesired dynamic behaviour which can affect the imprint quality. Examples of such cases have been listed in section 2.3.
- Second, two separate motions can be distinguished in the machine: the substrate transported through the NIL1100 and the cyclic motion of the stamp. The two objects make contact at the imprint roller, after which the two motions require synchronization, meaning that a relative velocity or displacement between the two objects will result in imperfections. The identified errors are an initial displacement at the start of the imprint motion between stamp and substrate, and an accumulated displacement between the two objects due to a relative velocity difference over time. In other words, the system uses two frames of reference which require alignment and synchronization with respect to each other.
- Third, the resist is deformed by the imprint roller, which applies mechanical pressure in a line contact over the width of the substrate. The contact mechanics of the roller can introduce additional loads which would result in mechanical deformation of the stamp and substrate. The elastic behaviour of the line contact has been analysed for roll-to-roll and rolling-mask soft lithography, in which the deformation of the mould is known to affect overlay [19, 22, 9]. However, the concept is fundamentally different to R2P imprinting and can potentially affect overlay in an alternative manner.
- Next, the resist is deformed to take on the nano-sized texture of the mould by applying a high pressure to a viscous resist. After the imprint roller, the stack of materials consisting of substrate, resist and mould, have to be transported to the UV-light source for curing. In between the imprint roller and UV-light, a relative displacement between substrate and mould could introduce an error. The displacement could be initiated by relaxation of the stamp after removal of the imprint pressure, variation of in-plane strain of the elastic mould, or a relative thermal expansion between the two components.
- Finally, curing of the resist by UV-light introduces thermal effects to the surrounding components. First, because of the exothermal curing process in which heat is released by the resist. Second, UV-light is absorbed by surrounding components based on the material properties and exposure to UV-light.

Additional causes could be considered as well, such as the effect of process parameters, deformation of the resist after curing or the deformation of the substrate due to the applied imprint loads. However, the causes presented here are considered to be the most relevant error sources considered at this moment.

A first impression of the R2P system leads to several causes for potential error sources, however it is not yet known which phenomena are most relevant. In section 3.2 a measurement will be presented in order to link the various error sources introduced to the observed errors from samples. To interpret the observed errors correctly, it is critical to have an expectation of the errors which potentially occur in the system and to know how these errors can be identified from experimental data. Overlay is a summation of different errors in a system, and decoupling the error sources will help to understand what type of errors are being observed. Similarly, it should give a prediction on how each error source will affect the overlay accuracy.

For the potential error sources considered in this section, the errors are expected to behave in a scalar, linear or higher-order deformation pattern. Scalar deformations include translations, linear deformations include rotation, scaling and shearing and higher-order deformations include non-linear deformation. The error source can be related to the behaviour of the pattern. In the coming section, experimental results will be used to observe errors, analyse the decoupled error components and relate observations to expectations from this section. Based on the results of the coming section, a problem will be for this thesis will be defined in section 3.4 and an outline for the remainder of this thesis will be presented.

## 3.2. Quantifying errors in overlay

So far, critical points in the imprint process which have an effect on the final overlay accuracy have been identified. In this section, two measurements will be used to quantify the different error components in overlay by relating the measurement results to the expectations from the previous section. Ideally, each imprint is exactly the same in terms of positioning on the substrate and relative positioning of features in the nano-pattern. However, experiments will prove that the nano-pattern is displaced and deformed in between imprints. The errors resulting from the measurement, will be decoupled into alignment and deformation errors in order to gain insight in the cause of overlay inaccuracies.

Moreover, the measurements can help to quantify system characteristics such as accuracy and repeatability. When comparing multiple imprints from the same batch the repeatability can be quantified, as will be shown in sub-section 3.2.1. Similarly, the machine-to-machine repeatability can be quantified by performing similar tests on different machines, which will be presented in sub-section 3.2.2. Altering imprint conditions amplifies specific errors and also enables us to include systematic errors in the analysis. From the coming two subsections the overlay, relevant error sources, system repeatability and accuracy can be quantified.

**Note:** The examples of this chapter are samples taken from a larger set of test-data. The complete test results are fully presented in appendix A, which includes an overview of the tests and the methods applied to perform and post-process the measurements.

### 3.2.1. Imprint repeatability

In order to quantify the repeatability of imprints, a batch of samples has been produced under similar conditions. To amplify deformations, a stamp was used on the largest possible imprint size ( $1.1 \times 1.3[m]$ ). The imprint pattern was equipped with several arrays of markers, which were measured with a repeatability of  $< 5[\mu m]$  in the x-direction and  $< 10[\mu m]$  in the y-direction. An image recognition algorithm was used to extract marker coordinates from camera imaging, using the marker illustrated in figure 3.3. The test setup and methods applied in this thesis have been designed during this thesis to enable a large quantify of overlay measurements on a large scale. The setup uses custom python software to automate the measurements, developed in this thesis, which will be explained in the appendix A.4. A visualization of the marker locations is given in figure 3.4a. The placement of markers is a result of the available mould design at Morphotonics. The marker positions are convenient for this thesis, as most markers are located on the outer edges of the imprinted area. Still, for a statistical analysis an evenly spaced grid of markers would be preferred in future research.

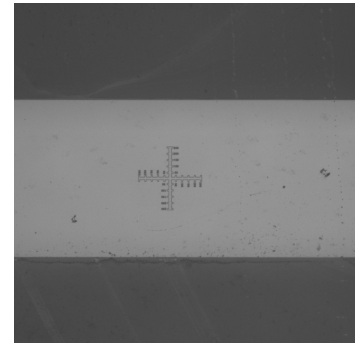


Figure 3.3: A zoomed image of a marker from which marker coordinates are obtained with a  $1.7\mu m$  resolution

The markers of each imprint are measured in the same frame of reference of the measurement setup, allowing for a direct comparison of marker coordinates. Each measured imprint results in a dataset of coordinates. From two datasets, the error between equivalent markers can be determined, which results in a vector field of error components. When visualizing the vector field directly, a large misalignment between the two imprints is found. Therefore, a least-squares fitting is used to compensate the translational and rotational error between the two datasets of coordinates, which enables analysis of the residual error after fitting. Additional methods for error decoupling will be discussed in section A.5 of the appendix. From the obtained translations and rotation the initial misalignment between the datasets can be approximated, including distortions due to the deformation of the imprinted area. The residual error after fitting can be used to analyse higher-order distortions, such as scaling, shearing and non-linear deformations of the imprint.

In figure 3.4b, two imprints have been compared after applying a translation and rotational fit to the two sets of marker coordinates. The fit applied to the 2D grid of coordinates, and the residual error after fitting, are summarized in table 3.1. The arrows used in the figure indicate magnitude and direction of the residual error. Looking at the figure, a clear relation in the vector field is visible, rather than random behaviour. Locally, the deformation is uniform in direction and magnitude. On a larger scale,

the resulting pattern resembles a more complex warping of the imprint. This example has a maximum error of approximately  $30[\mu m]$ , in a comparison between two imprints from the same batch under similar conditions. In other words, the repeatability of the imprint process.

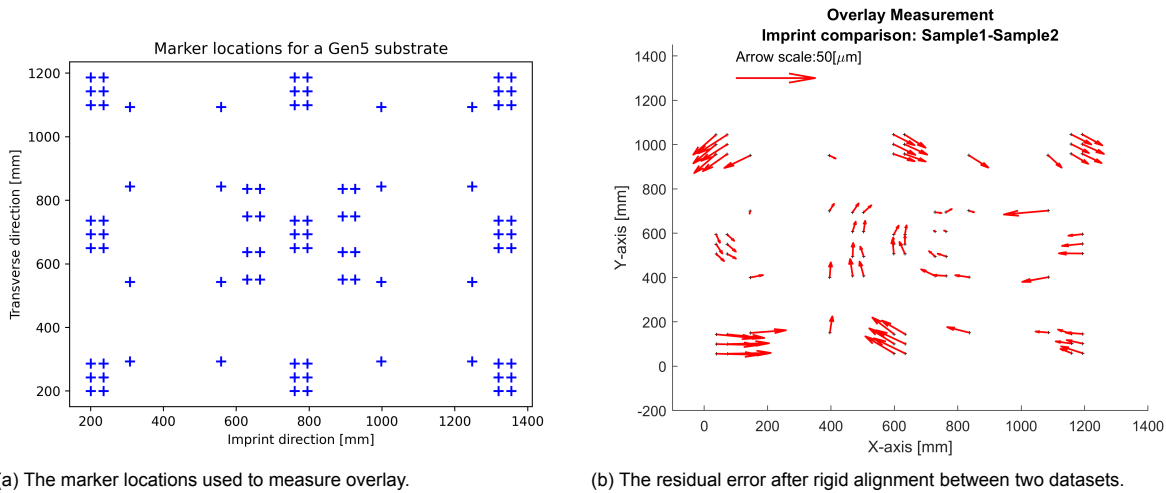


Figure 3.4: A quantitative comparison between two imprints, produced under similar conditions.

The residual error is broken down into two components: the rigid alignment used to fit the two samples and the residual error after applying the fit. In table 3.1, both of these components are given. In this case, the relative alignment between the two imprints is relatively large compared to the deformation in the imprint, and has the largest contribution to the errors in overlay. The content of the table does resemble comparable results from other samples or batches, as can be seen in the appendix A.

Rigid alignment			Absolute residual error			
Translation X [ $\mu m$ ]	Translation Y [ $\mu m$ ]	Rotation Z [ $\mu rad$ ]	Average error		Maximum error	
			X [ $\mu m$ ]	Y [ $\mu m$ ]	X [ $\mu m$ ]	Y [ $\mu m$ ]
-347.7	123.9	-480.3	10.2	7.4	28.0	18.0

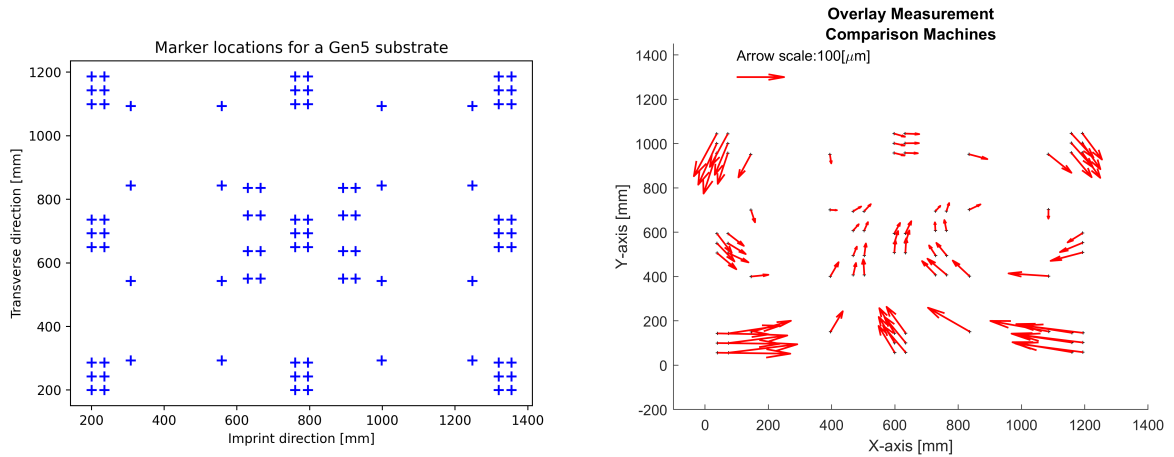
Table 3.1: The components which define overlay between two consecutive imprints. The rigid alignment defines the position accuracy between the two imprints, whereas the residual error quantifies the deformation of the pattern.

### 3.2.2. Machine to machine repeatability

The repeatability in the previous example, in figure 3.4b, masked the systematic errors present in both samples. By comparing samples from two different machines, using the same stamp (mould) and imprint conditions, the masked errors in a single machine would become observable. The motivation to perform measurements on multiple machines, is based on the expectations that machine design and tolerances affect the overlay accuracy.

The imprints are compared using the same methods from the previous example, a rigid transformation is applied, and the residual error is given in figure 3.5b and table 3.2. From figure ??, a similar deformation pattern is found compared to 3.5b, but with a larger magnitude of errors of approximately  $160[\mu m]$ . Again, adjacent vectors show a relation in magnitude and direction, indicating a local uniform deformation of the imprint. In addition, a curvature along the x-axis is visible as one side of the imprint lengths is placed in a positive strain and the other length is compressed. As two machines are compared, it would suggest that the errors observed are a result of a difference in machine components, and therefore that the machine has a big impact on the overlay accuracy.

Table 3.2 gives the residual errors for the machine comparison. The rigid alignment is left out, as the alignment between two machines is not controlled and can therefore not be compared. The order of magnitude for the errors ( $160[\mu m]$ ) is much larger compared to the repeatability of the imprint process, of approximately  $30[\mu m]$ . The significant increase in overlay inaccuracies, when considering two differ-



(a) The marker locations of the Gen5 nano-pattern used to measure over-(b) The residual error after applying rigid alignment between two measured imprints.

Figure 3.5: A quantitative comparison between two machines, by producing samples under similar conditions and using the same stamp.

ent imprint conditions, would suggest a large systematic error which was not observed in the previous example or has been introduced in between batches.

Rigid alignment			Absolute residual error			
Translation X [ $\mu\text{m}$ ]	Translation Y [ $\mu\text{m}$ ]	Rotation Z [ $\mu\text{rad}$ ]	Average error		Maximum error	
			X [ $\mu\text{m}$ ]	Y [ $\mu\text{m}$ ]	X [ $\mu\text{m}$ ]	Y [ $\mu\text{m}$ ]
-	-	-	44.0	41.5	153.7	127.6

Table 3.2: The machine to machine repeatability. The rigid alignment defines the position accuracy between the two imprints, whereas the residual error quantifies the deformation of the pattern.

From the result of this section, two important conclusions can be deduced. First, the comparison of imprints as shown in this chapter does not take into account an absolute comparison and can therefore mask errors relevant for overlay. Second, the significant increase in overlay inaccuracies for the machine comparison, suggest that a large error is introduced by machine parameters or components. Both batches have a repeatability of approximately  $30[\mu\text{m}]$ , with respect to imprint within the same batch, meaning that in between the two batches a systematic error of  $> 100[\mu\text{m}]$  has been introduced.

### 3.3. Problem analysis

The two comparisons made in figure 3.4 and 3.5b, are examples of a larger set of measurements and are representable for observations in other experiments. From these experiments, the errors can be related to aspects of the imprint process and machine design, according to our expectations of section 3.1. The results will determine the priorities in improving overlay accuracy in R2P NIL and develop a better understanding of overlay in the current system.

First, the rigid alignment, presented in table 3.1, gives a relative displacement of imprint of  $100 - 400[\mu\text{m}]$  and a rotation of roughly  $500[\mu\text{rad}]$ . Based on the expectations, the misalignment between samples is linked to the use of two frames of reference, namely the substrate and stamp, which is a synchronization error between the motions in the two respective frames. User experience of this system by Morphotonics supports this statement, which means that for the NIL1100 specifically, the synchronization is likely the cause of the translations and rotation error found. However, the values found in the experiment also contains measurement errors resulting from the use of a fit between the two objects, which can be distorted due to deformation of the patterns.

The second aspect of overlay is the residual error, which has been visualized in the figures 3.4 and 3.5b. The deformation seen in these figures shows a vector pattern with a visible relation in magnitude

and direction, representing a non-linear behaviour. Based on the underlying relation in the vector field, error sources such as thermal/hygroscopic expansion, tension variations or other linearly scaling components can be neglected as the dominant error component. Instead, the deformation is expected to be introduced by non-uniform strain along the width of the elastic mould. The idea is supported by literature, describing non-uniform strain profiles in webs as a result of machine imperfections, as introduced in section 2.3. This would relate the observations from the measurements to improper handling of the web, or elastic mould in the case of NIL. Based on the machine design this hypothesis is quite reasonable, as the current design does not consider the loads applied to the web to a great extent. It would explain how variations in imprint cycles can deviate slightly, whilst variations between machines show a much larger effect on overlay.

Comparing the figure 3.1 and 3.2, a hypothesis on the repeatability and accuracy of the system can be made as well. The first example compared the overlay within a single batch of production, which estimated a repeatability of  $\pm 30[\mu m]$ , which is supported by additional test results. The second example emphasized that a comparison between two machines resulted in much larger error components of  $\pm 150[\mu m]$ , which suggests that the two machines have a repeatable difference. Still, both the repeatability within a single batch and machine-to-machine repeatability, are expected to have a similar cause and can be solved by focussing on proper handling of the elastic mould.

In addition to the residual error, the rigid alignment between samples shows larger variations. However, it is assumed that the error is a result of an initial displacement at the start of the imprint cycle. This problem could be solved by an alternative design for the alignment between substrate and mould. There is no evidence yet, which would suggest a synchronization error over time is accumulated due to a relative velocity between the two components. Therefore, an improvement to the initial contact between mould and substrate should be sufficient.

### 3.4. Problem definition and outline

To summarize the content of this chapter, the machine topology of Morphotonics and the imprint process have been analysed, and different aspects of the imprint process were evaluated for potential errors. These errors were related to two measurements, which enabled us to quantify the error in the imprint process and relate the deformation to various sources. The deformation visualized in the resulting vector field indicated non-linear dominant error, as it was not relatable to 1-dimensional strain or expansion.

My conclusion, from the preliminary results, is that mechanical deformation of the stamp during the imprint process led to non-uniform in-plane strain of the elastic stamp. The mechanical strain is applied by the contact points of the stamp and machine on the rollers. This concept is derived from the literature on roller based web transport, as was introduced in chapter 2.

The assumption that mechanical strain is introduced by machine parameters could explain how the repeatability on a single machine is of the order  $30[\mu m]$ , whilst the overlay between machines was of the order  $150[\mu m]$ . To achieve a high overlay accuracy, the end-products of different machines should be comparable. Therefore, an understanding of how machine parameters and design have an effect on repeatability will be critical to improve overlay accuracy.

So far, the residual error after a rigid alignment has been discussed. However, also the translation and rotation error between imprints are quite significant, with errors ranging from  $100 - 400[\mu m]$ . These errors have been related to the initial positioning of the stamp and substrate at the start of the imprint cycle. The low repeatability has been caused by the transmission of the stamp in the NIL module, which is fundamentally related to the chosen transmission concept. To improve the alignment between the two components, a different actuation method and an alignment system with higher repeatability can be a great improvement. However, these implementations are related to the design of a machine and can be solved with conventional techniques available on the market.

Based on the hypothesis developed in this chapter, the remainder of this thesis will focus on the mechanical deformation in the elastic mould and the effect on overlay accuracy. Theory on roller based web transport will be used to quantify the dynamic behaviour and deformations of the elastic mould used in roll-to-plate imprinting. The web will be modelled using beam theory, as will be presented in chapter 4. Using the analytical descriptions for beam deformation and dynamics, chapter 5 will apply

the definitions in a numerical model to quantify the deformations resulting from machine design. In addition, the progression of deformations or disturbances in the web over multiple rollers will be considered. Modelling the dynamics of a web will result in an understanding of the observed behaviour in experiments and will be of help in relating error sources to machine design. The relation between the analytical models and observations in experiments will be presented in a verification step, as presented in chapter 6.

Having gained theoretical insight in the behaviour of a web, constrained by a set of rollers, the model will be used to identify critical parameters in the system which have impact on the overlay accuracy. Finally, having gained insight in the deformation in roll-to-plate imprinting, from both a theoretical and experimental perspective, suggestions will be presented to improve the handling of the elastic mould in overlay applications.



## Modelling of a web as a beam

In this chapter, the theory of web handling will be introduced to define a quasi-static model for a web constrained by a series of rollers. The literature describing the behaviour of a web will be discussed in order to understand the assumptions on which the models are built. From literature, it will become clear that a quasi-static analysis is not sufficient as the boundary conditions of a web vary over time and require an additional dynamic equation, which will be presented in section 4.4. Finally, the equations derived in beam theory will be used to quantify deformation of the web.

### 4.1. Introduction to web guiding

Rollers have been applied to guide and transport thin films in a field that can be categorized as web guiding. A web is herein defined as a material that is very long compared to its width and very wide compared to its thickness.

Generally, the web must follow a predetermined path in its longitudinal direction. Lateral deviations during this motion can result in a low product quality, or even failures in the production line. Too much lateral deviation will introduce slack of the web, or cause wrinkle formation. For this reason, the web tension, velocity and lateral position are important system parameters which require predictable behaviour in order to operate without disruptions. The handling of thin foils of various materials has been practised for a long time, especially in the paper, textile, polymer and metal industry. However, most of the knowledge on the design of roller systems was empirical and based on experience of the engineers.

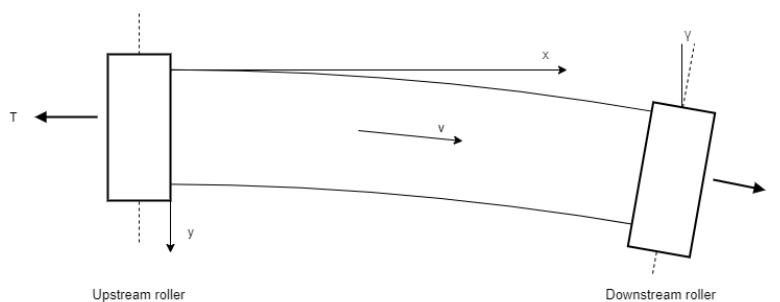


Figure 4.1: A schematic diagram of a web span between two consecutive rollers. The axis system of the web span is originated at the upstream roller. In the figure  $\gamma$  is the angle between the two rollers,  $T$  the constant web tension,  $v$  the transport velocity and  $x$  the transport direction. The convention in roller based transport is to define the roller from which the web exits as the upstream roller, and the roller on which the web enters as the downstream roller.

The focus of this chapter will be the lateral dynamic behaviour of the web over a series of rollers. When a web is exposed to disturbances, the web is able to move or translate in the lateral direction. As a result of the lateral displacement, the web will deform in between the two rollers. A web span, as

considered in this chapter, is visualized in figure 4.1. In the figure, a tensioned web with a longitudinal velocity is constrained by two rollers. Boundary conditions will be applied at the interface of the web and the rollers, and in the coming sections the dynamic behaviour of these boundary conditions will be elaborated.

## 4.2. Discussion on previous research

The first to combine empirical knowledge on web behaviour and formulate an accurate theoretical description of web shapes, deformations and dynamics was J.Shelton [37]. Shelton used beam theory to describe the shape of a web segment between two rollers. In his theory, Shelton distinguished models based on pure bending of the web and shear deformation.

With his approach, Shelton's model can accurately describe the shape of a web between two rollers and predict the lateral response of a web in dynamic behaviour. The formulation of Shelton could be applied to a single-web span, meaning that his methods did not couple the interaction of a multi-span system. Later, he would add to his previous research by converting his theory into a multi-span system using model estimation [49].

Shelton's work was referenced by many, as it was regarded as the first analytical web model in roller based transport. Various researchers would elaborate on the work performed by Shelton, such as L.Sievers and J.Brown who refined his work in their papers and review papers [43, 7]. Sievers focused on the state-space notation of a multi-span system, and also on the theoretical validation of assumptions applied in the description by both Sievers and Shelton. Brown has written multiple reviews and papers of different aspects in roller based transport [J.L.BrownAAND, 7, 6, 16, 32, 11]. In his work, he compares the different models by both Sievers and Shelton, by relating both methods to well-defined validation steps. Brown also collaborated with Shelton to discuss the quality of the previous research and from this analysis a good insight in the model, boundary conditions and assumptions was made.

The work of Shelton has been refined over the years and both Shelton, Sievers and Brown have found agreement on the description of the dynamic behaviour and the deformation in the web. The web is modelled as an Euler-Bernoulli or Timoshenko beam and the model can be used to describe the shape of the web and deformation in the web. From a quasi-static definition of the web between two roller contacts, the boundary conditions of the web can be described in analytical expressions. The quasi-static model can be further derived to come up with time-dependent expressions to convert the quasi-static model into a dynamic model and include lateral motion of the web. The output of the methods, as described by Shelton, Sievers or Brown, is a differential equation or transfer functions which defines the lateral acceleration of the web over time.

### 4.2.1. Shear in the Timoshenko beam model

According to Shelton, the steady-state shape of an elastic web can be derived from beam theory. The derivation depends on boundary conditions and initial conditions of the web. By applying beam theory, the conventions introduced by Timoshenko and Gere [40], will be used in all mechanical analysis. Previous work performed by Brown (and others) emphasized the importance of shear deformation to accurately describe the deformation in a web. Therefore, a preference was developed for the Timoshenko beam model over the Euler-Bernoulli model. Especially for short web spans with a length to width ratio of  $\frac{L}{W} < 2.5$ , which is the case in the systems of Morphotonics, the contribution of shear deformation is critical to the accuracy of the model. In figure 4.1, the conventions on a single web span can be seen.

The Timoshenko model is based on a distinction between bending and shear deformation. The shear deformation is an addition to the Euler-Bernoulli model, in which the shear stiffness of the beam is assumed to be infinitely stiff without deformation. By including the shear stiffness of the web, the slope of the beam consists of two components: the cross-sectional rotation  $\phi$  and the shear angle  $\psi$ .

$$\frac{\partial y}{\partial x} = \phi + \psi \quad (4.1)$$

So far, the lateral deformation of the web can be defined by the lateral position  $y$ , cross-sectional rotation  $\phi$  and shear angle  $\psi$ . Using these variables, Sievers applied Hamilton's principle to derive the

governing equations for a web segment. The derivations made by Sievers substantiate her research and the intermediate steps give insight in the methods she applied. However, these steps are rather complex to understand and do not add any value to the analysis performed in this thesis. If you are interested, I would suggest reading into the papers of Sievers and Brown [6, 43], for deeper understanding of the kinematic relation. From here on, the outcome of Sievers analysis will be directly applied, and her methods are assumed to be correct.

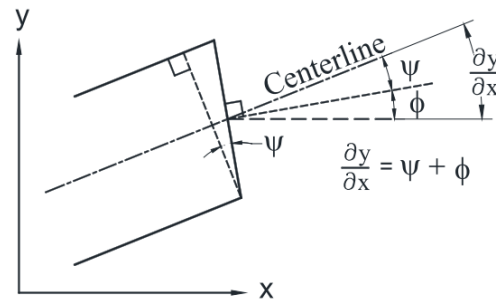


Figure 4.2: The convention of the Timoshenko beam model subdivides the slope of the web  $\partial y/\partial x$  in a bending component  $\phi$  and a shearing component  $\psi$ . [7]

### 4.3. Quasi-static beam model

The lateral dynamics of a moving web is described by Shelton, according to equation 4.2. Equation 4.2 is based on the assumption that the web mass can be neglected and describes the webs elastic curve which is derived from beam theory.

$$\frac{d^4 y}{dx^4} - K^2 \frac{d^2 y}{dx^2} = 0 \quad (4.2)$$

With

$$K^2 = \frac{T}{EI \left(1 + \frac{nT}{AG}\right)} \quad (4.3)$$

The parameter  $K$  is dependent on the web tension  $T$ , Young's modulus  $E$ , moment of inertia  $I$ , shear constant for a rectangular cross-section  $n = 1.2$ , cross-sectional area  $A$  and shear modulus  $G$ . The equation 4.2 is a fourth order linear differential equation. The general solution to the differential equation is given by equation 4.4:

$$y(x) = C_1 \sinh(Kx) + C_2 \cosh(Kx) + C_3 x + C_4 \quad (4.4)$$

The coefficients  $C_i$  of the static shape are dependent on the boundary conditions selected for the beam model. In addition, the Timoshenko beam model is applied and the boundary conditions at both ends of the web span are related to the rotational and shear deformation occurring in such a beam. In the full derivations, presented in appendix 4.3.1, Hamilton's principle is used to derive the equations for the cross-sectional rotation  $\phi$  and shear angle  $\psi$  according to the slope of a Timoshenko beam. This resulting definitions are:

$$\psi = -E I a \frac{n}{AG} y''' \quad (4.5)$$

$$\phi = y' + E I a \frac{n}{AG} y''' \quad (4.6)$$

#### 4.3.1. Boundary conditions

To solve the static web equation 4.4 four boundary conditions are required. The lateral position  $y$  at each end is a logical choice, and the other conditions are the cross-sectional rotation  $\phi$ . Subscripts 0

and  $L$  refer to the ends of the web-span at the contact point of the upstream- and downstream-roller. Note, that for an Euler-Bernoulli beam the rotation is equivalent to the slope of the web, whilst for a Timoshenko beam the slope also consists of a shear angle, as displayed in equation 4.1. Still, for both models the cross-sectional rotation as boundary conditions works, as both the lateral position and cross-sectional rotation should be continuous across a roller. The shear angle however, is not continuous and can differ for each web segment.

A roller is the interface of two consecutive web segments, and thus the boundary conditions meet. The boundary conditions of an upstream span should be equal to the downstream conditions for the following web span in order to be continuous. The shear angle sustained in a web span is constant and supported by the friction of the roller-web contact area. The shear angle is therefore discontinuous at the roller, meaning that the slope of the web differs at the entry and exit of the roller.

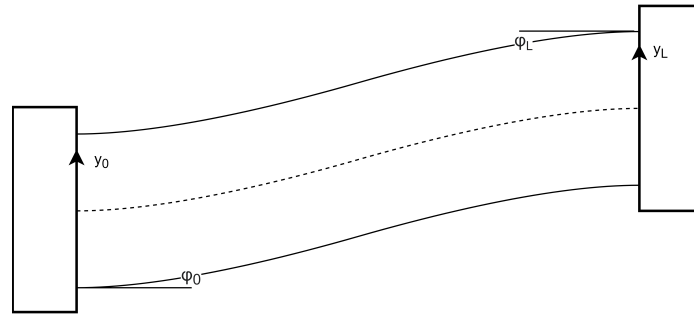


Figure 4.3: The four boundary conditions applied on a web span, as a result of contact with the rollers. At the upstream roller the cross-sectional rotation and lateral position from the previous web span gives  $\phi_0$  and  $y_0$ . The conditions at the upstream roller and the misalignment of the downstream roller  $\gamma$ , results in  $y_L$  and  $\phi_L$ .

With the cross-sectional rotation at the upstream roller  $\phi_0$  and downstream roller  $\phi_L$ , the resulting boundary conditions for a Timoshenko beam are:

$$\begin{aligned} y|_{x=0} &= y_0 & y|_{x=L} &= y_L \\ \phi|_{x=0} &= \phi_0 & \phi|_{x=L} &= \phi_L \end{aligned} \quad (4.7)$$

## 4.4. Dynamics of a web

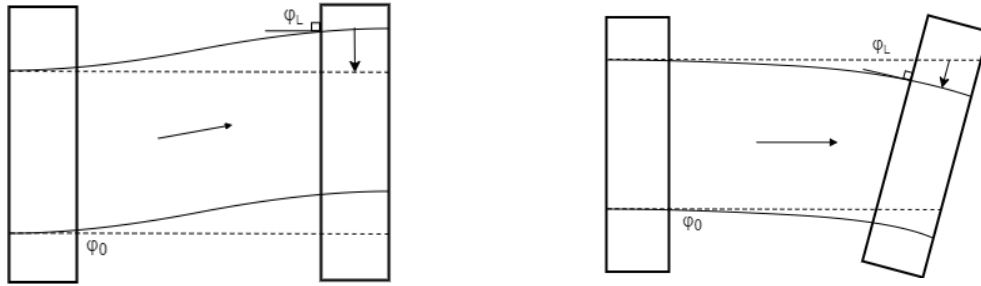
In the previous section, the four boundary conditions for a web are presented. However, the boundary conditions are presented as variables, as the exact values for the boundary conditions are time dependent. To describe how the boundary conditions vary over time a description of the dynamic behaviour is required, which is dependent on the so called "normal-entry" rule. From the normal-entry rule the lateral acceleration is derived.

In this thesis, the modified Sievers method is used to describe the lateral behaviour of the web in a multi-span system, based on the review of Brown [43]. To model the dynamics over multiple rollers, the continuous boundary conditions at the roller interface are used. Using these equations, the lateral behaviour and the progressions of disturbances over a series of roller are modelled.

### 4.4.1. Normal entry rule

The dynamic characteristics of a web span are derived from the "normal entry" - rule, which is widely accepted in the web industries. The normal entry rule states that a moving web has a propensity to align itself perpendicular to the roller axis. Meaning, that a misaligned roller will initiate a lateral motion of the web, until the web has aligned itself to a perpendicular entry on the roller surface. Consequently, if the web is not aligned perpendicular to the roller axis, it will deform in a 2D plane in order to meet the normal entry criteria. When a web has reached normal entry, it will not deform further or move in a lateral direction, as the web has reached a steady-state. This steady-state only refers to the lateral dynamics of the web, as the web does move in a longitudinal direction.

In figure 4.4, two examples are given for a laterally displaced web and a misaligned roller. In both figures, the entry angle of the web on the roller  $\phi_L$ , introduces a lateral motion to regain a perpendicular entry.



(a) Normal entry rule applied to parallel rollers. The web is initially displaced and will move in the lateral direction according to the arrow depicted on the downstream roller. (b) Normal entry rule applied to a misaligned roller. The web is initially straight but will move in the lateral direction until a normal entry to the downstream roller is achieved.

Figure 4.4: Two examples of the lateral motion initiated by the normal entry rule. The incoming web angle is initially not perpendicular to the roller axis, which results in a transverse motion of the web over the roller.

#### 4.4.2. Derivation of the lateral acceleration

The lateral dynamic behaviour is primarily driven by the web geometry as it enters the rollers at the downstream end ( $x = L$ ) of a span. The web conditions at the end of the span are determined by the conditions of the upstream roller at  $x = 0$  by  $y_0$  and  $\phi_0$ , as well as the roller misalignment  $\gamma_L$ , web dimensions, transport velocity  $v_0$ .

From the web geometry, Sievers found a relation for the lateral acceleration which describes the behaviour of the web end over time. The lateral acceleration is derived from the boundary conditions and web shape, which is presented in equation 4.8. The dynamic behaviour of the downstream roller is also taken into account, by the lateral velocity  $\frac{dy_L}{dt}$  and lateral acceleration  $\frac{d^2y_L}{dt^2}$  of the roller with respect to the world frame. In this thesis, only fixed rollers are considered which reduce both terms to zero. In equation 4.8, the subfunctions ( $g_i, h_i$ ) are introduced which are constant for a web span and are related to the web dimensions, material properties and transport conditions. The subfunctions are used to simplify the notation of algebraic equations and improve readability. The complete derivation, including the full notation, will be given in the appendix B.3, as the formulae are troublesome to work with.

$$\frac{d^2y_L}{dt^2} = (y_0 - y_L) \frac{v_0^2}{L^2} \left( g_1 - \frac{g_2 h_1}{h_2} \right) + \frac{g_2}{h_2} \left[ \frac{v_0}{L} \left( \frac{dz_L}{dt} - \frac{dy_L}{dt} \right) + \frac{v_0^2}{L} \gamma_L \right] + \frac{v_0^2 \phi_0}{L} \left( g_3 - \frac{g_2 h_3}{h_2} \right) + \frac{d^2z_L}{dt^2} \quad (4.8)$$

In addition to the lateral acceleration, one more equation is required for the cross-sectional rotation at the downstream web end  $\phi_L$ , as the boundary conditions at a web end will become the input conditions for a consecutive web span. The cross-sectional rotation can be derived as follows:

$$\phi_L = \frac{1}{h_2} \left( \frac{1}{v_0} \left( \frac{dz_L}{dt} - \frac{dy_L}{dt} \right) + \gamma_L - h_3 \phi_0 - \frac{h_1}{L} (y_0 - y_L) \right) \quad (4.9)$$

With a definition for the lateral acceleration and the boundary conditions at the downstream web end, a time-dependent model can be made to model the dynamic behaviour of a web. In chapter 5, these equations will be applied in a model which is representative for a system of passive rollers.

#### 4.4.3. Overview of assumptions

From the literature a dynamic model of a system of rollers can be made. Before going into the details of this method, the assumptions made in the models will be discussed shortly. As the description of a lateral dynamics model has been improved over the years, and different models have been defined, the assumptions are gathered from the initial model description of Shelton, as well as the additional work from Sievers and Brown [37, 49, 43]. The relevant assumptions for this thesis are listed below:

- No slip occurs at the roller surface
- Mass / inertia of the web is neglected
- The contact area of the web length compared to the free span length is small

- The web can never slack
- The web velocity and tension is constant
- All deflections are small
- The web is homogeneous and uniform in cross-section and material properties
- The web is isotropic and linearly elastic

Of the assumptions listed above, four are especially critical. First, the mass of the web is neglected, which is not realistic. However, the NIL applications considered in this thesis have such significantly low transport velocities, that the assumption seems reasonable. Second, the web is not isotropic, but rather anisotropic, which is relevant for the Timoshenko model considered in this thesis. In literature the use of isotropic materials is often considered as a possible error, however no alternative to the isotropic models have been published yet. In my opinion, the anisotropic behaviour is not critical for the models considered in this thesis, as the variation of material properties for anisotropic materials relatively small compared to the variations in materials considered in this thesis. In addition, the anisotropic behaviour is most relevant for the shear deflection of the Timoshenko beam and can be compensated by the shear modulus  $G$ . Third, the web is not completely homogeneous, as a nano-textured resist layer will be added to the stamp material. However, the effective thickness of the residual layer is relatively insignificant to the web thickness itself. Finally, the no-slack criteria is difficult to achieve in the setups of Morphotonics. Slack in the web is a result of a large enough curvature of the web, as through which the positive pretension over a part of the width is lost. The slack is therefore a result of improper handling of the web, as discussed in this thesis. Aside from angular misalignment, several additional causes can introduce a loss of pre-tension, as discussed in appendix E. In case slack in a web segment would occur, the theory applied in this thesis does not apply as no uniform tension of the web could be assumed.

## 4.5. Planar deformation of the web

In the description of lateral web dynamics, the Timoshenko beam model is applied to model the web as a beam. The previous sections focused on the dynamic behaviour at the web ends. The underlying equations model the beam and the beam deflection as a result of the boundary conditions. However, these relations are not actively applied as the industry of web handling focusses on the web behaviour at the interface of a roller. In the application of this thesis, the deformation in the 2D web span is also relevant.

In previous work, the strain and stress relations of the web span are not specifically mentioned, as it was not the point of interest. In this section, the beam equations will be used to describe the strain and stress relations of a 2D web segment. With the strain relations, the deformation can be quantified on each point on the web segment.

The strain relations for beam theory, valid for small rotations, can be defined using the Green-Lagrange finite strain theory. Figure 4.5 illustrates a beam under planar deformation. The beam uses the same conventions as applied to the web, with the origin in the web centreline.

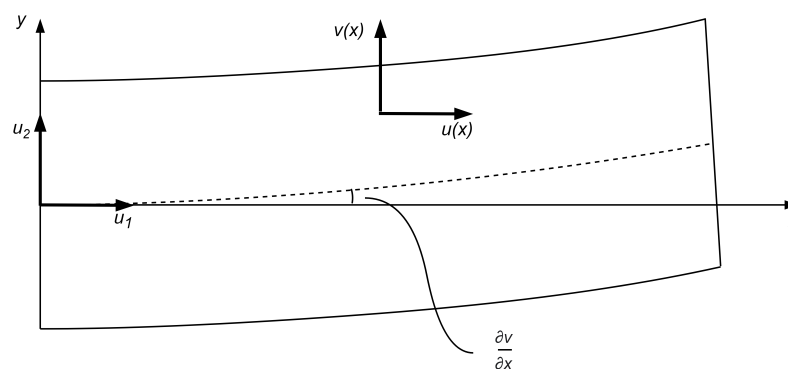


Figure 4.5: Schematic of beam conventions for planar deformation.

The displacement, fitting the notation of figure 4.5, are defined as follows:

$$\begin{aligned} u_1 &= u_{x,0}(x) - y\phi(x) \\ u_2 &= v(x) \\ u_3 &= 0 \end{aligned} \quad (4.10)$$

Substituting equation 4.10 into the Green Lagrange strain relations, gives the relevant strain terms for a web span.

$$\begin{aligned} \varepsilon_{11} &= \frac{\partial u_1}{\partial x} = \frac{\partial u_{x,0}}{\partial x} - y \frac{\partial \phi(x)}{\partial x} \\ \varepsilon_{22} &= \frac{\partial u_2}{\partial y} = \frac{\partial v(x)}{\partial y} = 0 \\ \varepsilon_{33} &= \frac{\partial u_3}{\partial z} = 0 \\ \varepsilon_{12} &= \frac{1}{2} \left( \frac{\partial u_1}{\partial y} + \frac{\partial u_2}{\partial x} \right) = \frac{1}{2} (-\phi(x) + \psi(x)) \\ \varepsilon_{23} &= \frac{1}{2} \left( \frac{\partial u_2}{\partial z} + \frac{\partial u_3}{\partial y} \right) = 0 \\ \varepsilon_{31} &= \frac{1}{2} \left( \frac{\partial u_1}{\partial z} + \frac{\partial u_3}{\partial x} \right) = 0 \end{aligned} \quad (4.11)$$

In these formulae, the tensile deformation is denoted by  $u_{x,0}$ . As a result of bending and shear deformation, a moment and shear force are applied. The moment results in a tensile strain according to  $-y(\partial\phi/\partial x)$ . The shear deformation is denoted by  $\partial v/\partial y$ .

With the strain equations presented above, the deformation in a beam can be expressed in the bending and shearing of a Timoshenko beam. The unique expressions for  $\phi$  and  $\psi$  will be presented in the appendix in B.2. In addition, the derivative of the cross-sectional rotation  $\frac{\partial\phi}{\partial x}$  is needed, which requires additional derivations also presented in appendix B.3.1 by equation B.31.

Using the strain equations, the deformation in the web has been quantified. An additional step is to analyse the stresses in the web span. Using the stress-strain stiffness relationship for isotropic materials, the strain vector can be used to obtain the stress vector of the web. The stress components can be rewritten using the Von Mises criterion to simplify the six directions into a single variable.

$$\begin{bmatrix} \sigma_{11} \\ \sigma_{22} \\ \sigma_{33} \\ \sigma_{23} \\ \sigma_{31} \\ \sigma_{12} \end{bmatrix} = \frac{E}{(1+\nu)(1-2\nu)} \begin{bmatrix} 1-\nu & \nu & \nu & 0 & 0 & 0 \\ \nu & 1-\nu & \nu & 0 & 0 & 0 \\ \nu & \nu & 1-\nu & 0 & 0 & 0 \\ 0 & 0 & 0 & 1-2\nu & 0 & 0 \\ 0 & 0 & 0 & 0 & 1-2\nu & 0 \\ 0 & 0 & 0 & 0 & 0 & 1-2\nu \end{bmatrix} \begin{bmatrix} \varepsilon_{11} \\ \varepsilon_{22} \\ \varepsilon_{33} \\ \varepsilon_{23} \\ \varepsilon_{31} \\ \varepsilon_{12} \end{bmatrix} \quad (4.12)$$

$$\sigma_{\text{vonmises}} = \sqrt{\frac{1}{2} \left[ (\sigma_{11} - \sigma_{22})^2 - (\sigma_{22} - \sigma_{33})^2 + (\sigma_{33} - \sigma_{11})^2 \right] + 3(\sigma_{12}^2 + \sigma_{23}^2 + \sigma_{31}^2)} \quad (4.13)$$

## 4.6. Conclusion

In this chapter, the Timoshenko beam model has been used to model a web span in between two rollers as a beam. Using the beam model, expressions for the web shape and deformation have been found. In addition, the dynamic behaviour of the beams boundary conditions have been defined, which will be applicable to model the deformation of a web over time. The methods to build such a dynamic model will be introduced in chapter 5, using the lateral acceleration equation derived in this chapter.

To conclude the content of this chapter, a static example of the web deformation will be given. In this example, a beam in between two non-parallel rollers will be considered. The boundary conditions are chosen, such that the boundary conditions at the upstream roller are perfect ( $y_0 = 0, \phi_0 = 0$ ), and an imperfection at the downstream roller is assumed of  $y_L = -50[\mu m]$  and  $\phi_L = 100[\mu rad]$ . These four boundary conditions are visualized in the figure 4.6.

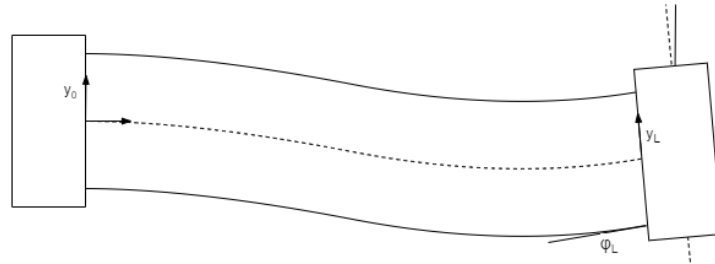
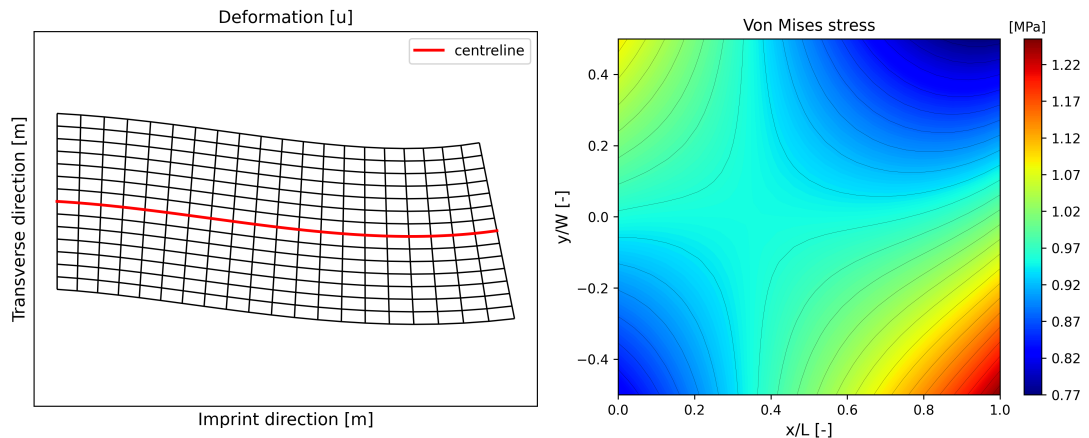


Figure 4.6: A deformed web with applied boundary conditions. The downstream roller has a misalignment of  $\phi_L = 100[\mu rad]$  and a lateral displacement of  $y_L = -50[\mu m]$ .

Using the theory of this chapter, the lateral deformation of the centreline can be quantified as well as the planar deformation of the web as shown in figure 4.7a. In addition to the theory from literature, this chapter introduced the stress and strain relations for a web span. For the example considered here, the Von Mises stresses have been visualized in figure 4.7a. In the example, the boundary conditions have been applied to a beam with length  $L = 1.5[m]$  and width  $w = 0.6[m]$ .



(a) The planar web deformation and the web centreline, as a result of roller misalignment. The deformation in this figure has been scaled. (b) The Von Mises stresses in a web span. The axis of the web are converted to a dimensionless scaling for comparison.

Figure 4.7: Deformation analysis of a web span using beam theory.



# 5

## Implementation of lateral web dynamics

In the previous chapter, the behaviour of a web in contact with rollers has been discussed. First, a quasi-static analysis was performed to describe the web as a beam with boundary conditions at the contact point with the rollers. Then, the dynamic behaviour was quantified to model how the boundary conditions vary over time.

In this chapter, the dynamic web behaviour from chapter 4 will be used to develop a dynamic model in Python. An Object-Oriented Programming (OOP) structure was chosen to efficiently implement the analytical descriptions to model both quasi-static and dynamic webs. The resulting model is able to perform and post-process numerical simulations in several seconds, enabling time efficient analysis of the systems at hand. The preference for Python as a software package is based on the accessibility of the methods in an open-source programming language.

The theory and analytical descriptions for a web in both quasi-static and dynamic behaviour have been validated and verified in previous research on experimental setups. However, the correct implementation of the theory in Python will still need to be validated, which will be presented in section 5.2. The verification will be obtained in chapter 6, in combination with a test on overlay accuracy. To support the models build in this chapter, simple examples of boundary conditions will be used to verify the correct behaviour of the models and gain understanding in the dynamic behaviour.

The goal of modelling the dynamics in a web span system, is to quantify the deformation as a result of machine imperfections. From the results obtained in this chapter a feeling can be developed for the severity of specific distortions to the web and the progression of errors over multiple web spans. In order to obtain these results the following objectives, or functionality, should be met by the model:

1. Model the quasi-static deformation in a free web span, between two rollers.
2. Model the dynamic behaviour of the web boundary conditions at the roller contact.
3. Model the progression of distortions over multiple web spans.
4. Map the deformation of the web onto a static point in the world frame to quantify the deformation found in imprints.

### 5.1. Model description

In section 4.4 the lateral acceleration of a web segment has been derived, as a result of imperfections in web handling, by equation 4.8. The equation is dependent on the boundary conditions at the upstream roller  $[y_0, \phi_0]$ , web properties  $[E, L, W, h, v]$ , roller alignment  $\gamma$  and time derivatives  $\dot{y}$ . A single web span in between two consecutive rollers can therefore be described by the building block as shown in figure 5.1. In the building block, two functions are solved: the lateral acceleration at the downstream roller  $\ddot{y}_L$ , and the cross-sectional rotation at the web end  $\phi_L$ .

Figure 5.1, is the building block for a single web span. The input is dependent on the previous web span,

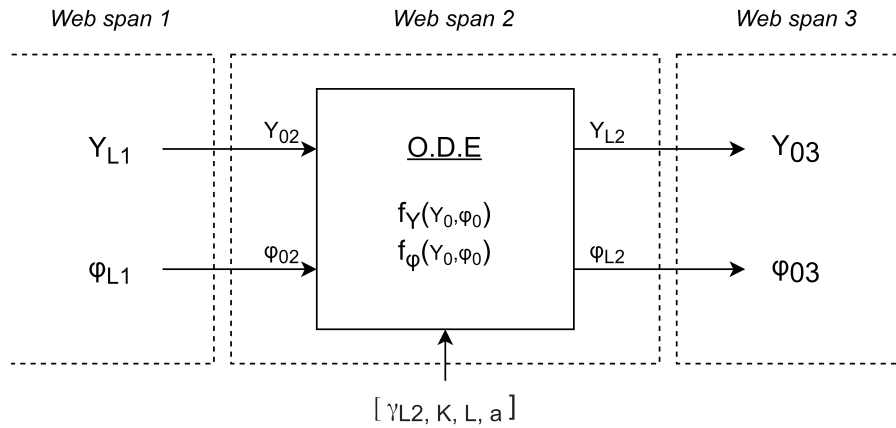


Figure 5.1: A schematic of a roller O.D.E. block which can be placed in a series of roller to form a multi-span system. The output of the O.D.E.'s become the input for the consecutive web span. The functions  $f_Y(y_0, \phi_0)$  and  $f_\phi(y_0, \phi_0)$  depict the equations solved to determine  $y_L$  and  $\phi_L$  of the web span.

and similarly the output of a block can be used as input for a consecutive web segment, also referred to as the up- and down-stream web spans. In a multi-span system, the blocks can be connected in series to relate the boundary conditions of an upstream web span  $i$ , to a downstream web span  $i + 1$ . The upstream boundary conditions  $[y_{i,L}, \phi_{i,L}]$  at  $x = L$ , will be equivalent to the boundary conditions  $[y_{i,0}, \phi_{i,0}]$  at  $x = 0$ .

From this generic structure, modelling a multi-span system is simple and accessible. Each span can have unique properties in terms of geometry and alignment. However, the dynamic model always requires a defined starting condition at the first modelled web span, namely  $y_{i=0,0}$  and  $\phi_{i=0,0}$ . The incoming web dynamics are therefore assumed to be known. This assumption is quite critical, as the chosen input conditions should be representable for the actual dynamics in a system. On the other hand, the input condition can now be chosen to model the progression of an input disturbance in a system, which is beneficial for research purposes.

In addition, the lateral position of the roller could be actuated to model a displacement guide. The lateral position  $z$  could be actuated in a closed loop system for active control, which is included in the model but not used as this thesis focusses on a system of passive rollers.

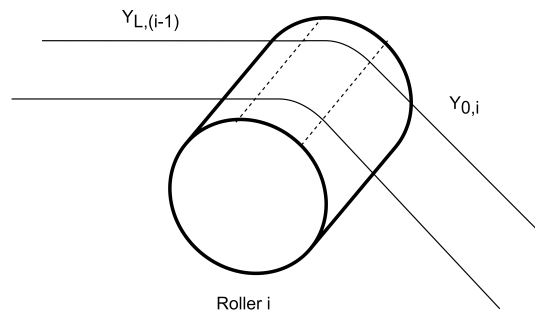


Figure 5.2: Physical interpretation of the roller building block. The coverage of the web over the roller circumference is referred to as the 'wrap-angle'. The dynamic models considered in this thesis neglect the length of the roller circumference due to the assumption of sufficient friction.

So far, the model building block is used to represent the roller. However, the physical interpretation of the block, and the accompanying assumptions are just as valuable. In figure 5.2, the interface between two consecutive web spans on the contact area with a roller is visualized. The area of the contact surface is dependent on the so called 'wrap-angle' of the web, referring to the coverage of the web over the roller. It is assumed that the contact area has sufficient friction to prevent slippage of the web over the roller, therefore being 'fixed'.

The web length covering the roller contact area is not considered in the block model. The result is an instant connection between two consecutive roller spans, without a time or displacement delay. Whilst in reality, a fixed point on the moving web will exit the roller after completing the circumference of the 'wrap-angle'. Naturally, neglecting the web length covering the roller does not represent a physical multi-roller system. However, including a delay with respect to time or displacement is numerically troublesome, whilst it does not alter the resulting dynamics. In the field of web guiding, the connected entry and exit conditions on a roller interface is widely accepted, due to the no-slip condition. Still, this assumption should be considered when interpreting the results from a numerical simulation to web dynamics.

### 5.1.1. Building a multi-span system

In figure 5.3, an exemplary system of four rollers is illustrated. As discussed, the wrap-angle of the web over the rollers can be neglected and is therefore not visualized in the schematic view. The translation of such a roller topology to a model, as described in this thesis, is given in the flow-diagram of figure 5.4.

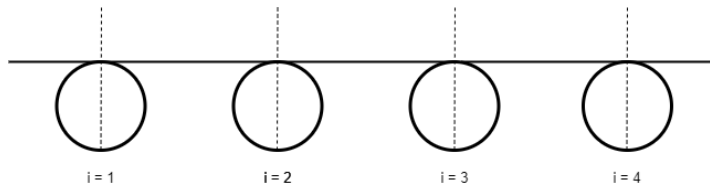


Figure 5.3: A system of  $i = 4$  rollers with a continuous moving web of infinite web length.

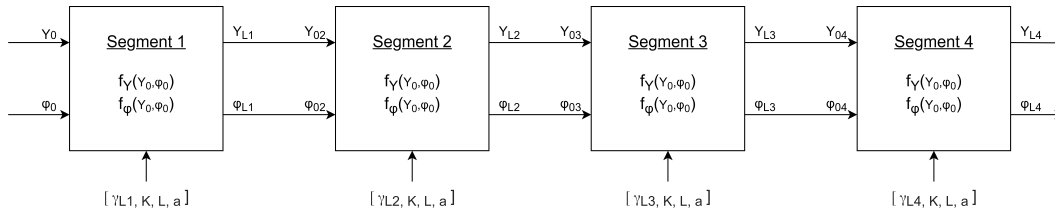


Figure 5.4: A schematic of a multi-span system, modelled by a chain of block models to couple the dynamics. Each web span has its unique input parameters and at each interface the down-stream boundary conditions are passed down to the following span as up-stream boundary conditions.

## 5.2. Validation of models

Brown used a step input to validate the implementation of the lateral dynamics model. In his example, he compared the reaction of an Euler-Bernoulli and Timoshenko-Gere beam model on a multi-span system. The example is quite relevant to illustrate the physical difference between a web span including or excluding shear deformation. In addition, the example can be used to validate the implementation of his theory in this thesis. The validation step by Brown included a system of five rollers ( $R_0, R_1, R_2, R_3, R_4$ ) with varying web lengths in the configuration depicted in figure 5.5. The parameters of the system are given in table 5.1. At roller  $R_0$ , a step input is introduced at the start of the simulation.

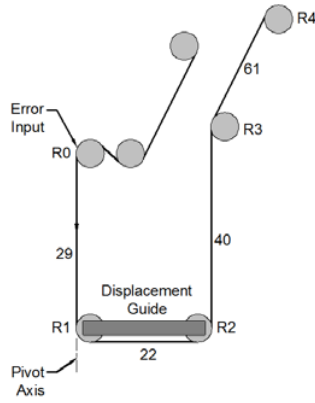
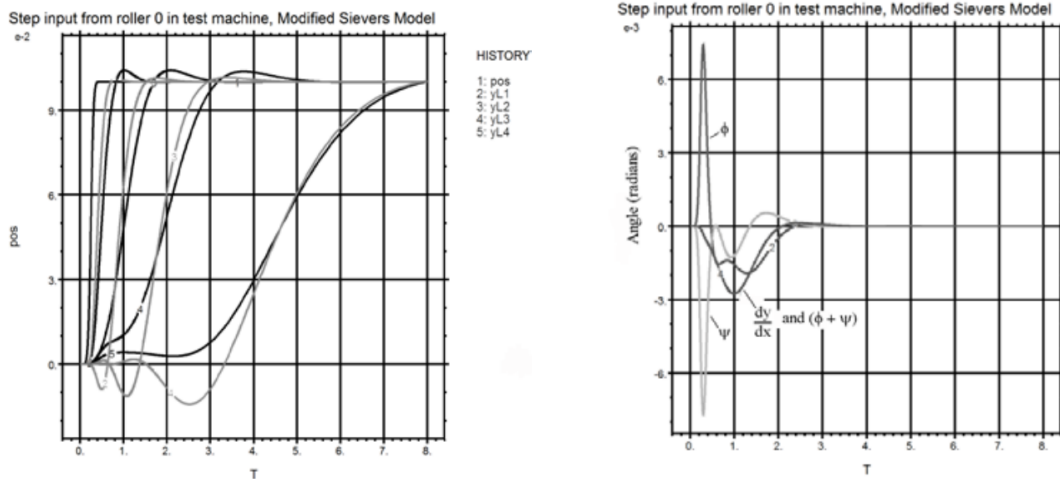


Figure 5.5: The test setup used by L.Sievers, as documented by J.Brown [J.L.BrownAAND]

Parameter	Imperial		Metric	
	Value	Unit	Value	Unit
$L_1$	10	inch	0.254	m
$L_2$	22	inch	0.559	m
$L_3$	40	inch	1.016	m
$L_4$	120	inch	3.048	m
$w$	44.5	inch	1.313	m
$h$	0.0034	inch	86e-6	m
$E$	550.000	psi	3.8	GPa
$\nu$	0.3	-	0.3	-
$\nu_0$	200	fpm	1.013	m/s
$T$	1	lb/inch	175	N/m
$\frac{nT}{AG}$	0.0017	-	0.0017	-
$K$	0.07036	-	0.07036	-

Table 5.1: Parameters used in the example by J.Brown using the Modified Sievers method, as modelled in this thesis. [7].

The response of the four downstream rollers ( $y_{L1}, y_{L2}, y_{L3}, y_{L4}$ ) is plotted in figure 5.6a, in which both the Euler-Bernoulli responses (light-grey) and the Timoshenko response (dark-grey) are visualized. From this analysis, a significant difference in dynamic behaviour can be expected for a web neglecting or including shear deformation. Especially at  $t = 0$  a unique behaviour can be observed as the Euler-Bernoulli model translates in the opposite direction to the disturbance, a phenomenon referred to as nonminimum phase behaviour by Brown. This effect has been observed in lab experiments as well.



(a) Brown's step input example for an Euler-Bernoulli (light-grey) and (b) The angular components ( $\phi_{2,L}, \psi_{2,L}, \frac{dy_2}{dx} \Big|_{x=L}$ ) of the second web Timoshenko-Gere (black) beam model [7].

Figure 5.6: A step response modelled by J.Brown to validate his model, using both the Euler-Bernoulli and Timoshenko method [7]. From his example, he validated the correct behaviour for both models and related the behaviour to observations in experiments.

### 5.2.1. Replicating Browns model

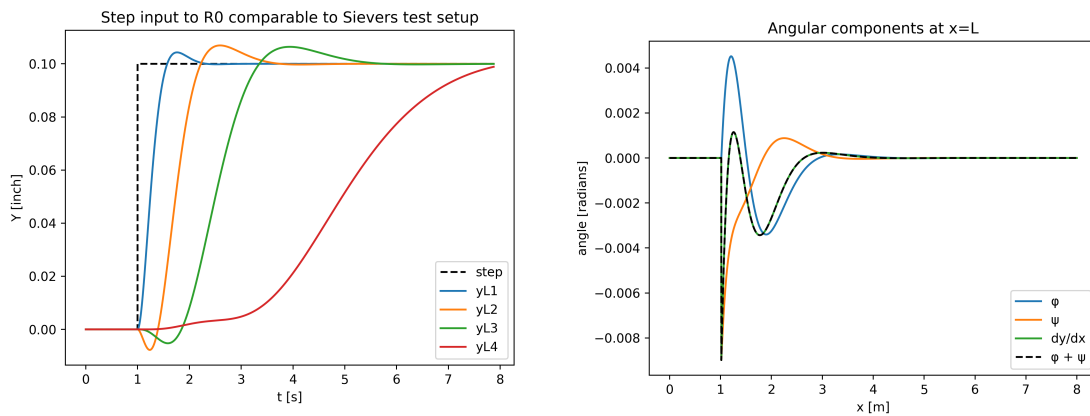
Brown's example can be replicated to validate the implementation of his model description in this thesis. In order to keep the visualization simple, the difference between the Euler-Bernoulli and Timoshenko beam model will be separated into two examples. The distinction between the two models is made by setting the shear coefficient  $n$  for a rectangular cross-section to  $n = 1.2$  for the Timoshenko beam or to  $n = 0$  for the Euler-Bernoulli beam. As described in chapter 4 the variable  $a = 1 + \frac{nT}{AG}$  will reduce to  $a = 1$  for an Euler-Bernoulli beam. As a result, the beam equations for web deformation or web dynamic behaviour will also reduce to the simplified Euler-Bernoulli lateral dynamics model.

At this point, I would like to emphasize on the physical meaning of the Euler-Bernoulli beam compared to

the Timoshenko beam. In the Euler-Bernoulli beam model the web slope is equal to the bending angle of the web, such that:  $\frac{dy}{dx} = \phi$ . The Timoshenko beam model introduces an additional deformation to this equation, by taking into account shear deformation, such that:  $\frac{dy}{dx} = \phi + \psi$ . The Euler-Bernoulli model neglects shear deformation and assumes an infinitely stiff web in the lateral direction, therefore the shear angle  $\psi$  is assumed to be zero. In the coming examples, the effect of neglecting or introducing shear deformation will be visible.

First, let's look at the Timoshenko beam model by replicating the system as described by Brown. A step input is used by defining a signal for the incoming lateral position at  $R_0$ . In this case, the step input is not initiated at the start of the numeric simulation, in order to observe the stability of the simulation. At  $t \geq 1[s]$ , the lateral position  $y_0$  is set to  $0.165[inch]$  or  $4.19[mm]$ .

The modelled dynamic behaviour of the web is visualized in figure 5.7a for the four rollers and the step input. In addition, the angular components of the second web segment at  $R_2$  are visualized in 5.7b. In the figure, the line of  $\frac{dy}{dx}$  and  $\phi + \psi$  overlap, as they are equivalent.



(a) The lateral position converging towards a step input under the assumption of a Timoshenko beam model ( $n = 1.2$ ).

(b) The angular components in the second web span at  $x = L$

Figure 5.7: A step response modelled for the Timoshenko beam model, similar to the validation presented by J. Brown from figure 5.6. Based on the replicated results a difference in the response at  $t = 1$  is found, whilst overall the response seems similar in response time and overshoot.

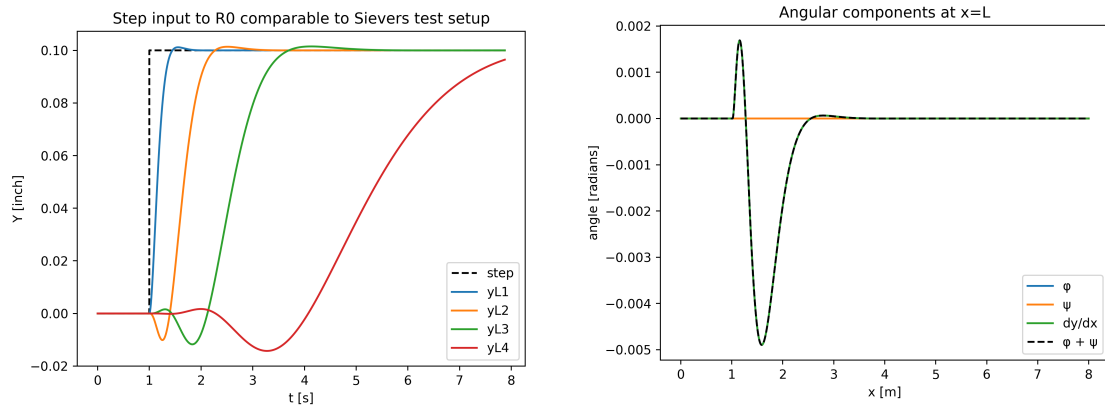
The same approach has been performed for the Euler-Bernoulli beam model. In this case the shear coefficient is set to zero ( $n = 0$ ). The resulting dynamic behaviour is visualized in figure 5.8a and the accompanying angular components in the second segment are given in figure 5.8b. The shear angle  $\psi$  is zero, as was expected for the beam with an infinite shear stiffness.

The replicated step responses from figure 5.7 and 5.8 show good similarities to the example given by Brown in figure 5.6, as well as some clear discrepancies.

First, the convergence towards the step reference value is similar to Brown's model for all roller within a comparable time. Moreover, the same difference between webs with or without shear can be observed in the models produced in this thesis. The overshoot for the Euler-Bernoulli beam is lower compared to the Timoshenko beam, and the nonminimum phase behaviour is also present for the Euler-Bernoulli model.

However, in spite of a good overall similarity between Browns simulations and the simulations performed in this thesis, the behaviour at  $t = 1[s]$  deviates from Browns results. The initial motion for the Timoshenko beam shows nonminimum phase behaviour which closer represents the Euler-Bernoulli beam model from Brown. The difference in results is most clearly notable when comparing the angular components in the second web span from Brown in figure 5.6b, and the results from this thesis in figure 5.7b. In figure 5.7b, the step input results in an immediate shear angle to accommodate the deflection. Whilst for Brown, both  $\phi$  and  $\psi$  gradually increase over time, which would suggest that the step input applied by Brown is not an instantaneous deformation, but rather a fast but smooth motion.

Arguably, the method by which the step input is introduced in the numerical simulation is different in my



(a) The lateral position converging towards a step input under the assumption of an Euler-Bernoulli beam model ( $n = 0$ ). (b) The angular components ( $\phi_{2,L}$ ,  $\psi_{2,L}$ ,  $\frac{dy}{dx}|_{x=L}$ ) in the second web span at  $x = L$ .

Figure 5.8: A step response modelled for the Euler-Bernoulli beam model, similar to the validation presented by J.Brown from figure 5.6. Based on the results, the implementation of web dynamics in this thesis has been validated, as the response is an exact replica of the results from J.Brown.

this thesis models compared to Brown, which has a relevant effect on the models including shear deformation. This also explains why the Euler-Bernoulli models match quite well, as that specific model has no shear deflection, and how the overall response to the step input is similar. The Timoshenko models on the other hands, show a different initial response to a disturbance and then converge in an equivalent manner to the step reference value.

As the method by which Brown has implemented his step input is not mentioned in his work, it is difficult to make an ideal comparison. An attempt has been made to use a fourth order set-point to replicate the work of Brown, which made the comparison better but still not perfect. Still, by diving further into the differences between the two models the imperfection can also be reasoned. Disregarding the shear deformation at  $t = 1$ , the models show good coherence with the dynamics of Brown's paper. Therefore, the implementation of the Modified Sievers method in this thesis is theoretically validated.

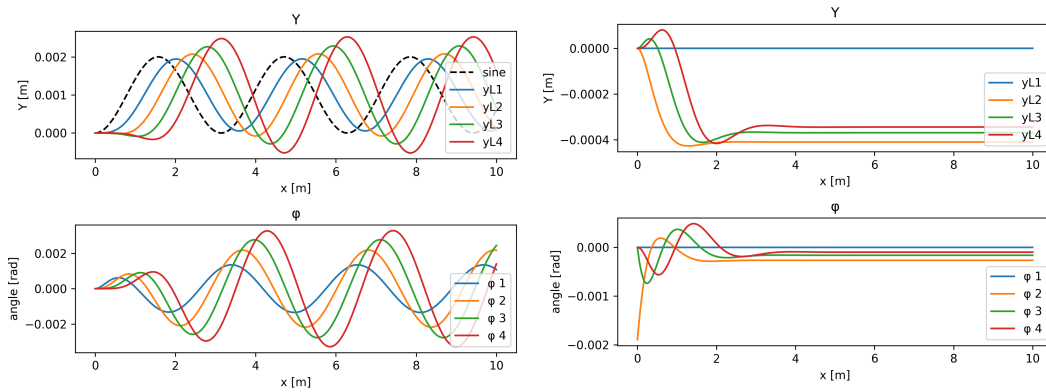
### 5.3. Case study

Besides the step input, additional examples can be studied to validate the lateral behaviour modelled in this thesis. In this section, several cases will be studied to relate the modelled dynamics to our expectations, based on the insights obtained so far as well as descriptions from literature.

Relevant examples are the effects of a specific error introduction and the progression of an error over time and over a set of multiple rollers. Therefore, a sine wave is used to track the progression of an error, the effect of a single roller misalignment is modelled and the eccentricity of a single roller is modelled. All simulations are performed on a system of four rollers, to represent the design of Morphotonics. The web spans all have an equal length of  $1[m]$ , width of  $1[m]$  and material properties of the standard stamp design of Morphotonics. The examples apply a Timoshenko beam as the literature has emphasized the importance of the shear deflection in short web spans. The same models have been performed with the Euler-Bernoulli beam as well, which can be found in the appendix C.1.

#### 5.3.1. Sine input

A sine wave as input to a system of rollers is a common example to model error progression over multiple web segments. Naturally, the error is dependent on the properties of the web and the dimensions of the system in addition to the frequency and amplitude. In figure 5.9a an example is visualized for a four-roller system of equal lengths. The shear deflection of the web and the short span lengths result in an amplification of the incoming error.



(a) A sine wave disturbance introduced at the entry of the first roller, with an amplitude of  $1$  [mm] and frequency of  $\frac{2\pi}{6}$  [rad/s]. (b) A web response to an angular misalignment of  $-1$  [mrad] introduced at the second rollers. As a result, the second and downstream rollers move in the lateral direction.

### 5.3.2. Roller misalignment

A critical aspect to this thesis is the dynamic response of a web to roller misalignment. This error is a result of machine tolerances and assembly errors, and will affect the dynamic behaviour of a web. As the accuracies in alignment are finite, the effect of these error sources are relevant to analyse performance. In figure 5.9b the effect of a misalignment on the second roller is visualized. As a result of this misalignment, a lateral motion of the web is initiated which affects all downstream web segments. Notably, the downstream web segments do not converge towards the same equilibrium as the lateral position is dependent on four boundary conditions:  $[y_0, y_L, \phi_0, \phi_L]$ , which mean that the bending angle  $\phi$  is not equivalent in the downstream segments.

### 5.3.3. Eccentricity

The field of web guiding focuses on web dynamics over a perfect cylindrical roller, which is representative for modelling the lateral behaviour. In case of a non-ideal roller, geometrical imperfections can affect the lateral dynamic behaviour as well. Roller misalignment from the previous example is one of the scenario's considered. Another imperfection is the eccentricity of a roller. Two types of eccentricities can be considered, one case in which the geometrical centre of the roller is not aligned with the axis of rotation, and the other being an angular misalignment between roller and axis of rotation. The second example can be modelled as a sinusoidal motion of the angular alignment, in which the web velocity and roller radius determine the frequency of the angle. This can be modelled with the existing block model, as is illustrated in figure 5.10. From the figure, an oscillatory behaviour can be observed which dampens over the web segments.

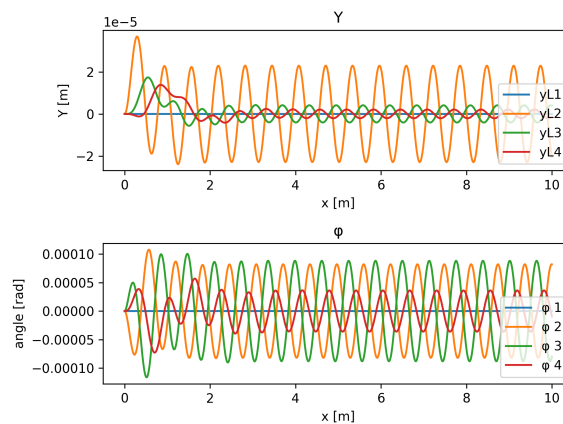


Figure 5.10: The effect of roller eccentricity which causes an oscillatory disturbance to the web input.

## 5.4. Mapping of web deformation

To relate the deformation and position of the stamp to the deformation in the final product an additional step is required. Figure 3.2 from section 3.1 illustrated the imprint process in which the stamp is laminated onto a substrate whilst mechanically deforming a resist to the nano-structure. After laminating the two components, the resist is cured using UV-light, after which the structure has solidified and assumed to be fixated in its positioning. Before curing the stamp is sealed to the substrate with a viscous resist in between, which can allow a viscous flow or displacement of the stamp. After curing, the solidified resist is assumed to be rigid and unable to deform.

This thesis does not address the complex viscous flow in between stamp and substrate, or the relative displacement between these two components. The complexity of this fluid dynamics problem exceeds the scope of this thesis project. However, identifying the possible error source and its underlying complexity is relevant for possible future research, as will be recommended in chapter 11.

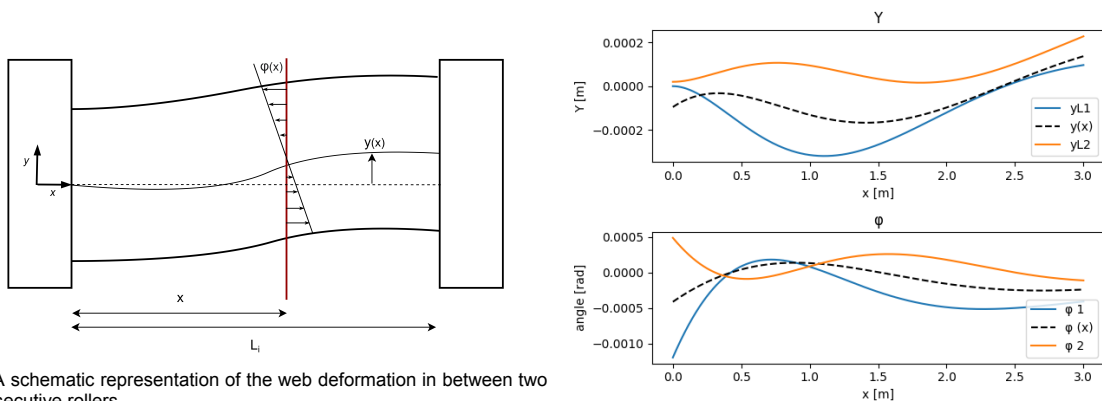
For now, it is assumed that the viscous friction of the uncured resist does affect the overlay accuracy, but can not be quantified. Even though the behaviour of the resist as a viscous fluid is unknown, two extreme scenarios can be considered to approximate the deformation:

1. By neglecting the viscous friction on the stamp, in contact with the substrate, the stamp can be modelled as a free-span. As a result the web is assumed to be unconstrained in its deformation and the web shape as modelled so far can be mapped directly onto a substrate.
2. Assuming infinite viscous friction the web does not deform after contact with the resist and substrate. In this case the web deformation at the imprint roller can be mapped directly to the imprint, assuming no relative displacement between stamp and substrate after initial contact.

In reality, the viscous friction will allow displacement of the stamp with respect to the substrate and the resulting imprint overlay will be a combination of the two scenarios described above. Quite possibly, the exact deformation will be dependent on the process parameters such as layer thickness of the resist, viscosity and in-plane web tension. For now, the two scenarios considered will be elaborated on to give a first impression of imprint deformation.

For a free span, the web is assumed to be unaffected by the contact with the substrate, and the deformation can be quantified by the quasi-static beam theory from chapter 4. The planar deformation will depend on the boundary conditions  $[y_0, y_L, \phi_0, \phi_L]$  at the web ends. For a position  $x$  on the free web span, the local deformation is dependent on  $y(x)$  and  $\phi(x)$  as illustrated in figure 5.11a.

An example is visualized in figure 5.11b, for  $x = 0.5[m]$  on a web span of  $L = 1[m]$ . From these equations the deformation, as described in 4.5 can be applied to map the deformation onto a substrate as seen in figure 5.12a.



(a) A schematic representation of the web deformation in between two consecutive rollers.

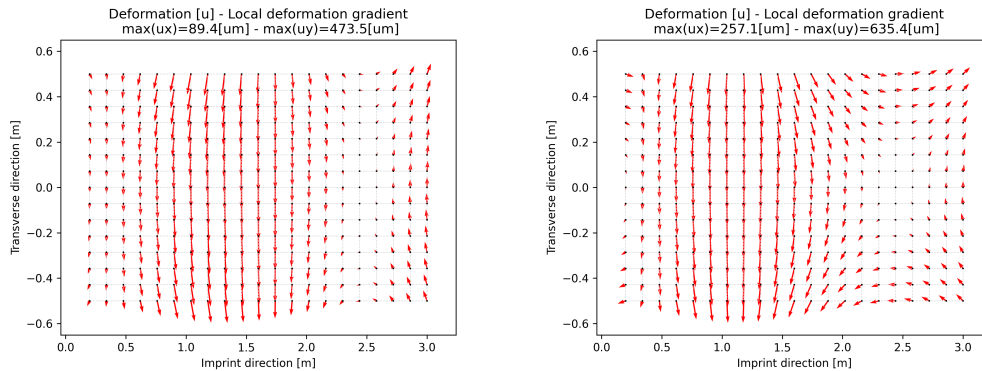
(b) The boundary conditions over time, including the web lateral position and angular rotation at a location on the free-span.

Figure 5.11: A visualization of the relation between web lateral dynamics and deformation of a web in between two consecutive rollers.



The alternative scenario does not allow for a relative displacement between stamp and substrate. Therefore, the stamp is assumed to maintain its shape after the NIP contact at  $x = 0[m]$ . Mapping the deformation of  $\gamma_0$  directly onto the imprint results in a different deformation pattern, which is visualized in figure 5.12b. From the figures, the main difference is found in the imprint direction, as close to the imprint roller the largest angular deflection is expected. The behaviour close to the boundary conditions is clearly visible in figure 4.7b from the previous chapter.

The two scenarios focus on the mechanical deformation in the stamp, resulting in an overlay inaccuracy of the imprint. The thought experiment exercised in this section takes two extreme scenarios by neglecting or by excluding the possibility of relative displacement. In reality, a more complex dynamic behaviour will determine the exact deformation which will require additional research from a new point of view. Still, the results shown in figures 5.12 give us insight into the mechanical behaviour of a stamp, which can be related to the measurements performed during this thesis.



(a) The web deformation at a location  $x = 0.5[m]$  on the stamp mapped onto a substrate. (b) The web deformation at a location  $x = 0[m]$  on the stamp mapped onto a substrate.

Figure 5.12: An exemplary mapping of stamp deformations to imprint deformation. A four roller system is modelled for the arbitrary angular misalignments:  $\gamma = (\gamma_1, \gamma_2, \gamma_3, \gamma_4) = (900, -700, 300, -600) [\mu rad]$ .

### 5.4.1. Main deformation components

From the model, various deformation patterns can be observed depending on the model conditions. To summarize the observations, several main deformation components can be identified, namely: translation, rotation, warping and shearing. Each deformation is visualized in figure 5.13.

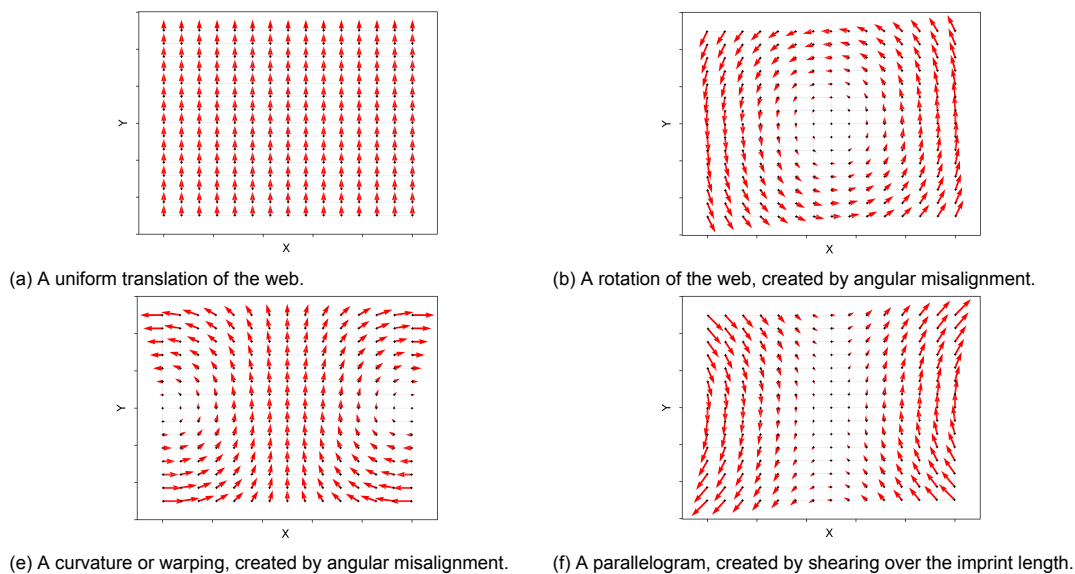


Figure 5.13: The main deformation components, which have been observed in dynamic simulations of a multi-span system.



# 6

## Verification

So far, the lateral web dynamics has been derived from beam theory and the implementation of the descriptions into a model has been validated. Examples presented in chapter 5 presented the behaviour of a web over multiple rollers, including the progression of a disturbance or error over multiple web spans. The lateral behaviour has been verified in experimental setups in numerous papers. However, the relation between lateral web dynamics and overlay accuracies, as researched in this thesis, is yet to be proven. Therefore, this chapter will present a verification test in which the knowledge of web guiding is applied to quantify the effect on overlay accuracy in R2P nanoimprint lithography.

The machines available at Morphotonics will be used to introduce a disturbance to the flexible mould and measure the resulting deformation in the end-product. Keep in mind, that the machine of Morphotonics is no dedicated test setup, but rather a complete system with additional complexity. The same measurement methods are applied as in section 3.2, to compare the relative deformation in the imprint process. The same mould and marker design has been used to produce imprint on Gen5 scale ( $1.3 \times 1.1[m]$ ). The verification test presented in this chapter has two objectives:

- Prove the relation between lateral web dynamics and overlay by a relative comparison between imprints with and without a disturbance to web handling.
- Relate the observed deformation in imprints and the positioning of the imprint on a substrate to results obtained in models presented in chapter 5

From the test results, a quantitative conclusion can be drawn on the results obtained in dynamic models, as well as prove the reasoning presented in this thesis.

### 6.1. Verification method

The two samples presented in section 3.2 quantified the relative difference in imprints produced under or varying conditions. The repeatability of imprints was estimated to be  $\pm 30[\mu m]$ , and a comparison between machines resulted in residual errors up to  $150[\mu m]$ .

Similarly, in this verification test a relative comparison will be made between imprints with the addition of a forced disturbance. The disturbance will be an angular misalignment introduced at one of the rollers, and imprints will be made for various angular positions. These imprints can be compared relative to each other in order to observe the effect on overlay. To do so, three batches of three imprints have been made. The first batch acts as a reference for the nominal state of the machine, and afterwards two batches will be produced with a small and larger angular disturbance of the roller. It is important to introduce an error significant enough to be observed and overcome the repeatability error in the system. The tests performed are given in the table 6.1.

Batch	Sample displacement	Angular
1	1	0.0 [mrad]
	2	0.0 [mrad]
	3	0.0 [mrad]
2	4	0.43 [mrad]
	5	0.43 [mrad]
	6	0.43 [mrad]
3	7	1.22 [mrad]
	8	1.22 [mrad]
	9	1.22 [mrad]

Table 6.1: An overview of the samples produced in the verification of this thesis.

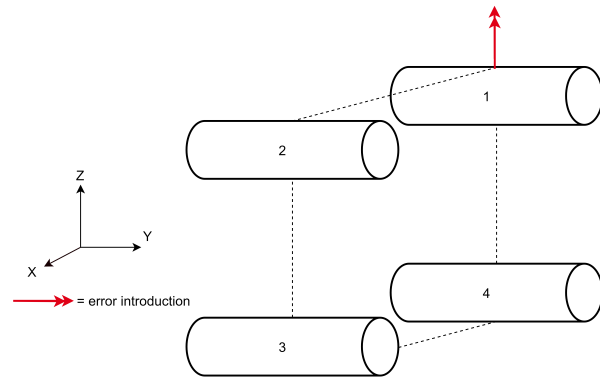


Figure 6.1: A schematic overview of the four rollers of the NIL1100. A roller 1 is given an angular misalignment indicated by the red arrow in this figure. In between roller 3 and 4 the web is in contact with the substrate.

The angular misalignment can be applied on a single roller in the NIL1100, which is labelled as roller 1 in figure 6.1. The roller is supported by two bearing housings with a rough adjustment, and the displacement of the housing is measured with respect to a fixed point on the frame. As the roller is not located near the curing position of the substrate, the observations of this test will focus on the progression of disturbances over multiple web spans, as discussed in chapter 5.

## 6.2. Expectations based on model results

The introduced angular misalignment is applied to roller 1, and is expected to introduce a lateral motion based on the examples from chapter 5. The resulting dynamic behaviour progresses towards downstream rollers, with a critical point in between roller 3 and 4 where the web is in contact with the substrate. The model representing the NIL1100 with an angular displacement can be visualized schematically as in figure 6.2. It is assumed that the roller misalignment will be notable due to a lateral displacement of the imprint and additional overlay inaccuracies due to a deformation of the web.

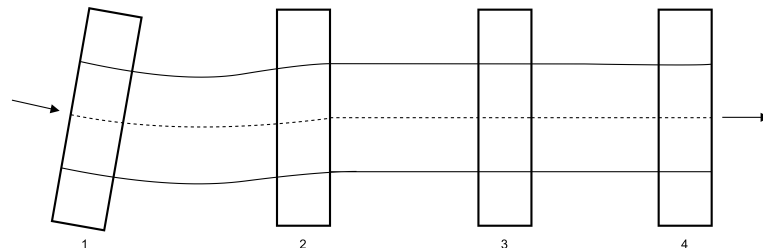


Figure 6.2: A schematic overview of the series of rollers. Roller 1 has an angular misalignment, which will result in an error downstream. The error is a combination of a lateral displacement and two-dimensional deformation in the web.

The representative model for the four-roller system, is given in figure 6.2. Unfortunately, the possible disturbances introduced to the system are unknown, such as the relative alignment of rollers and the incoming web motion at the first roller span. Therefore, the system dynamics is approximated by assuming perfect conditions except for the introduced misalignment at roller 1. This assumption is critical, however given the circumstances it is a reasonable solution.

Using the representative model, the effect of various angular disturbances is analysed. Based on the models presented in previous chapters, the dynamic effect can be quantified in the lateral positions and cross-sectional rotation at each roller  $[y_i, \phi_i]$ . The most notable parameter is the lateral translation of the web, which progresses towards downstream rollers. When taking the lateral displacement of the web in between roller 3 and 4, an expectation for the test can be formed.

In the model, a range of angular displacements is used to quantify the expected lateral displacement of the imprint. The resulting relation is a linear trend in the lateral displacement and angular misalignment of roller 1. Figure 6.3 illustrates the modelled data points. The linear relation between lateral dis-

placement and angular misalignment can also be supported by the acceleration equation 4.8 derived in chapter 4, in which the angular misalignment appears linearly.

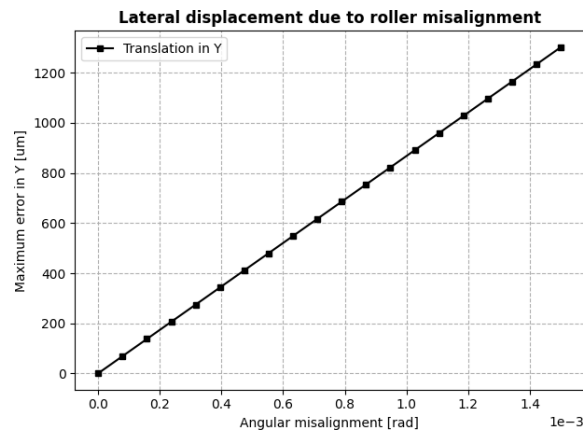
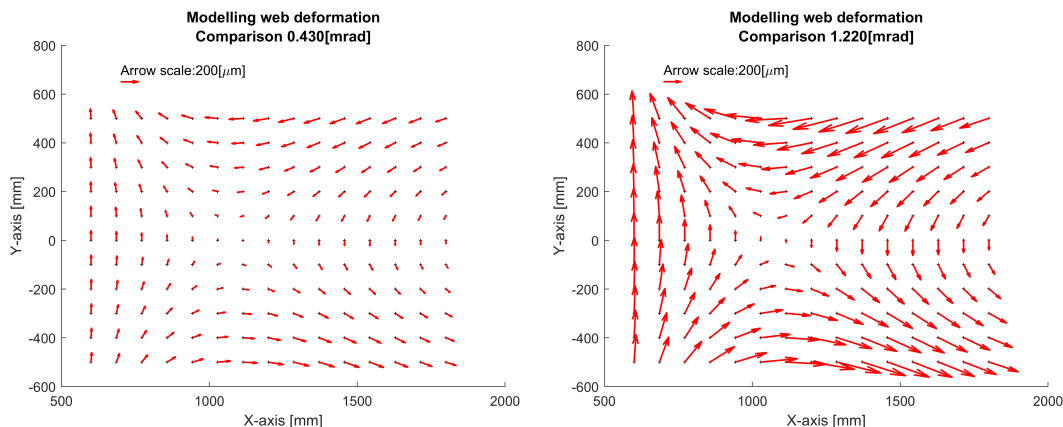


Figure 6.3: The obtained lateral displacement, at the curing position at half the web length between roller 3 and 4, as a result of an angular disturbance. The figure illustrates a linear relation between the disturbance angle and the lateral displacement.

In addition to the lateral displacement of the web on the roller, the resulting deformation of the web is studied. The verification test performed in this chapter, uses three distinctive batches which can be compared relative to each other. Using the results obtained from the model, the rigid alignment is performed similarly to the post-processing of test results. In this case, there are no coordinate sets of markers, but a grid of points on the web for which the deformation is observed. The grid is compared between a deformed and undeformed state, for both angular disturbances in figure 6.4.



(a) The resulting deformation pattern as a result of a  $0.43[mrad]$  disturbance to the web. (b) The resulting deformation pattern as a result of a  $1.22[mrad]$  disturbance to the web.

Figure 6.4: The modelled and post-processed deformation of the elastic mould, obtained by dynamically modelling the web response as a result of machine misalignment for several angular disturbances.

## 6.3. Results

Each of the 9 samples has been measured with the same methods as introduced in chapter 3, which resulted in a 2D grid of coordinates for each sample. The samples can be compared relative to each other, in which a relation between the batches is expected. For the analysis of this chapter the error due to repeatability or due to the forced misalignment of a single roller have to be distinguished, in order to draw clear conclusions.

All the samples have been compared relative to sample 2, which was found to be representative for the first batch of imprints. Each comparison consists of a rigid alignment between the two set of coordinates,

which applied a translational and rotational fit. The residual error is analysed which resulted in an average error, max value and min value. These results have been summarized in table 6.2. Within a single batch of 3 imprints, produced under similar conditions, the imprints are expected to have a repeatability of  $\pm 30[\mu m]$  which seems to hold up.

The most notable results, from table 6.2, are the translation in the y-direction of the fitting, and the maximum and minimum errors obtained. First, the lateral translation has increased stepwise with the increase in angular misalignment and a maximum translation of over  $2[mm]$ . Second, the overall overlay accuracy has decreased significantly, which is represented both by the average error for all markers and the maximum and minimum residual errors. The progression of lateral displacement is visualized in figure 6.5, including a linear trend line to emphasize the underlying relation. For the lateral translation, also the expectations from the model has been included in the figure as well. The linear expectation has been given the same offset as the trend-line of the data points for comparison. Furthermore, the maximum and minimum error components have been visualized in figure 6.6, including a trend line. Based on the data points, it seems as if the errors are repeatable over the series of imprints. The trend line emphasizes the increasing error in overlay as a result of the forced disturbance exposed to the system.

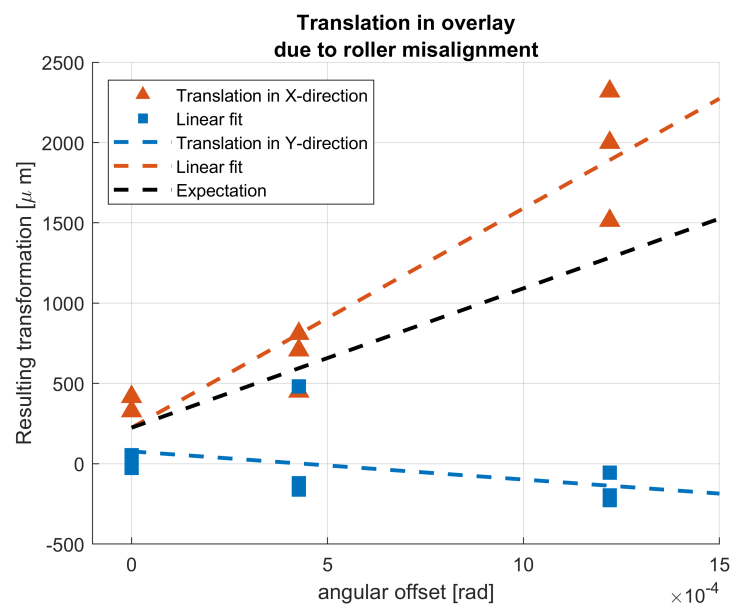
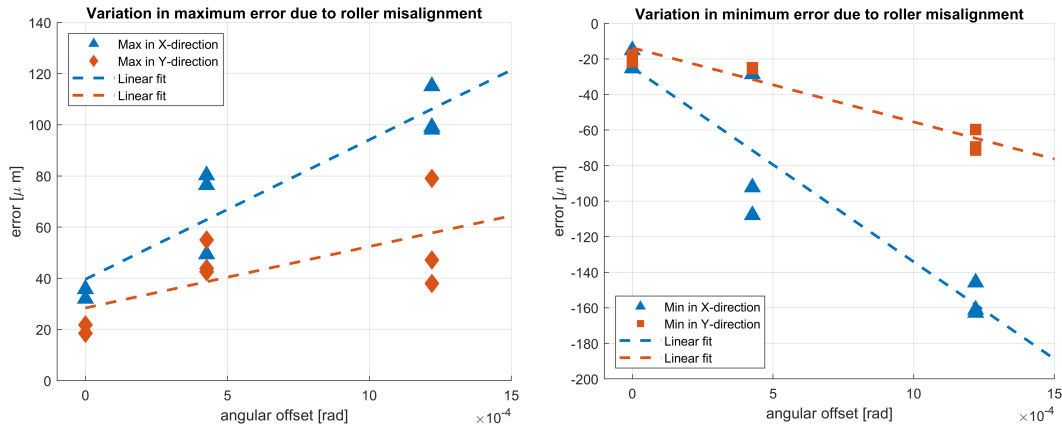


Figure 6.5: The translation in the X- and Y-direction, plotted from the results of table 6.2. A linear trend line is included to fit the data points, as well as the expectations from figure 6.3. The linearly expected translation is transposed to the same value on the y-axis for comparison, as the trend line does not go through the origin of the plot.

Batch	Sample	Absolute residual error						Transformation		
		Average		Max		Min		Translation		Rotation
		X [ $\mu m$ ]	Y [ $\mu m$ ]	X [ $\mu m$ ]	Y [ $\mu m$ ]	X [ $\mu m$ ]	Y [ $\mu m$ ]	X [ $\mu m$ ]	Y [ $\mu m$ ]	Z [ $\mu rad$ ]
1	1	8.1	9.6	35.8	21.8	-15.1	-17.8	-53.9	-328.0	385.8
	2	0.0	0.0	0.0	0.0	0.0	0.0	0.0	0.0	0.0
	3	11.1	9.4	32.0	18.5	-25.3	-22.0	25.9	-416.9	-112.8
2	4	11.0	16.4	49.4	43.9	-28.6	-25.3	120.9	-706.9	684.9
	5	25.5	13.1	80.3	55.0	-92.2	-25.5	159.8	-809.9	789.7
	6	34.3	12.2	76.5	42.5	-107.9	-24.9	-481.4	-450.5	272.6
3	7	29.7	20.6	98.1	79.0	-145.8	-59.8	226.9	-1513.9	475.0
	8	38.7	27.3	115.1	47.2	-162.8	-71.3	196.2	-1999.5	626.8
	9	34.4	26.3	99.1	38.0	-161.1	-69.4	54.6	-2319.1	1006.8

Table 6.2: An overview of the relative comparison with respect to sample 2. A rigid alignment fit is applied to obtain the translation in the x- and y-direction and a rotation.

The overlay performance in this thesis is quantified by observing the residual error and summarizing the result by the average, minimum and maximum residual error. However, the underlying relation between vector components also contains valuable information, which can not be comprised in one of the previously mentioned parameters. A visualization of the vector field is a good method to interpret the observed deformation, so figure 6.9 depicts the comparison of each sample with respect to sample 2. From the figures, a similar deformation pattern is found within each batch. The samples in batch 1 have a relatively good overlay accuracy, whereas the samples from batch 2 and batch 3 show larger vector components and an underlying relation in the deformation pattern.



(a) The maximum residual error over all marker pairs for each sample. All data points are compared to sample 2. (b) The minimum residual error over all marker pairs for each sample. All data points are compared to sample 2.

Figure 6.6: The test results summarized in two figures. The test data is plotted over the error introduced at the roller. The data points have a large variation, which was expected based on previous results and machine specifications. However, a significant linear trend is visible for both figures.

### 6.3.1. Visual comparison of imprint deformation

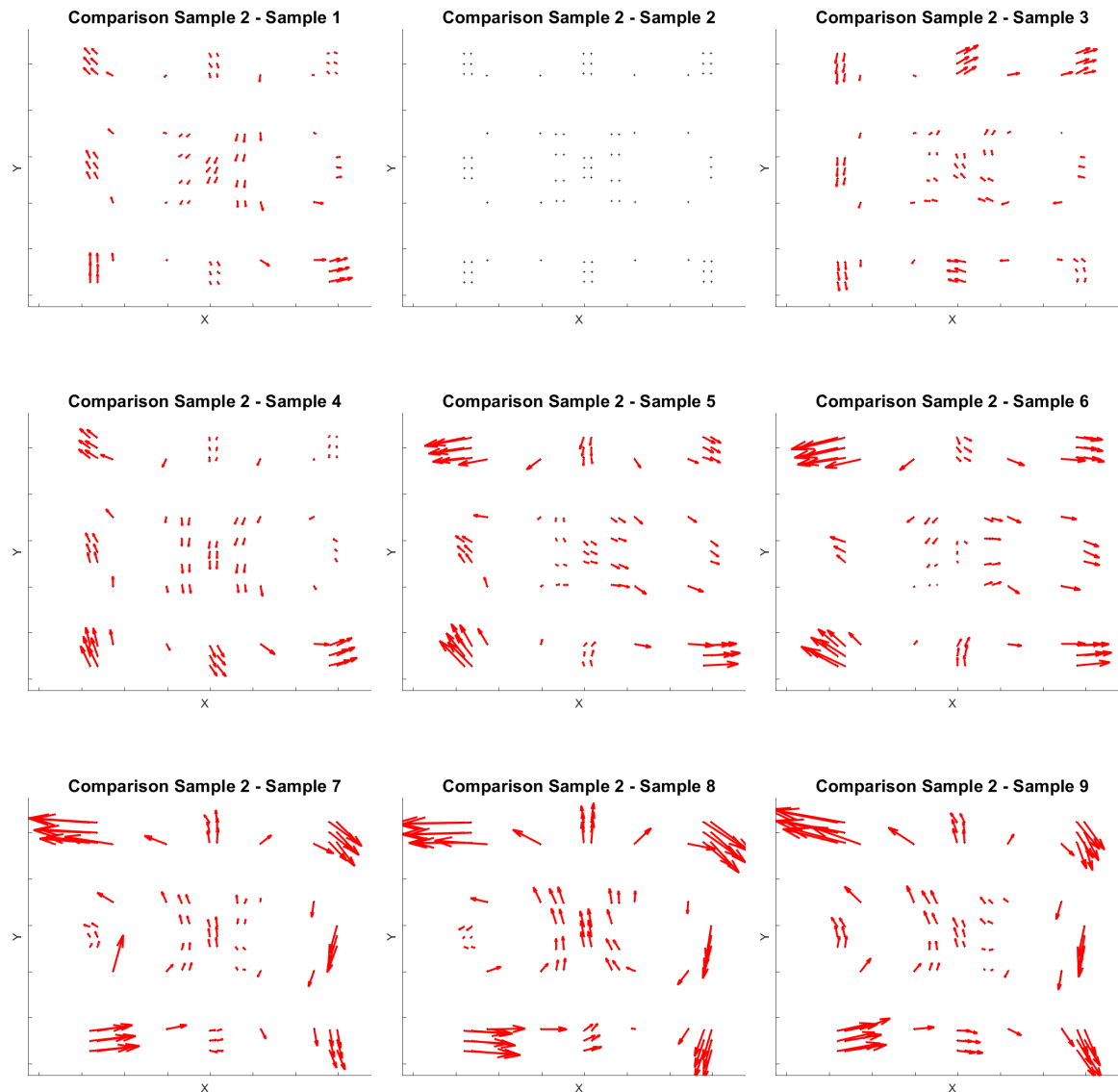


Figure 6.9: A relative comparison for each of the 9 samples, compared to sample 2. The methods applied is a rigid alignment with a translation and rotation fit. For each sub-figure, the arrows indicate the residual error between the two samples with the same scaling factor in order to compare the results. Over the series of samples repeated deformation patterns are identified for samples within a batch.

## 6.4. Discussion and conclusion of results

The results obtained in section 6.3 relate theory and models applied in this thesis to experimental results obtained on machines of Morphotonics. The results are presented by table 6.2 and figures 6.9 and 6.6, in which the overlay of the samples can be compared to a single reference, namely the reference sample 2 obtained from batch 1. In the table and figure, an interesting increase in overlay inaccuracies was found as a result of the introduced misalignment.

First, the table summarized the positioning of the nano-pattern on the substrate by fitting a rigid body alignment for each imprint. The translations which resulted from the rigid body transformation show a large increase in lateral displacement as a result of the roller misalignment, on a scale which has not been observed in other experiments. In the worst case, a  $1.22[mrad]$  misalignment resulted in a maximum translation of  $2.3[mm]$  and maximum residual error of  $162[\mu m]$ . The lateral displacement complies with the expectations from section 6.2, in which a linear relation was expected based on model results. The linear trend is fitted to the data points, however the data points do show a large



variation, making it difficult to verify the linear relation. The variation is caused by the repeatability of the NIL module itself, and a settling behaviour in which the web finds an equilibrium position over multiple imprint cycles.

Interestingly, based on the model expectations, the translation was estimated to have less effect than observed in this measurement. The difference between the model and measurements can be explained by the angular displacement not being an independent parameter. The roller, to which the misalignment is introduced, is coupled to multiple components in the NIL1100, which all affect the behaviour of the web in the imprint process. This is a result of machine design for the NIL1100 specifically, but does give a hypothesis for the larger errors observed in the measurements. An alternative reason for the discrepancy between model and results, can be the deformation of the nano-pattern affecting the fit of the rigid alignment. The least-squares method applied could be compensating the deformation of the imprint with a translation in the y-direction.

Furthermore, the translation in the X-direction is rather repeatable. Based on the values found in the table, the data points would fall within the  $\pm 200[\mu m]$  specifications of the NIL1100. Nevertheless, based on the trend line fitted to the data points, I would reason that the data points show a deformation opposite to the lateral deformation, which can simply be related to the finite length of the web. However, there are insufficient data points to make an exact statement.

Secondly, the residual error for all markers on the imprint after the rigid body transformation is represented by the average error, maximum value and minimum value. The table indicates an increase of errors found in overlay, however the underlying relation or exact deformation is not taken into account. Nevertheless, a clear relation can be observed when looking at the figures from 6.9, in which the deformation for each batch shows a repetitive pattern. This means we can expect a repeatable deformation as a result of the misalignment introduced, and that the deformation is significantly large relative to the system repeatability. The results suggest that a roller misalignment can be repeatable, which is a valuable conclusion. However, in order to obtain accuracy an additional calibration of the roller alignment would be required.

Despite a clear result for the lateral behaviour of the imprinted nano-pattern, the deformation is not exactly similar to the deformation found in figure 6.4. Part of the difficulty of comparing the modelled and measured deformation, was relating the absolute model results relatively to each other. In the end, the same rigid alignment mapping for post-processing of measurements was used.

In addition, the largest difficulty faced in replicating the deformation from measurements, were mostly related to the input conditions for the model. The verification test, presented in this chapter, involved the assumption of a perfect system of rollers with a single disturbance. Still, the actual system is composed of multiple disturbances which can not be quantified. The system functions as a black box, and from the results obtained in this chapter the exact deformation can not yet be related to modelled results. Possibly due to a lack of accuracy in the modelling methods, or due to additional distortions exposed to the imprint process as a result of the introduced roller misalignment.

In conclusion, the experiment showed a significant response in overlay, comprised of a lateral displacement and deformation of the nano-pattern on the substrate. The lateral displacement could roughly be related to results obtained in models. The deformation of the sample was found to be repeatable in the imprint process, but the exact deformation field could not be related to model results. Still, the lateral behaviour from literature and the error progression over multiple web spans have been observed in this chapter. Therefore, the verification presented in this chapter proved insightful and relevant to improving overlay accuracy in R2P NIL.

Based on the verification results, combined with the knowledge of elastic webs from literature, the implementation of beam theory in roll-to-plate imprinting proved to be an important conceptual step. Although not perfect, the beam model helps to explain the behaviour and deformation patterns first observed in chapter 3. Therefore, the coming chapters will use the theoretical descriptions from chapter 4 and 5 to analyse the effect of parameters in the models of this thesis. Chapter 7 will perform a parameters study for a four roller system, and chapter 8 will combine the conclusions from various chapters to propose design considerations and suggestions when handling web materials.





# Parameter study

From previous chapters, the quasi-static and dynamic analysis of a web modelled as a beam has been performed. In both the quasi-static and dynamic model the influential parameters have been identified, however the relative importance of the parameters with respect to each other is unknown. This chapter will perform a parameter study to compare the sensitivity of the system to a given parameter, in order to assess the critical aspects in a web span from a theoretical point of view. To compare the sensitivity of various parameters, a logarithmic sensitivity is applied, which scales the sensitivity down to a dimensionless number and enables a direct comparison between variables. In addition, a larger range of values is analysed for critical parameters, as the results of the analysis is found to be very dependent on the chosen values in the design space.

To perform the sensitivity analysis, a four roller system is assumed similar to the topology of the NIL1100 by Morphotonics, as will be presented in section 7.2. All web spans are assumed to have equal lengths. The sensitivity analysis uses the deformation in the imprint, as presented in section 5.4, to find the maximum deformation in both x- and y-direction. These maximum values will be the objective of the sensitivity analysis.

## 7.1. Logarithmic sensitivities

A sensitivity analysis relates the response of a system's objective  $f$  to its system parameters  $\mathbf{q}$ . The design variables in our case are the web properties, dimensions and initial boundary conditions of a modelled system of rollers. A logarithmic sensitivity analysis is a method to convert the sensitivity of each design variable into a comparable dimensionless number. This allows for a quantitative comparison of a multivariable system analysis. For the application of this thesis, the objective is the maximum error in both the x- and y-direction. The logarithmic sensitivity is defined as follows:

$$\frac{d_L f}{d_L q} = \frac{d(\log f)}{d(\log q)} = \frac{\frac{1}{f} df}{\frac{1}{q} dq} = \frac{q}{f} \frac{df}{dq} \quad (7.1)$$

As said, the logarithmic sensitivity allows for relative comparison between design variables as the value is dimensionless. In addition, the relative sensitivity of a parameter to other design variables can be compared as follows:

- > 1; influential parameter
- << 1; less relevant parameter

The derivative  $\frac{df}{dq}$  can be derived using a finite difference method. Common types are first-order forward and backward finite differences. For this thesis, the central difference method is applied:

$$f'_{central}(x) = \frac{f(x+h) - f(x-h)}{2h} + O(h^3)$$

## 7.2. Model parameters

The sensitivity analysis requires a model as input, which should be representable for the system at hand. Therefore, a four roller system is modelled of equal lengths. In figure 7.1, the four roller system is visualized with the labelled rollers and indication of web transport direction. In the NIL concept of Morphotonics the web makes contact with the substrate in between roller 3 and 4. In this model, the resist is assumed to be cured at half the segment length in between roller 3 and 4.

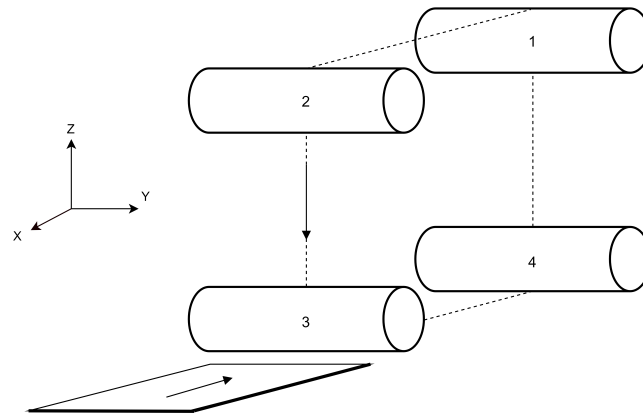


Figure 7.1: A schematic representation of the system modelled in the sensitivity analysis.

For the system, two types of model parameters can be identified:

<b>Input conditions</b>	The input conditions are parameters which introduce an imperfection to the web. To model the response of a web system, an assumption for web imperfections is required. The response of the sensitivity analysis will be dependent on the introduced input conditions and the result can differ based on the assumed conditions. In this case, the considered input conditions are initial lateral displacement of the web on a roller contact and the relative in-plane alignment between rollers: $[\gamma_{01}, \gamma_{02}, \gamma_{03}, \gamma_{04}, \gamma_{01}, \gamma_{02}, \gamma_{03}, \gamma_{04}]$ .
<b>Design parameters</b>	Given a set of input conditions, the response of the system is dependent on material and geometrical parameters: $[E, v, T, h, w, L]$ . The design parameters are aspects of the system which can be tuned to reduce the error response for a given deformation. For the sensitivity analysis the relative importance of the design parameters will be critical.

The selection for input conditions is critical for the response of a system, and the choice for specific input conditions will affect the outcome of the sensitivity analysis. So, to make an educated estimate of the most important parameters, a study to the effect of input parameters is performed. Having defined the most critical input parameters, a model can be made to observe the sensitive at a given disturbance. So first, a logarithmic sensitivity analysis is applied to the input conditions of the system. In this analysis, the initial input conditions are set to zero, to model the sensitivity of the individual parameters. The result is visualized in the bar plot in figure 7.2. In addition to the logarithmic sensitivities, the objective function of each input condition was observed over a large range for each input condition to relate the local sensitivity to the global behaviour of the parameter. This result is given in appendix section D.1. The conclusion is in practice rather simple, the input condition of each roller is equivalently important. This idea is supported by the error progression model in chapter 5, in which the error progression over a series is presented.

Therefore, in the coming section the effect of a lateral displacement and angular misalignment of a single web span on the full system will be modelled. The two parameters  $(y_i, \gamma_i)$  will be introduced individually and the effect of design parameters on each of the two disturbances will be discussed.

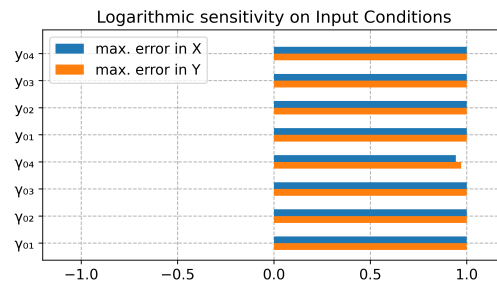


Figure 7.2: The sensitivity of each input condition to a four roller system. The results show similar results for all the input conditions, emphasizing the effect of error propagation in a multi-span system. Each disturbance has a direct effect on the downstream deformations.

## 7.3. Results

In the coming two examples, the sensitivity of design parameters to lateral displacement and angular misalignment is quantified. For both examples, additional material is presented in the appendix D, such as a convergence study to the step size applied in the logarithmic sensitivity.

The results are presented in a bar plot, visualizing the logarithmic sensitivity of the design parameters as a result of a disturbance. In the figures a positive sensitivity value, means that an increase of the design parameter results in an increase of error. From the sensitivity analysis the critical parameters can be obtained, with a distinction between errors in the imprint (X) and transverse (Y) direction. From the positive or negative sensitivity and value, the parameters effect on overlay can be found, which is important in the design of a system.

### 7.3.1. Sensitivity analysis on angular misalignment

The sensitivity of the design parameters, in response to an angular disturbance, is given in figure 7.3. As observed in the previous section, the disturbance parameter  $\gamma_{03}$  is critical for the overlay and has a large value. From the design parameters, the web properties are found to have limited to no effect on overlay. However, the geometrical parameters for length and width have a larger impact on overlay. Especially the web length has a critical aspect in the lateral error, as the web will be able to make a larger lateral displacement for an increased web length.

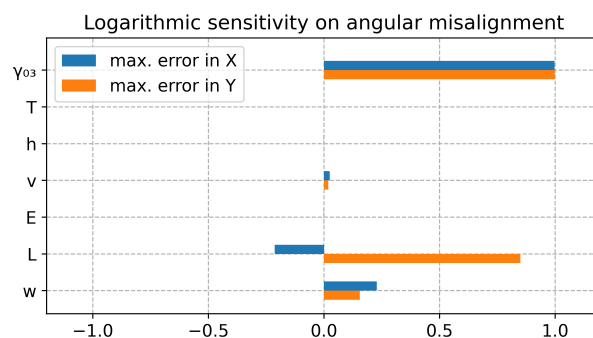
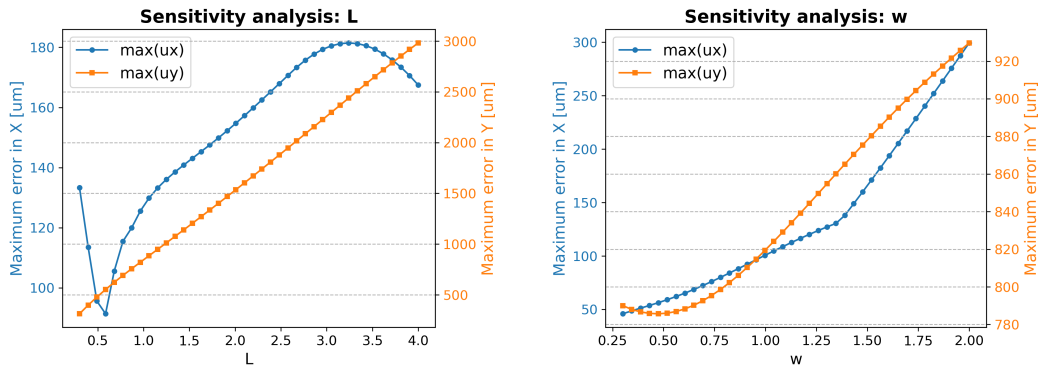


Figure 7.3: The sensitivity of a four roller system exposed to an angular misalignment:  $\gamma_{03}$ . The system parameters are:  $h = 86[\mu m]$ ,  $w = 1.313[m]$ ,  $L = 1.016[m]$ ,  $E = 3.8[GPa]$ ,  $\nu = 0.3[-]$ ,  $T = 175[N/m]$ .

When observing a larger range for both  $L$  and  $W$ , it can be concluded that the web length is critical for the transverse error of a web due to the lateral motion of a web over a roller. For the imprint direction the web length the results are less clear, however a clear relation for the mid-range values is found. For incredibly short web spans, the numerical results are doubtful, which is understandable for a length width ratio of less than  $\frac{1}{2}$ . The width of the web is also critical for the overlay inaccuracies, which complies with modelling results obtained in this thesis. Additional plots and results are presented in the appendix D section D.2.1, such as a parameter sweep for each individual parameter over a larger



(a) The relation between the error in each respective direction and the design parameter  $L$ . (b) The relation between the error in each respective direction and the design parameter  $W$ .

Figure 7.4: A study to the impact of the web length and width, exceeding the parameter set considered in figure 7.3.

range.

### 7.3.2. Sensitivity analysis on lateral displacement

Similar to the angular misalignment, the effect of a lateral displacement of the web can be modelled. In figure 7.3, the sensitivity with of the system is illustrated in a bar plot. From the results a large sensitivity to the web length is found, whilst no other system parameter apparently has a significant influence on overlay on first glimpse.

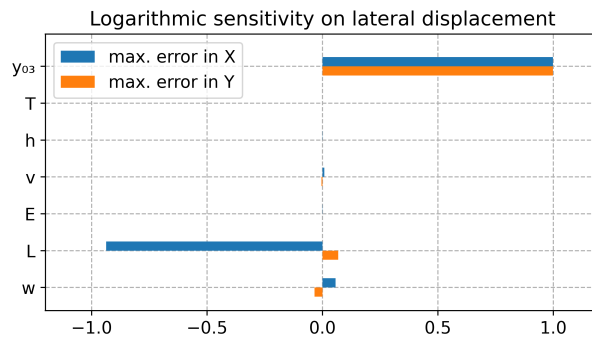
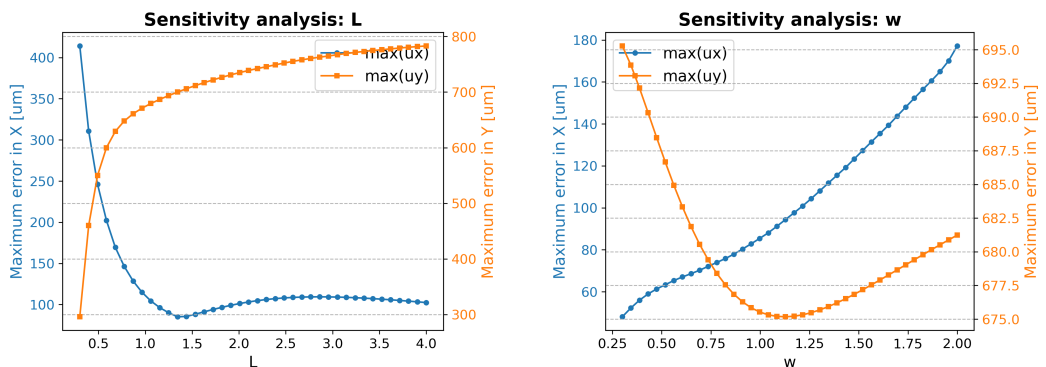


Figure 7.5: The sensitivity of a four roller system exposed to an initial lateral displacement at roller 3:  $y_{03}$ . The system parameters are:  $h = 86[\mu m]$ ,  $w = 1.313[m]$ ,  $L = 1.016[m]$ ,  $E = 3.8[GPa]$ ,  $v = 0.3[-]$ ,  $T = 175[N/m]$ .



(a) The relation between the error in each respective direction and the design parameter  $L$ . (b) The relation between the error in each respective direction and the design parameter  $W$ .

Figure 7.6: A study to the impact of the web length and width, exceeding the parameter set considered in figure 7.5.

When observing the system parameters over a larger range of values, a better understanding is gained. For the web length, it is clear that a short web span results in large errors in the imprint direction, whilst the error in the transverse direction flattens out. The length width ratio, appears to play a significant role in the internal strain developed in the web.

## 7.4. Conclusions to parameter study

This chapter has presented the most relevant results from a parameter study to parameters in a dynamic web system. An emphasis on the geometrical parameters was found, which meant that the material properties were found to be less influential for overlay. Still, the visualization of results for all parameters is given in appendix D. From this short analysis, several conclusions can be drawn.

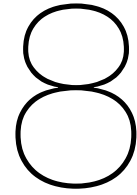
First, in section 7.2 the two types of system parameters were given: input conditions and design parameters. The input conditions cover imperfections introduced to the web. Figure 7.2, illustrated the importance of each variable considered in the four roller system. This observation complies with the expected behaviour of error progression over a series of rollers, in which upstream disturbances result in a downstream imperfection. When considering a four roller system, in which the deformations of the final web segment are observed for overlay, the upstream components are found to be equivalently critical as the alignment in the web segment itself. The complexity of the system has therefore increased significantly, compared to a concept with less components.

Moreover, the results from section 7.3 show a large sensitivity for geometrical parameters such as web length and width, whilst material properties of the web seem to have no significant impact on overlay. This result is understandable, as the beam model applied in this thesis uses geometrical boundary constraints on both web ends. Therefore, the in-plane stiffness of the web will increase the internal stress of the web, but does not affect the resulting strain profile.

Still, the behaviour of the web length and width is not trivial. As the lateral position of the web on a roller is time-dependent, the system parameters affect both the lateral position and the deformation of the web. This results in the contradicting behaviour, of a longer span having less internal deformation whilst having a larger lateral displacement when exposed to a disturbance. However, a larger length width ratio is still preferred as the lateral position of the web on the roller can be repeatable.







# Suggestions and design considerations

So far, beam theory has been applied to model the behaviour of a thin elastic material in a roll-to-plate imprint process. By modelling a web span as a beam, a theoretical understanding of web deformation was formulated. The deformation patterns observed in measurements are expected to originate from the deformation of the elastic mould, which has partly been verified in chapter 6. The beam model applied to a web span gave insight in the relevant parameters for deformation in a web span with the appropriate boundary conditions. It is believed that a correct handling of the elastic mould in roll-to-plate imprinting will improve the overlay accuracy. Therefore, this chapter will use the model, measurements and parameter study of chapter 7, to propose design considerations for future concepts.

## 8.1. Critical degrees of freedom

Chapter 5 focussed on the progression of disturbances over a multi-span system, from which could be concluded that deformations in a single span are dependent on upstream imperfections. Therefore, the complexity of a system scales with the number of consecutive web spans. In other words, the number of degrees of freedom considered in a system. To elaborate this train of thought, the critical degrees of freedom for a web span will be identified and analysed for the concept of Morphotonics.

A web segment is defined by the web constrained between two consecutive rollers, with on each roller two boundary constraints  $[y_i, \phi_i]$  and relative dimensions between the rollers  $[L_i, \gamma_i]$ . Each roller can be considered as a three-dimensional body with 6 degrees of freedom, namely three translations and three rotations. Inherently, a single rotation of the roller is unconstrained as it is allowed free rotation around its axle, referred to as  $R_y$ .

In case of a single web span, the position of the web is defined by the four boundary conditions at the roller contact points. The lateral position  $y_0$  and  $y_L$  at the up- and downstream roller are undetermined in a dynamic system, as the lateral position shifts as a result of disturbances in the web handling. The angular alignment  $\gamma_i$  represents the parallelism of the two roller axes. This relative alignment between

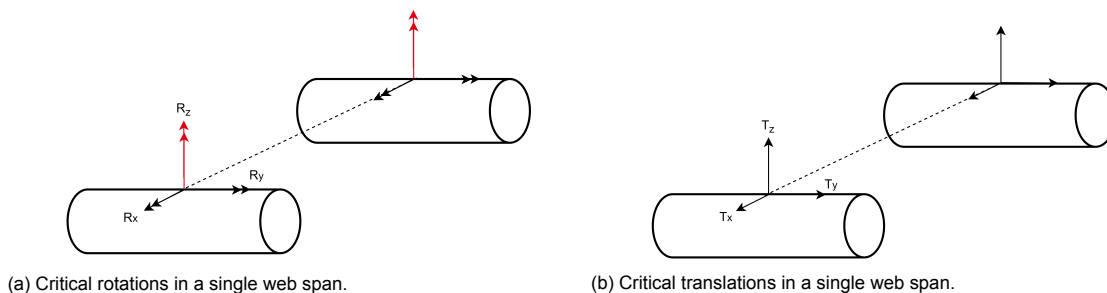


Figure 8.1: Identifying the degrees of freedom of a single web span.

the up- and downstream roller require accurate positioning of both components, resulting in two critical degrees of freedom. The critical rotations  $R_z$  have been visualized in figure 8.1a, in which the rotational vector is perpendicular to the web plane and highlighted in red.

The body frames of the two rollers in figure 8.1a are chosen with  $R_z$  perpendicular to the web plane, which is convenient for a single span system. However, when considering a multi-span system, the roller functions as the interface between the entering and exiting web span. Figure 8.2 has visualized a roller, including the normal vectors for both the entry and exit web-span. The wrap-angle is the angle between the web entry and exit, which in theory can have any arbitrary value. Each web span has a critical alignment, which can be expressed as a normal vector  $n_i$  in the body frame of the roller  $B$  as a function of the rotational vectors  $R_x$  and  $R_z$ . Depending on the wrap angle, the rotational vectors would be more or less critical. If the wrap-angle is  $90^\circ$ , the angular alignment of both  $R_x$  and  $R_z$  would be equivalently critical, whilst for a  $180^\circ$  angle only a single rotation would be critical.

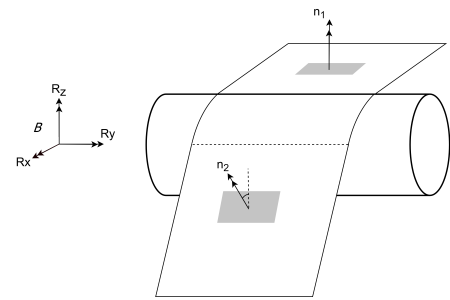


Figure 8.2: A roller having a non-perpendicular wrap angle. The normal vectors to the entry and exit span are given by  $n_1$  and  $n_2$ .

### 8.1.1. Degrees of freedom in Morphotonics' concept

In the case of Morphotonics, multiple contact points can be considered, of which four at the rollers and two at the clamped web ends. The web segments are placed perpendicular to each other in series, meaning that two rotational degrees of freedom of a roller are perpendicular to a tangent web span, and both rotations are equally critical. As a result, the complexity of the system alignment quickly increases.

In addition to the rotations, the translations of the system can also be considered. In the concept of Morphotonics the web has a finite length and is constrained at its end points. As a result, the lateral position of the end points will act as a possible disturbance input from which errors can arise. The lateral positions at the contact points with a roller still remain undetermined due to the dynamic web transport. Therefore, system consist of two critical translations, located at each web end. The remaining translations are undetermined due to lateral web dynamics. The critical rotations and translations for the concept by Morphotonics are visualized in figure 8.3. The deduced critical degrees of freedom from

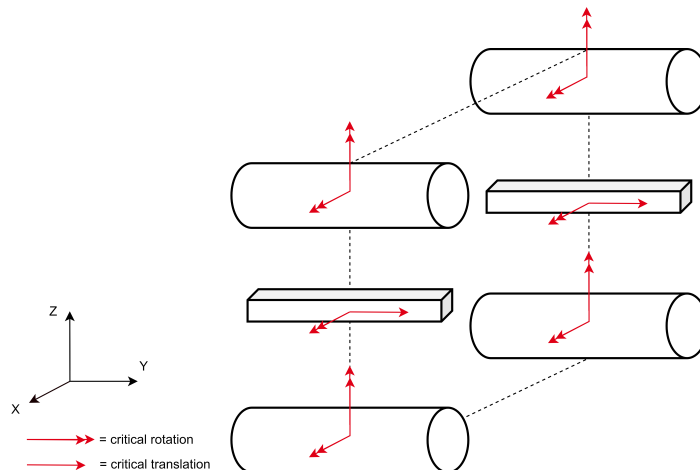


Figure 8.3: The critical rotations of the six contact points in the NIL1100 by Morphotonics. The perpendicular topology of the rollers make the angular alignment of 2 rotations per roller critical.

figure 8.3 indicate the complexity of the system and the elements in the system which require a defined level of alignment. The system has been analysed by defining the number of contact points and the critical degrees of freedom are identified. The resulting properties have been summarized in table 8.1.

Properties:	#
Contact points	6
Degrees of freedom	36
Critical rotation	10
Critical translations	2

Table 8.1: The deduced properties for system of rollers visualized in figure 8.3.

### 8.1.2. Tolerances on alignment

The methodology of this section identifies critical DOF's, which would require alignment in order to prevent disturbances from entering a system. Results from chapter 5 and the verification experiments from chapter 6, showed the progression of errors from upstream rollers and how it can affect overlay in NIL. The train of thought of this section, can be used to identify critical DOF's to re-design a machine topology to reduce the complexity of the critical degrees of freedom. Simplifying a system by eliminating critical DOF's would reduce the requirements on alignment of upstream rollers.

When simplification of a system is not optional, the alignment of the critical DOF's will determine system performance. The experimental results, used as verification, suggested that a  $1.22[mrad]$  misalignment would result in a maximum lateral displacement of  $2.3[mm]$  with additional deformation of the nano-pattern. The results have emphasized the importance of roller alignment in order to prevent deformation of the elastic mould and distortions in the nano-pattern. Such properties are especially relevant when considering accuracy, instead of repeatability. When assuming that R2P NIL should compete with alternative imprint techniques, which perform in the (sub-) micron range, the requirements on roller alignment will be more challenging. Considering the results of this thesis, tolerances of micron-radians would be suggested for future systems in order to obtain micro-meter overlay accuracy.

## 8.2. Web dimensions

The results presented in this thesis are based on the machine topology of Morphotonics, in which extremely short web spans are applied on a system of four rollers. The beam theory applied to the web spans, as shown in chapter 4, considers deformation due to bending or shearing of the web. Shear deformation is considered relevant for length width ratio's  $< 2\frac{1}{2}$ , which is definitely the case in system of Morphotonics. Both angular components will deform relatively easily for short spans. Therefore, a larger length width ratio would be better from a conceptual perspective, in order to achieve a better overlay performance. The results are supported by the parameter study from chapter 7. However, in the parameter study, to maximum absolute error was considered, in which larger web lengths also resulted in larger lateral displacement when exposed to roller misalignment. However, the in-plane deformation of the web, would be reduced.



# 9

## Discussion of the results

To summarize, this thesis focussed on large-scale overlay in roll-to-plate nanoimprint lithography. An experimental study was performed to quantify the overlay performance on the NIL1100 imprint module available at Morphotonics. Based on preliminary test results, an understanding of positioning and deformations in R2P imprinting was developed, resulting in a focus on the deformation patterns observed in experiments. This led to a literature study to the dynamics of web materials over a series of rollers, in which beam theory was applied to quantify web deformation. The theory has been applied to models, as described by chapters 4 and 5, and the relation between web dynamics and overlay was roughly verified in chapter 6. Afterwards, the application of web dynamics is used to perform a parameter study to relevant parameters and propose suggestions for future concepts. Even though the relation between web dynamics and overlay was observed in experiments, the interpretation of the data and the conclusions drawn from the results in this thesis should be critically reviewed.

### 9.1. Discussion

First, the measurement performed in a preliminary phase of the project, proved to be extremely valuable as new insights in the effect of overlay are obtained due to the observed deformations patterns. However, to draw clear conclusions, the data required additional post-process steps, which were susceptible to measurement errors, variations in measurements and defects in the measured samples. The post-process steps removed part of the information in order to decouple the error components or sources, which was good for insight in the problem but also required a different definition for overlay. Therefore, the metrology applied in this thesis differs from the methods applied in the semi-conductor industry, where a Gaussian distribution is common practice. Therefore, the methods for R2P overlay should be revised in order to relate better to the metrology applied in the overlay industry.

In addition, in the interpretation of results only relative comparisons between imprints were made, as the original objects was unknown. This limited the results to repeatability, rather than absolute deformations in the imprint.

Furthermore, a relation between deformations in the experimental results from chapter 3 and the literature, led to an approximation of web deformations using a beam model. The model described the planar deformation of a web, as well as a lateral displacement of the web when exposed to misalignment in the rollers. The relation between the lateral web dynamics, derived from beam theory, was verified in an experiment in chapter 6. The lateral displacement over the series of imprints was a clear result of the angular disturbance applied to the web system. Similarly, the observed deformation pattern showed consistency and repeatability over multiple imprints. However, the measurements could not easily be related to deformations found in the models. Partly, due to the complexity of the imprint process, in which multiple aspects affecting overlay are not yet well understood. Also, the mapping of absolute deformation to relative deformation between two imprints proved difficult. The disturbances in the NIL module operated as a black box, in which the existing misalignment or defects were unknown, let alone the variations in system parameters. Therefore, the implementation of beam theory is valu-

able to gain insight in the behaviour of a web in a dynamic system, but has also been challenging to relate to observations of this thesis.

Possibly, the models would be easier to relate to experimental results when using a comparison of the imprints to an absolute reference of the original object, instead of relative to each other. Practically, this was not yet possible within the current state of Morphotonics. As the original object replicated by the imprint process is not exactly known, it proved difficult to quantify all errors present in the imprint process. Still, the observed deformation patterns from experiments and the model showed similar vector fields, even though it was not possible to relate the errors to exact system parameters. Ideally, a known reference object was used to compare the imprints too, which would be the elastic mould itself. Unfortunately, the elastic mould can not be measured in a condition which represents the mould geometry during the imprint process.

In spite of the sidenotes in the experimental results, the implementation of beam theory to describe overlay errors is roughly verified. The use of a beam model gave insight in the behaviour of deformations within a web span, the dynamic behaviour on the interface with a roller, and the progression of errors/disturbances in a system of multiple rollers.

From the theoretical understanding, chapter 7 and 8 emphasized the relevant parameters affecting overlay accuracy. It could be concluded that overlay is determined by the geometrical parameters of the web span, rather than material properties, in combination with the disturbances applied to the system. So, based on the theory of lateral web dynamics, material properties would be less critical to deformations. Of course, modelling a beam with geometrical boundary conditions inherently implies the importance of geometrical parameters, but from a theoretical perspective it appears to be grounded. Still, the material properties can play an important role when considering alternative distortions, such as the response to thermal variations or in-plane bending due to additional loads non-related to web dynamics. It is important not to exclude additional error sources, as it has not been verified that the lateral web dynamics is the only imperfections present in R2P NIL.

Looking back on the results obtained from the experiments and models in this thesis, the implementation of web dynamics in roll-to-plate imprinting proved insightful. Using the concepts applied in web dynamics, the elastic mould could be approximated with a beam model in both quasi-static and dynamic conditions. Especially, the progression of web deformations or errors over multiple rollers was unexpected, but verified in experiments. This result emphasized the importance of web handling, as a disturbance far away from the point of observation (imprint) resulted in a significant error.

# 10

## Conclusions

In this thesis, a study to large scale overlay has been performed using a roll-to-plate nanoimprint lithography fabrication process. The thesis consists of two distinctive parts, namely the general experimental study to overlay performance using the facilities of Morphotonics, and the detailed study to errors in large-scale overlay resulting from improper handling of the elastic mould. In this chapter, the main conclusions of this thesis are presented.

First, the main objective of this thesis was to characterize the overlay accuracy in roll-to-plate nanoimprint lithography, in collaboration with Morphotonics. At the start of the project the understanding of overlay in the facilities of Morphotonics was limited. With the experimental results presented in chapter 3, a new insight in large-scale overlay was obtained from the deformation patterns observed in the experiments. The system was analysed for a range of potential causes, and the results obtained in measurements were used to prioritize relevant error components. The test results provided the understanding needed to improve overlay accuracy within the concept of Morphotonics. With the results obtained from the preliminary measurements, the first objective was achieved. However, as discussed in chapter 9, the measurements only quantified relative errors in the imprint process, rather than an absolute deformation with respect to a universal reference object. Therefore, the measurement methods applied in the experiments masked repeatable errors in the imprint process, which could be significant in magnitude. Currently, such an absolute reference object is not yet known, but would be valuable as a standard to compare multiple imprints over a larger range of imprint conditions.

The second objective of this thesis, was stated after the preliminary study to the various error components in R2P overlay. The objective for the remainder of this thesis was to relate the higher-order deformation pattern found in the residual error to a specific error cause. The vector field visualizing the residual error in a two-dimensional field, showed strong underlying relation in both direction and magnitude of the vector components. Based on literature, the pattern was related to mechanical deformation in the elastic mould (stamp), which could be explained by the concepts applied in the field of web dynamics. Implementing the knowledge from web dynamics made it possible to model the deformation of the elastic mould over time and identify the relevant machine parameters which affect the elastic mould. The relation between web dynamics and overlay was verified in chapter 6, and proved the relevance of web dynamics in the use of the elastic mould. Introducing web dynamics into roll-to-plate imprinting proved to be a significant step, as many defects in webs are related to the dynamic descriptions applied in this thesis.

The chapters 7 and 8, used the definitions from lateral web dynamics and numerical results to identify the critical aspects of machine design which affect the overlay accuracy. This resulted in a focus on the geometrical parameters of the system, namely the boundary conditions applied at the roller interfaces and the dimensions of the web. The alignment of rollers proved critical for both the lateral positioning of the web on the rollers, as well as the deformations which are introduced in the web span. The dimensions of the web proved critical in the response to the boundary conditions applied, which are geometrical conditions. Therefore, the material properties of the web itself seemed irrel-

evant. This conclusion could be argued, as applying geometrical boundaries will inherently result in a focus on geometrical parameters as opposed to load induced boundary conditions. However, the boundary conditions applied in literature have been reviewed extensively and multiple sources have found agreement on the use of the boundary conditions as presented in this thesis, and are therefore assumed to be correct.

Even though the content of this thesis proved well applicable to the dynamics of the web and progression of disturbances over multiple rollers, the theory is not satisfying enough to quantify the behaviour of the web in contact with the substrate. This part of the web handling is not fully covered within the scope of this project and requires additional research. Still, this theory gave insight in the relevant aspects which will need to be addressed, as will be presented in chapter 11.

In addition, the results obtained to verify the validity of this research proved a relation between the residual errors in overlay and misalignment in the system. However, this does not mean that the deformation patterns observed in experiments are limited to the errors resulting from roller misalignment. Rather, the quasi-static beam model showed how the web deformation is dependent on the boundary conditions at the roller interfaces. Clearly, roller misalignment is one of the causes for overlay inaccuracies. However, other aspects of the system could also affect the boundary conditions in a similar manner, resulting in a comparable deformation pattern.

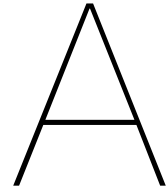
Overall, the results of this thesis have been delivered new insights in the behaviour of large-scale overlay in roll-to-plate NIL. The overlay performance of Morphotonics has been characterized, from which points of improvement have been derived for the future generation of R2P imprint machines. The theory applied in this thesis proved relevant and insightful to relate observations to system parameters. In addition, so the implementation of beam theory was valuable in order to quantify deformation, whilst improvement to the modelling accuracy could result in a better analysis of the overlay inaccuracies. The methods by which the beam model can be improved will be presented in chapter 11.



11

## Recommendations





# Measurement of overlay

To analyse the overlay accuracy in roll-to-plate nano-imprint lithography a measurement had to be defined to measure the positioning of nano-textures on a substrate. Such a tool was not yet available at Morphotonics, so an alternative solution was found in which an existing XYZ gantry stage was used to actuate a high resolution camera over a large area.

This chapter will focus on the methods and results obtained from the measurements. The measurements which will be discussed have been gathered over the course of several months, in which the understanding of the overlay inaccuracies became more detailed. Each measurement consists of a batch of samples (imprints), which have been produced / measured within the same time-slot. First, a relative comparison within a single batch will be relevant to address the possible inaccuracies present during production. Next, selective comparisons between batches will introduce a new perspective to the definition of overlay. The effect of machine parameters will be addressed, and variations in parameters will be researched. Finally, a test will be discussed in which the models and theory of this thesis will be validated.

## A.1. Test description

The tests discussed in this chapter consist of measurements performed on the end-product of the nano-imprint lithography production process. First, a batch of samples would be produced on the machines available at Morphotonics, after which the batch of imprints would be measured using a high-resolution camera and a XYZ gantry stage. The steps performed in the production process and the methods applied to perform the measurement using the camera are explained in detail in the section A.4. Having completed the measurement on the distinctive features of all substrates, the sets of coordinates can be post-processed to identify various error components or to define the overlay accuracy. The methods used in the post-processing steps will be presented in section A.4 of the appendix.

The final product of the imprint process is used to draw conclusions on the overlay accuracy. However, no additional measurements during the imprint process can be used to relate the inaccuracies to machine parameters or hardware, which is troublesome. still, the relative comparison of the final products include all the possible error sources and give a detailed insight in the most dominant error components contributing to overlay.

## A.2. Test objectives

As said, the test presented in this chapter have been gathered over the course of several months. Initially, the measurement was used to make a first estimate of overlay in the current imprint process. However, over time the measurements became more insightful and the comparison of various test results gave additional understanding in the challenges of overlay accuracy.

As a result, the objectives of the various tests have shifted over time, as the understanding of the system

raised new questions which required research. To summarize the tests performed, the following test objectives can be identified:

1. Quantify the deformation of imprints in the imprint process
2. Isolate error components to identify error sources
3. Compare various production processes of imprints:
  - (a) Compare the repeatability of imprints under similar conditions
  - (b) Compare imprint parameters
  - (c) Compare the imprint accuracy from various machines
  - (d) Compare the performance of different stamp materials

From the tests various unique properties or system characteristics can be identified, which is common in fields that apply overlay such as the semi-conductor industry. The system characteristics refer to the definition of accuracy and precision introduced in section 2.1, which distinguish systematic and random errors. These errors can be quantified by relative comparisons between tests, such as systematic errors between machines (machine-to-machine) or random errors within a single machine.

To define the systematic or random errors within a test batch or test comparison, specific error components will be identified during the post-process step. The translation and rotational error between imprints will be removed to reduce a repeatability error of the imprint module (NIL1100). In addition, the residual error can be further reduced by extracting linear scaling or shear components. The remaining error refers to higher-order deformation, which is summarized by an average error or standard deviation.

### A.3. Overview of performed tests

In table A.1 the tests used in this thesis are presented. Three distinctive tests have been performed in which the imprints have been produced in measure within the same batch, thus under similar conditions. Each test introduces a variation, which allows for a quantitative comparison of samples and measure the effect on the overlay accuracy. The most notable difference in test conditions is the use of two machines to produce the same end-product and the use of a different stamp material.

By comparing test 1 and 2 the effect of a different stamp material can be analysed and compared to numerical analysis of the stamp behaviour, seen in chapter 5. The comparison between machines gives insight in the machine-to-machine repeatability of the system. The relative error between samples of two different machines amplifies systematic errors, which would otherwise not be visible in a measurement.

Test	Machine	Stamp	Objective	ID	Substrate	Pressure
<b>1</b>	Machine A	Standard stamp design	Nominal comparison	1	3mm	medium
			Nominal comparison	2	3mm	medium
			Pressure comparison	3	3mm	high
			Pressure comparison	4	3mm	low
<b>2</b>	Machine A	Enhanced stamp design	Nominal comparison	1	3mm	medium
			Nominal comparison	2	3mm	medium
			Nominal comparison	3	3mm	medium
			Nominal comparison	4	3mm	medium
			Pressure comparison	5	3mm	low
			Pressure comparison	6	3mm	high
<b>3</b>	Machine B	Standard stamp design	Nominal comparison	1	3mm	medium
			Nominal comparison	2	3mm	medium
			Pressure comparison	3	3mm	high
			Pressure comparison	4	3mm	low

Table A.1: A summary of the various tests which will be used for analysis in this thesis. Each of the three tests was designed to compare various system properties, such as machine specific deformation or process parameters.

Aside from the tests under similar conditions (1-3), test 4 focuses on the effect of roller alignment within

a single machine. An intended misalignment of one of the components is used to validate models developed in chapter 5.

## A.4. Test setup and methods

### A.4.1. Test equipment

The following equipment was used to complete the test:

- PC with Ethernet port
- Portis NIL1100: an imprint module for R2P imprint lithography designed by Morphotonics.
- Portis Coater1100: a machine of Morphotonics with an accurate XYZ-stage and a build in camera
- Software to read out the marker positions. In this case custom scripts were used:
  - PyCharm 2020.1.3
  - Python 3.7 (open-source)
  - Open-CV for python (open-source)
- Gen5 substrates of 3mm
- Camera setup:
  - Camera 2448x2048 pixels and  $1.7\mu\text{m}$  resolution
  - Telecentric lens
  - Ethernet cable
  - PLC interface with Coater1100
  - Coaxial LED spot
- Matlab 2020a

### A.4.2. XYZ stage

The positioning stage of the Portis Coater1100 by Morphotonics was used to perform the measurements on marker recognition. The Coater1100 is equipped with a XYZ linear stage and a high resolution camera equipped on the end-effector. By positioning the camera on the desired marker locations, the coordinates of the gantry and image of the marker could be used to derive the exact marker positions. The XYZ stage has proven to be very repeatable, having a repeatability of  $5[\mu\text{m}]$  in the X-direction and  $10[\mu\text{m}]$  in the Y-direction. The high repeatability makes the measurement very suitable for relative comparison between imprints, rather than an absolute measurement of the marker positions.



Figure A.1: A photo of the Coater1100, used to perform overlay measurements on Gen5 substrates.

The Coater1100 has a gantry using a series configuration, meaning that the Y-axis is build on top of the X-axis and the Z-axis on top of both X- and Y-axis. Therefore, a lower stiffness of the Y-axis was visible during the measurement, as well as a possible curvature of the linear stage. These errors reduce the accuracy of the system in the Y-axis by  $10 - 30[\mu\text{m}]$ . However, as said before, the repeatability allows for relative comparison in which case these effects can be mitigated.

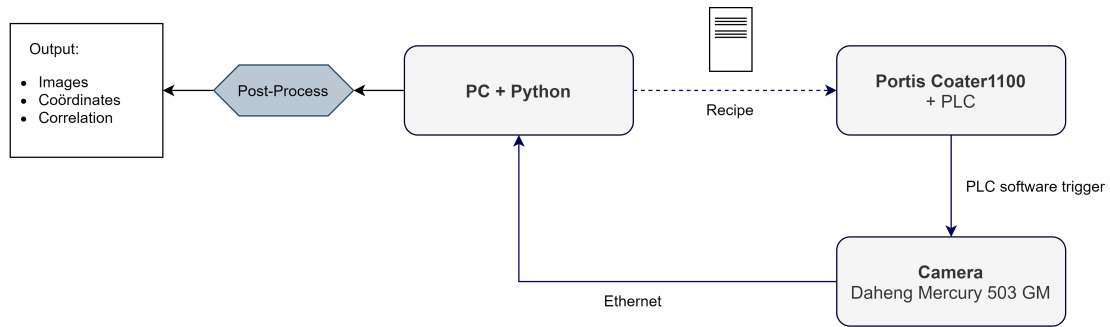


Figure A.2: Schematic overview of the components in the test setup. A PC with Python installed writes a recipe for the XYZ gantry stage of the Coater. The Coater actuates the stage and uses a software trigger to actuate the camera. The resulting images are used in a post-process step in python to retrieve the relevant data, given as output of the measurement.

### A.4.3. Image processing

Using image recognition from OpenCV the marker coordinates are obtained from a first image. The location of the marker in the image and the coordinates of the coater are combined to define the accurate positioning of the marker in a two-dimensional field. The iteration of marker positions from a first measurement, to an accurate positioning is illustrated below.

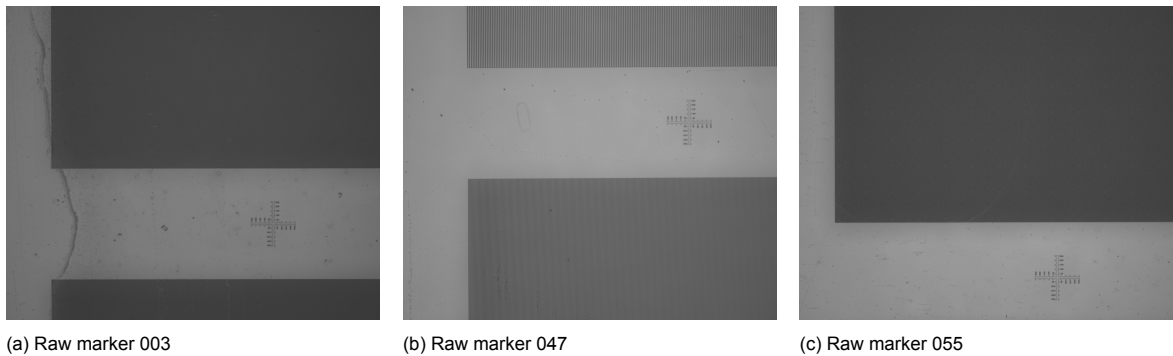


Figure A.3: Examples of measured markers in a first iteration.

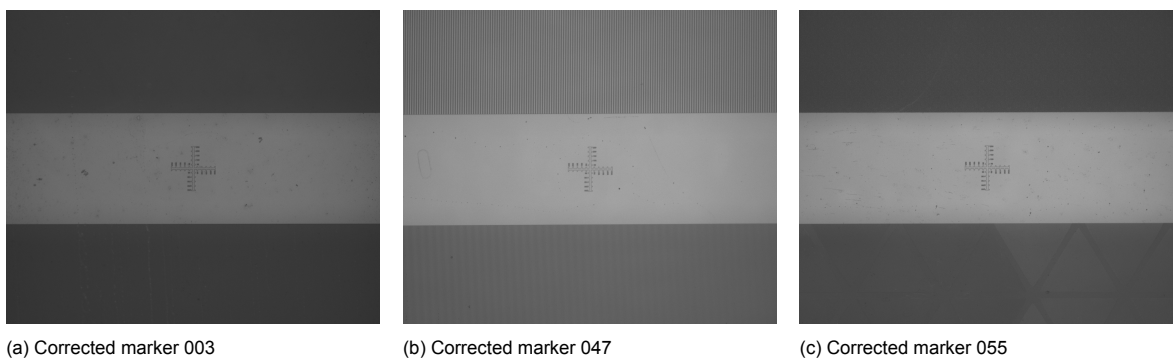


Figure A.4: Examples of improved marker positions after an iteration cycle.

### A.4.4. Software

The marker position is extracted by matching a template to the image. The pixel with the highest correlation is assumed to be the correct marker position in the image. The marker position follows from the pixel coordinates, multiplied with a fixed constant for pixel size. The image is 2448x2048 pixels, meaning that a marker at the edge of the image has a larger error compared to a marker close to the origin of the image. This error results from the error in the pixel constant. To compensate this error in the algorithm, each marker position is measured once in a raw measurement. After which the coordinates

are iterated in a post-process step. The following three measurements will have the markers accurately at the centre of the image, by which the error due to a pixel constant is mitigated. An example of the raw marker position and the iterated marker position is given in figures A.3 and A.4.

The custom software used was written in Python 3.7. The software uses packages which were distributed with the camera, to actuate and read-out the data from the camera. Additional packages were used from OpenCV to apply image recognition. A template matching algorithm was used, in which a given template would be fitted on each pixel of the image. The highest correlating pixel would be used as reference for the marker position. The software would take a batch of images and process the entire batch, to then give the correlation value, marker position and logbook of the applied methods as output.

#### A.4.5. Image processing

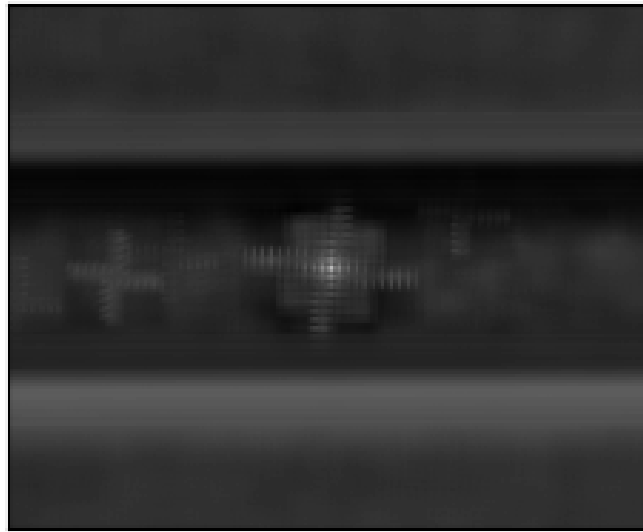


Figure A.5: Example of the correlation per pixel, with white indicating a high correlation.

Evaluating the determined marker position for multiple imprints indicates the repeatability of the measurement. The normalized correlation value, given between 0 and 1, can be used to determine the fit of the template. A low fit, means the marker template can not be fit well onto the image, due to distortions, damage or deformation to the marker. Additionally, the correlation value for the entire image can be plotted for each pixel, which indicates how unique the marker position is. Ideally, the template find a single match. However, if the algorithm finds multiple correlating values it can be concluded that the method is not robust.

### A.5. Analysis of Overlay

From each measurement a data-set of marker coordinates is obtained. To translate the coordinates into a definition for overlay, additional post-process steps are required. In this section, the various methods to quantify overlay and isolation of overlay components will be introduced. The methods discussed have been used in a post-process tool such as Matlab or Python to interpret the results.

#### A.5.1. Rigid alignment

The most basic definition of overlay is a rigid transformation which aligns two sets of corresponding points in a 2D field. This requires a translation and rotation which minimizes the error between the two sets of points. In doing so, the set retains its shape as the relative distance between points is not affected.

The method to find the optimal fit between two sets of coordinates is commonly described by a least-square rigid motion using SVD [39]. The method considers two data sets  $\mathcal{P} = \{\mathbf{p}_1, \mathbf{p}_2, \dots, \mathbf{p}_n\}$  and  $\mathcal{Q} = \{\mathbf{q}_1, \mathbf{q}_2, \dots, \mathbf{q}_n\}$  in  $\mathbb{R}^d$ . The goal is to find a rigid transformation using a rotation  $R$  and translation  $\mathbf{t}$ ,

such that:

$$(R, \mathbf{t}) = \underset{R \in SO(d), \mathbf{t} \in \mathbb{R}^d}{\operatorname{argmin}} \sum_{i=1}^n \|(R\mathbf{p}_i + \mathbf{t}) - \mathbf{q}_i\|^2 \quad (\text{A.1})$$

Without including the steps and reasoning, the steps to find the rotation  $R$  and translation  $\mathbf{t}$  are:

1. Compute the centroids of both sets of points:

$$\bar{\mathbf{p}} = \frac{\sum_{i=1}^n \mathbf{p}_i}{\sum_{i=1}^n 1}, \quad \bar{\mathbf{q}} = \frac{\sum_{i=1}^n \mathbf{q}_i}{\sum_{i=1}^n 1} \quad (\text{A.2})$$

2. Computed the centred vectors:

$$\mathbf{x}_i := \mathbf{p}_i - \bar{\mathbf{p}}, \quad \mathbf{y}_i := \mathbf{q}_i - \bar{\mathbf{q}}, \quad i = 1, 2, \dots, n \quad (\text{A.3})$$

3. Compute the  $d \times d$  covariance matrix:

$$S = XY^T, \quad (\text{A.4})$$

where  $X$  and  $Y$  are the  $d \times n$  matrices which have  $\mathbf{x}_i$  and  $\mathbf{y}_i$  as their columns.

4. Compute the singular value decomposition  $S = U \Sigma V^T$ . The SVD is a accessible as a function in most programming languages such as MATLAB or python. The rotation becomes:

$$R = V \begin{pmatrix} 1 & & & & \\ & 1 & & & \\ & & \ddots & & \\ & & & 1 & \\ & & & & \det(VU^T) \end{pmatrix} U^T \quad (\text{A.5})$$

5. Compute the optimal translation:

$$\mathbf{t} = \bar{\mathbf{q}} - R\bar{\mathbf{p}} \quad (\text{A.6})$$

For the application of this thesis, a 3-dimensional matrix will result from this method for both rotation and translation. To compute the rigid transformation of one set of points to another, a set of linear transformations is used. The residual error  $\mathbf{e}_i$  after applying the rigid transformation can be obtained by subtracting the transformed set of coordinates from the original set:

$$\mathbf{q}'_i := R\mathbf{p}_i + \mathbf{t}, \quad \mathbf{e}_i := \mathbf{q}'_i - \mathbf{p}_i, \quad i = 1, 2, \dots, n \quad (\text{A.7})$$

The rigid alignment method discussed uses an algebraic notation. The same method can also be written in a matrix notation, as the method is still a linear computation.

$$\mathbf{q}'_i := RT\mathbf{p}_i \quad (\text{A.8})$$

$$\mathbf{q}'_i := \begin{bmatrix} \cos(\theta) & -\sin(\theta) & 0 \\ \sin(\theta) & \cos(\theta) & 0 \\ 0 & 0 & 1 \end{bmatrix} \begin{bmatrix} 1 & 0 & t_x \\ 0 & 1 & t_y \\ 0 & 0 & 1 \end{bmatrix} \mathbf{p}_i \quad (\text{A.9})$$

## A.5.2. Affine transformations

To add to the rigid alignment from the previous subsection, higher order deformations can be included as well. Affine transformations include all linear transformations, such as translation, rotation, shear and scaling. Previously, we have seen the matrices for rotation and translation and their derivations. A similar approach can be taken towards additional linear transformation. In the table A.2 the transformation matrix for various linear cases are shown and the respective deformation which results from such a transformation.



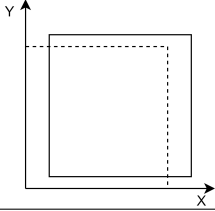
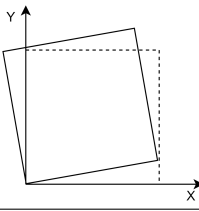
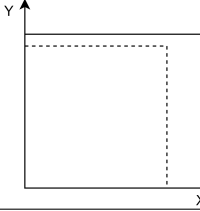
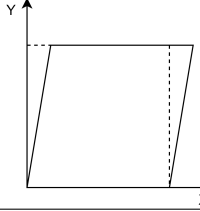
Translation	Rotation	Scaling	Shear
$\begin{bmatrix} 1 & 0 & t_x \\ 0 & 1 & t_y \\ 0 & 0 & 1 \end{bmatrix}$	$\begin{bmatrix} \cos(\theta) & -\sin(\theta) & 0 \\ \sin(\theta) & \cos(\theta) & 0 \\ 0 & 0 & 1 \end{bmatrix}$	$\begin{bmatrix} s_x & 0 & 0 \\ 0 & s_y & 0 \\ 0 & 0 & 1 \end{bmatrix}$	$\begin{bmatrix} 1 & c_x & 0 \\ c_y & 1 & 0 \\ 0 & 0 & 1 \end{bmatrix}$
			

Table A.2: Transformation matrices for linear transformations in a 2 dimensional plane.

Including additional transformations increases the complexity of finding the optimal fit. Luckily, most software packages, such as MATLAB and python, have build in functions which make the computations more accessible. In the case of MATLAB, the function `fitgeotrans()` offers various transformations such as linear transformations and even 3<sup>rd</sup> or 4<sup>th</sup> order polynomials.

Using affine transformations, linear deformations in imprints can be filtered from the data, by isolating linear error components such as thermal expansion or tension variations. From the fitted transformations components, a cause for the error can be deduced, which helps in analysing the test results. Additionally, the residual error after applying a transformation will lower, and the higher-order terms will become more visible.

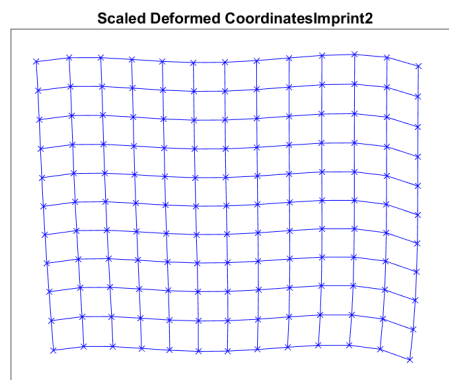
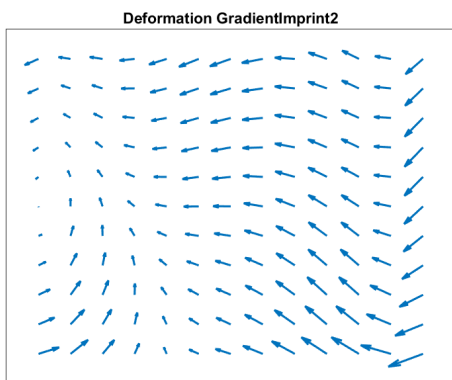
### A.5.3. Polynomial transformations

For higher-order transformations, a polynomial fit can be applied. This affects the transformation applied to a set of points, as matrix multiplication will not be suitable for non-linear computations. Rather, a polynomial can be used such as equation A.10.

The polynomial equation is an addition to the transformation so far, as the coefficients ( $C_1, C_2, C_3$ ) can be related back to the affine transformations. The polynomial adds 2<sup>nd</sup> and higher order terms, up to the desired order to give a desired fit. For the application of this thesis, a 3<sup>rd</sup> order polynomial is sufficiently accurate to quantify a large portion of the residual errors.

$$U(X, Y) = C_1 + C_2X + C_3Y + C_4XY + C_5X^2 + C_6Y^2 + C_7X^2Y + C_8XY^2 + C_9X^3 + C_{10}Y^3 \dots \quad (A.10)$$

$$V(X, Y) = C_1 + C_2X + C_3Y + C_4XY + C_5X^2 + C_6Y^2 + C_7X^2Y + C_8XY^2 + C_9X^3 + C_{10}Y^3 \dots \quad (A.11)$$



(a) Example of 3<sup>rd</sup>-order polynomial deformation gradient.

(b) Example of 3<sup>rd</sup>-order polynomial deformation

## A.6. Test results

From the tests proposed in table A.1 different conclusions can be drawn. First, imprints within a single test are assumed to be produced under similar conditions and can easily be compared relative to each other. Ideally, the imprints are compared to a known object such as the reference geometry from which the imprints have been duplicated. However, this is not possible for this application, as the production process of the stamp also introduces errors which would be more dominant compared to the errors of the imprint process itself. Therefore, the most logical method is to compare the imprints relative to each other also referred to as inter-imprint overlay. This has been performed for each of the tests and the results can be found in table A.3.

In the coming sections, several results will be presented to summarize the observations of the performed tests:

- First, a relative comparison of imprints within a single test. All imprints will be compared to the first imprint of the batch, as an example. The comparison includes imprint produced under similar and varying imprint conditions, such as a variation in imprint pressure or a variation in machine and stamp design.
- Second, a selective comparison will be made for the imprints of different stamp designs. Samples have been produced under similar conditions, using a different stamp materials. The comparison gives insight in the behaviour of the stamp.
- Next, a selective comparison will be made for imprint from two different machines. The same stamp has been used under similar imprint conditions on both machines, which has also been presented in chapter 3.
- Finally, a selective comparison is made for imprint under various imprint conditions. For all tests the same variation in imprint pressure has been applied, which enables a comparison of low and high pressure for each machine and stamp design.

### A.6.1. Inter-Imprint comparison

From each test the imprints can be compared to each other to quantify the random deformation in the imprint process. To do so, the rigid alignment is subtracted from the data sets and the residual error is quantified by the average, maximum and minimum residual error. A summary of the test results is presented in table A.3. The accompanying visualizations are presented below.

Test	ID	Absolute residual error						Transformation		
		Average		Max		Min		Translation		Rotation
		X [ $\mu m$ ]	Y [ $\mu m$ ]	X [ $\mu m$ ]	Y [ $\mu m$ ]	X [ $\mu m$ ]	Y [ $\mu m$ ]	X [ $\mu m$ ]	Y [ $\mu m$ ]	Z [ $\mu rad$ ]
<b>1</b>	1	8.1	9.6	35.8	21.8	-15.1	-17.8	-53.9	-328.0	385.8
	2	0.0	0.0	0.0	0.0	0.0	0.0	0.0	0.0	0.0
	3	11.1	9.4	32.0	18.5	-25.3	-22.0	25.9	-416.9	-112.8
<b>2</b>	4	11.0	16.4	49.4	43.9	-28.6	-25.3	120.9	-706.9	684.9
	5	25.5	13.1	80.3	55.0	-92.2	-25.5	159.8	-809.9	789.7
	6	34.3	12.2	76.5	42.5	-107.9	-24.9	-481.4	-450.5	272.6
<b>3</b>	7	29.7	20.6	98.1	79.0	-145.8	-59.8	226.9	-1513.9	475.0
	8	38.7	27.3	115.1	47.2	-162.8	-71.3	196.2	-1999.5	626.8
	9	34.4	26.3	99.1	38.0	-161.1	-69.4	54.6	-2319.1	1006.8

Table A.3: An overview of the tests performed in this thesis. All samples have been compared to the first imprint of each test, using a rigid alignment fit. The residual error after fitting is presented, as well as the transformation applied in the fit.

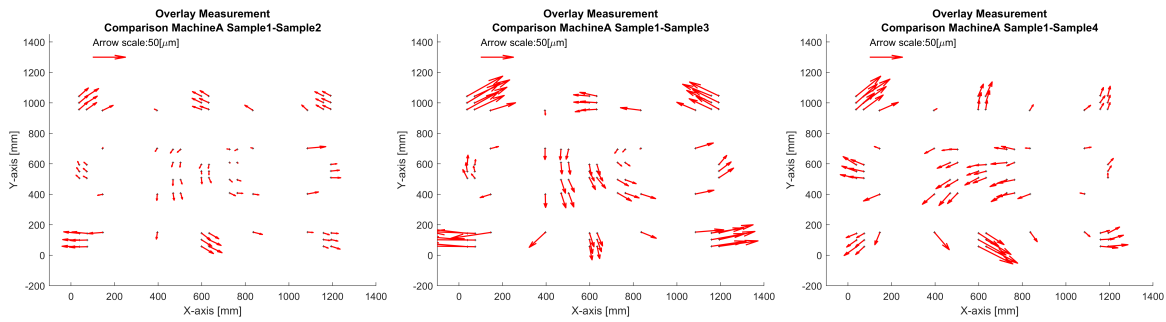


Figure A.7: A relative comparison for the samples produced for Test 1. All samples have been compared to sample1 and are produced on Machine A using the standard stamp design of Morphotonics.

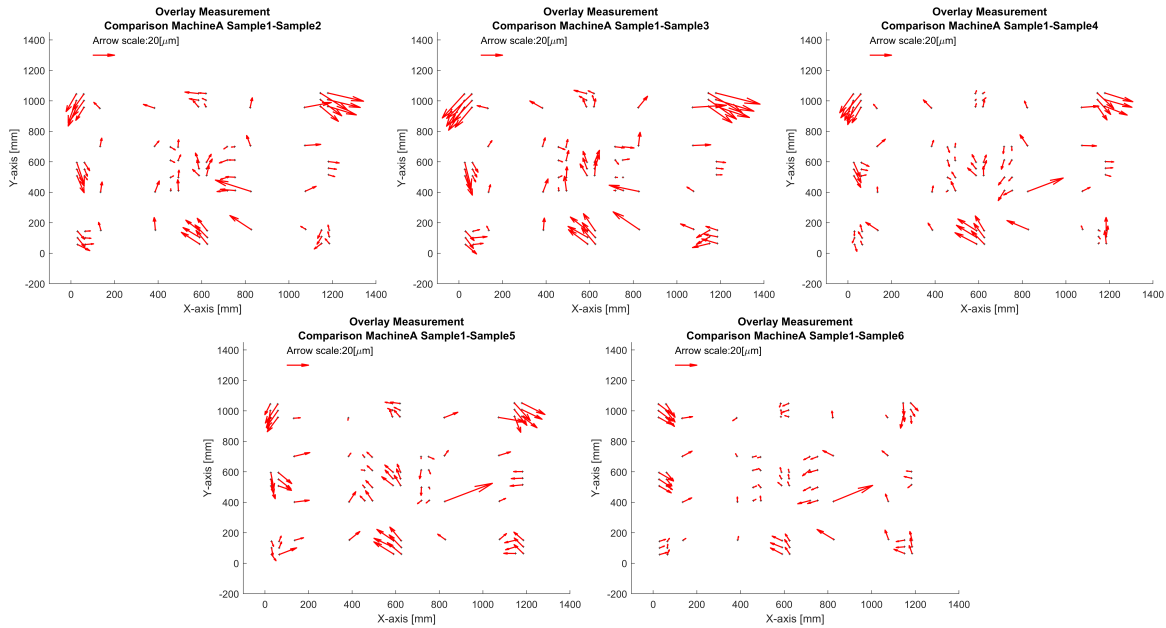


Figure A.8: A relative comparison for the samples produced for Test 1. All samples have been compared to sample1 and are produced on Machine A using the enhanced stamp design of Morphotonics.

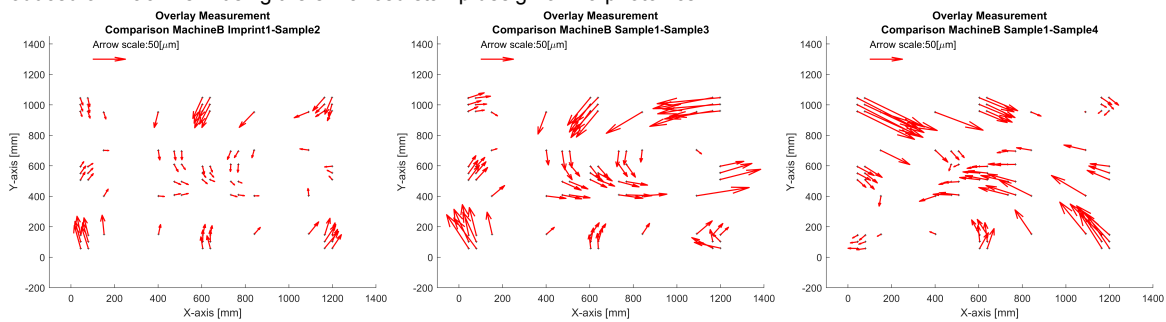


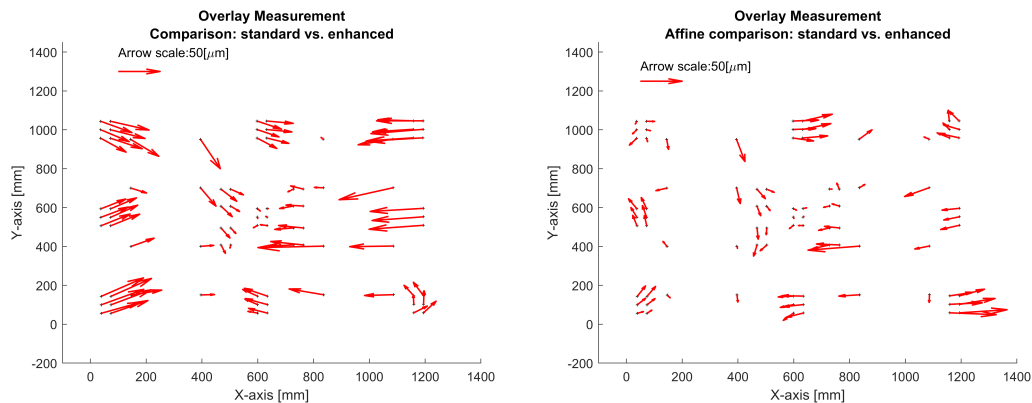
Figure A.9: A relative comparison for the samples produced for Test 1. All samples have been compared to sample1 and are produced on Machine A using the enhanced stamp design of Morphotonics.

### A.6.2. Stamp material comparison

Two of the tests are performed on the same machine and imprint conditions, but with a different stamp material. One stamp is the most commonly stamp design used by Morphotonics, the other stamp is an enhancement to the original stamp design with higher in-plane stiffness. The enhanced stamp, compared to the standard design, has a factor 6 higher tensile stiffness  $\frac{EA}{L}$  and a higher in-plane bending stiffness  $EI$  of a factor 8.

According to the literature on web dynamics, discussed in chapter 4, the in-plane stiffness is not directly related to the deformation as the boundary conditions are geometrical constraints and not load constraints. Therefore, it is assumed that the effect of a different stamp stiffness is not visible for the deformation we are researching. However, the higher stiffness is relevant for additional loads which are not included in the theory for web dynamics. Similarly, other error sources such as thermal expansion will behave differently for other material properties. For the interpretation of the results, such considerations will be critical to deduce the correct conclusions from these test results.

The measurements are compared by a linear fit, including translation and rotation, and an affine fit with an additional scaling and shearing component. The linear fit is visualized in figure A.10a, in which a clear uniform strain in the X and Y direction can be identified. Therefore, the affine transformation given in figure A.10b will be more appropriate.



(a) The residual error after rigid alignment fitting of the averaged standard and enhanced stamp imprints. (b) The residual error after affine fitting of the averaged standard and enhanced stamp imprints.

Figure A.10: Comparison of two test results using different stamp materials.

The linear strain in X and Y can be a result of temperature differences or tension differences in the stamp during production or the measurement. From the affine transformation the strain components can be identified, which are given in table A.4. From the relation between strain in X and Y the error can not directly be related to pure mechanical deformation or homogeneous expansion, but more likely a combination of both.

After applying the affine transformation the residual error is rather close to the residual errors found within the same batch of imprints. The translations and rotation are much larger as the imprints have been produced with a different initial position.

	Transformation					Absolute residual error			
	Translation	Translation	Rotation	Scaling	Scaling	Average error		Maximum error	
	X	Y	Z	X	Y	X	Y	X	Y
	[ $\mu m$ ]	[ $\mu m$ ]	[ $\mu rad$ ]	ppm	ppm	[ $\mu m$ ]	[ $\mu m$ ]	[ $\mu m$ ]	[ $\mu m$ ]
Rigid alignment	-3835.4	-692.2	-4182.3	-	-	28.6	12.0	78.5	50.4
Affine alignment	-3876.1	-726.5	-4180.5	71.5	31.6	14.1	8.8	61.6	38.0

Table A.4: The transformation components applied in the comparison between imprint from a standard or enhanced stamp design, and the residual error after the transformation.

### A.6.3. Machine comparison

The systematic error in a machine can be deduced by comparing imprints from two different machines. This has been performed by comparing imprints from the same stamp and same imprint conditions,

produced by two machines. Similar to the stamp comparison, the imprints can be analysed using a rigid alignment and affine transformation. The residual error has been visualized in figure A.11.

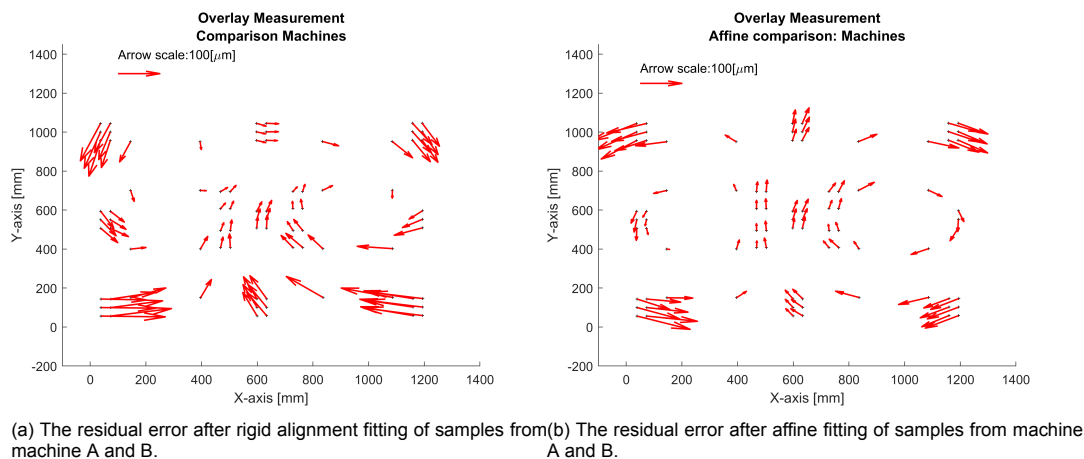


Figure A.11: Comparison of result obtained from two different machines, using the same imprint process and elastic mould.

From the figures a clear pattern can be seen, which resembles a curvature of the imprint pattern. Table A.5 proves that the error is not a linear scaling in the X or Y-direction, as seen in the previous example. Rather, the deformation is largely determined by higher-order components. The result complies well with deformations seen in the dynamic modelling of web's in chapter 5, as over the entire imprint direction (X-axis) a uniform rotation over the width of the imprint is visible.

The residual error has a maximum of 100–150[ $\mu m$ ], is a factor 3 larger compared to the residual errors found within a single batch. This means that the systematic error within a single machine is significant, and the introduction of the error is repeatable.

	Transformation					Absolute residual error			
	Translation X	Translation Y	Rotation Z	Scaling X	Scaling Y	Average error		Maximum error	
	[ $\mu m$ ]	[ $\mu m$ ]	[ $\mu rad$ ]	[ppm]	[ppm]	X [ $\mu m$ ]	Y [ $\mu m$ ]	X [ $\mu m$ ]	Y [ $\mu m$ ]
Rigid alignment	-5354.8	-1304.2	-48.8	-	-	44.0	41.5	153.7	127.6
Affine alignment	-5382.7	-1352.4	-72.0	77.5	112.1	36.6	32.0	126.9	63.2

Table A.5: The transformation components applied in the comparison between two machines, and the residual error after the transformation.

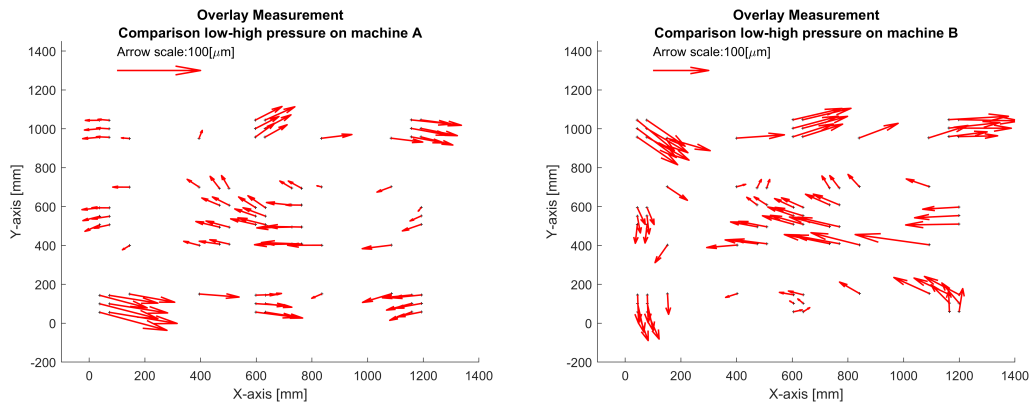
#### A.6.4. Imprint pressure

Chapter 4 and 5 model a web as a beam by applying boundary conditions to the web at the contact points with a roller. Literature describing the behaviour of such a web in dynamic conditions, assumes no additional loads are applied to the web as the web is considered to be a 'free-span'. Applying this assumption to an imprint system of rollers, this would be valid up to the point where the stamp and substrate make contact. Therefore, applying the theory from the field of web guiding directly on an imprint application is not without risks. The initial contact points of the stamp and substrate is referred to as NIP and the pressure created in the NIP applies additional loads to the web, which are not taken into account yet.

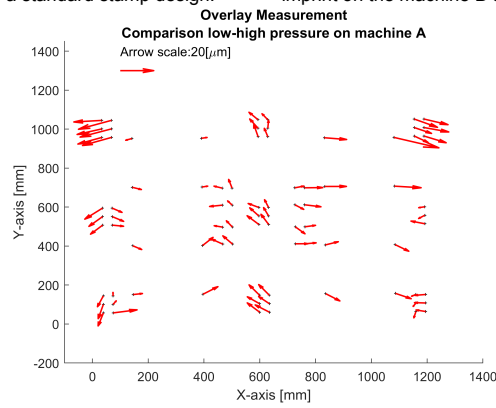
Neglecting the free-span assumption is a possible point of failure for the models discussed in this thesis. The contact mechanics in the NIP is an interesting research topic in itself, which is definitely a relevant topic for future research. However, a more direct method is to set up a measurement to quantify the effect of the NIP and the loads induced at this contact point. The simplest method is to introduce various imprint loads, which has been performed for each of three tests presented in table A.1.

In each of the three tests, a lower and higher pressure is used compared to the nominal imprint conditions. The overlay inaccuracies due to a pressure difference is amplified the most by directly comparing an samples under low and high pressure. These results have been plotted in figure A.12. From the figures the significance of imprint pressure on the overlay accuracy can be determined, with errors

exceeding  $200[\mu\text{m}]$  for figure A.12b.



(a) The deformation between a low pressure and high pressure imprint on the machine A using a standard stamp design. (b) The deformation between a low pressure and high pressure imprint on the machine B using a standard stamp design.



(e) The deformation between a low pressure and high pressure imprint on machine A using an enhanced stamp design.

Figure A.12: Comparison of samples produced under various imprint pressures. Each test has produced additional imprints to quantify the effect of imprint pressure.

# B

## Derivations in beam theory

### B.1. Coefficients derived for the static web shape

$$C1 = \frac{KLa\phi_0 e^{KL} + KLa\phi_0 + Kay_0 e^{KL} + Kay_0 - Kay_L e^{KL} - Kay_L - \phi_0 e^{KL} + \phi_0 + \phi_L e^{KL} - \phi_L}{Ka (KLa e^{KL} + KLa - 2e^{KL} + 2)} \quad (B.1)$$

$$C2 = - \frac{\left( KLa\phi_0 e^{2KL} + KLa\phi_0 - 2KLa\phi_L e^{KL} + Kay_0 e^{2KL} - 2Kay_0 e^{KL} + Kay_0 - Kay_L e^{2KL} + 2Kay_L e^{KL} - Kay_L - \phi_0 e^{2KL} + \phi_0 + \phi_L e^{2KL} - \phi_L \right)}{Ka (e^{KL} - 1) (KLa e^{KL} + KLa - 2e^{KL} + 2)} \quad (B.2)$$

$$C3 = - \frac{Kay_0 e^{KL} + Kay_0 - Kay_L e^{KL} - Kay_L + \phi_0 e^{KL} - \phi_0 + \phi_L e^{KL} - \phi_L}{KLa e^{KL} + KLa - 2e^{KL} + 2} \quad (B.3)$$

$$C4 = \frac{\left( K^2 La^2 y_0 e^{2KL} - K^2 La^2 y_0 + KLa\phi_0 e^{2KL} + KLa\phi_0 - 2KLa\phi_L e^{KL} - Kay_0 e^{2KL} + 2Kay_0 e^{KL} - Kay_0 - Kay_L e^{2KL} + 2Kay_L e^{KL} - Kay_L - \phi_0 e^{2KL} + \phi_0 + \phi_L e^{2KL} - \phi_L \right)}{Ka (e^{KL} - 1) (KLa e^{KL} + KLa - 2e^{KL} + 2)} \quad (B.4)$$

### B.2. Derivation of boundary conditions

From Hamilton's principle, two governing equations for a web can be derived:

$$\left( \frac{AG}{n} + T \right) y'' - \frac{AG}{n} \phi' = 0 \quad (B.5)$$

$$EI\phi'' + \frac{AG}{n} (y' - \phi) = 0 \quad (B.6)$$

These equations can be further reduced to a single equation with one dependent variable, resulting in an equation also introduced by Shelton. Shelton's approach was based on beam theory and a derivation of the steady-state mechanical analysis. Both methods resulted in the following fourth order differential equation:

$$\frac{d^4 y}{dx^4} - K^2 \frac{d^2 y}{dx^2} = 0 \quad (B.7)$$

The parameter  $K$  is dependent on the web tension  $T$ , Young's modulus  $E$ , moment of inertia  $I$ , shear constant for a rectangular cross-section  $n = 1.2$ , cross-sectional area  $A$  and shear modulus  $G$ . The equation B.7 is a fourth order linear differential equation. The general solution to the differential equation is given by equation B.8:

$$y = C_1 \sinh(Kx) + C_2 \cosh(Kx) + C_3 x + C_4 \quad (B.8)$$

The coefficients of the static shape are dependent on the boundary conditions selected for the beam model. Shelton's work focused on the derivation of such boundary conditions for various roller systems. In this thesis, systems of roller guides are considered with a fixed alignment. In addition, the Timoshenko beam model is applied and the boundary conditions at both ends of the web span are related to the rotational and shear deformation occurring in such a beam. These boundary conditions will be defined in the following paragraphs.

### B.2.1. Boundary conditions

The coefficients to the static web shape B.8 follow from the static boundary conditions. The position  $y$  and slope of the web is assumed to be known, which result in four boundary conditions. Subscripts 0 and  $L$  refer to the ends of the web-span at the contact point of the upstream- and downstream-roller.

For a Timoshenko beam, the slope in the web is build up from the cross-sectional rotation and shear angle in the beam, as displayed in equation 4.1. In a multi-span system, the slope of the web varies over the length of the web and is unique in each web segment. A roller forms the interface of two consecutive web segments, and thus the boundary conditions meet. The shear forces sustained in a web span is constant and supported by the friction of the roller-web contact area. The shear angle is therefore discontinuous at the roller, meaning that the slope of the web differs at the entry and exit of the roller. However, the cross-sectional rotation  $\phi_i$  is preserved, making it a logical choice for the boundary condition at the web ends.

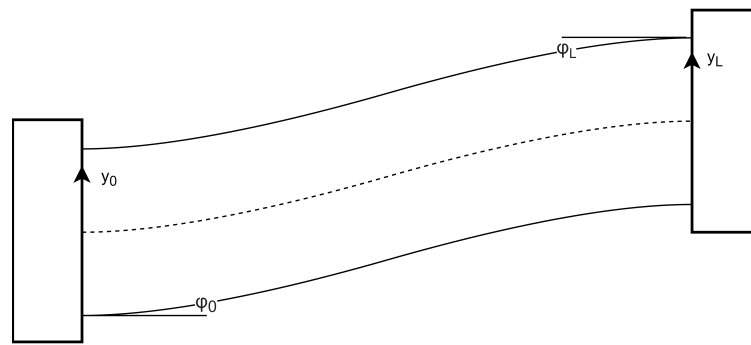


Figure B.1: The four boundary conditions applied on a web span, as a result of contact with the rollers. At the upstream roller the cross-sectional rotation and lateral position from the previous web span gives  $\phi_0$  and  $y_0$ . The conditions at the upstream roller and the misalignment of the downstream roller  $\gamma$ , results in  $y_L$  and  $\phi_L$ .

With the cross-sectional rotation at the upstream roller  $\phi_0$  and downstream roller  $\phi_L$ , the resulting boundary conditions for a Timoshenko beam are:

$$\begin{aligned} y|_{x=0} &= y_0 & y|_{x=L} &= y_L \\ \phi|_{x=0} &= \phi_0 & \phi|_{x=L} &= \phi_L \end{aligned} \quad (\text{B.9})$$

To define the boundary conditions, a description of the shear angle and cross-sectional rotation is required, in order to quantify the slope at each end. A unique description for  $\phi$  and  $\psi$  can be derived from equation B.5. Differentiation with respect to  $x$  results in:

$$\phi'' = y''' a \quad (\text{B.10})$$

Where:

$$a = 1 + \frac{nT}{AG} \quad (\text{B.11})$$

By substituting equation 4.1 as  $\psi = y' - \phi$  a definition for both the cross-sectional rotation and shear



angle is derived as follows:

$$\psi = -E I a \frac{n}{A G} y''' \quad (\text{B.12})$$

$$\phi = y' + E I a \frac{n}{A G} y''' \quad (\text{B.13})$$

$$y|_{x=0} = y_0 \quad \frac{dy}{dx}|_{x=0} + E I a \frac{n}{A G} \frac{d^3 y}{dx^3}|_{x=0} = \phi_0 \quad y|_{x=L} = y_L \quad \frac{dy}{dx}|_{x=L} + E I a \frac{n}{A G} \frac{d^3 y}{dx^3}|_{x=L} = \phi_L \quad (\text{B.14})$$

These unique expressions can be used to describe the boundary conditions of the Timoshenko beam, as well as for the strain relations which will be introduced in section 4.5.

To describe  $\phi_0$  and  $\phi_L$  the first and third order derivative of  $y$  are required. Equation B.8 can be differentiated in order to obtain  $\frac{dy}{dx}$  and  $\frac{d^3 y}{dx^3}$ .

$$\frac{dy}{dx} = C_3 + C_1 K \cosh(Kx) + C_2 K \sinh(Kx) \quad (\text{B.15})$$

$$\frac{d^3 y}{dx^3} = C_1 K^3 \cosh(Kx) + C_2 K^3 \sinh(Kx) \quad (\text{B.16})$$

Solving equations B.8 and B.15 at each end of a web span, so  $x = 0$  and  $x = L$ , results in the following four equations:

$$\begin{aligned} \phi_0 &= C_3 + C_1 K a \\ \phi_L &= C_3 + K a (C_1 \cosh(KL) + C_2 \sinh(KL)) \\ y_0 &= C_2 + C_4 \\ y_L &= C_1 \sinh(KL) + C_2 \cosh(KL) + C_3 L + C_4 \end{aligned} \quad (\text{B.17})$$

The equations given above, will be solved simultaneously in a system of equations to obtain the four coefficients:  $C_1$ ,  $C_2$ ,  $C_3$  and  $C_4$ . Notably, the coefficient are dependent on  $\phi_0$ ,  $\phi_L$ ,  $y_0$ ,  $y_L$ ,  $L$ ,  $a$  and  $K$ . With these coefficients, the static web shape from equation B.8 is fully defined. The coefficients are quite troublesome and long equations, therefore they are placed in the appendix in section B.1. Sievers decided to rewrite the static web shape  $y(x)$  to sort the terms by the input conditions  $[\phi_0, \phi_L, y_0, y_L]$ . Reorganizing the terms and using substitute functions  $g_i$  to describe the terms, results in the following description:

$$y(x) = y_0 + (y_0 - y_L) g_4(x, L) + \phi_L g_5(x, L) + \phi_0 g_6(x, L) \quad (\text{B.18})$$

where,

$$\begin{aligned} g_4(x) &= [\cosh(Kx) + \cosh(KL) - \cosh(KL - Kx) - Kax \sinh(KL) - 1]/R \\ g_5(x) &= [KLa(\cosh(Kx) - 1) - Kax(\cosh(KL) - 1) - \sinh(Kx) \\ &\quad - \sinh(KL - Kx) + \sinh(KL)]/KaR \\ g_6(x) &= [\sinh(Kx) - \sinh(KL) + \sinh(KL - Kx) \\ &\quad - KLa(\cosh(KL - Kx) - 1) + Ka(L - x)(\cosh(KL) - 1)]/KaR \end{aligned} \quad (\text{B.19})$$

and,

$$R = KLa \sinh(KL) - 2(\cosh(KL) - 1) \quad (\text{B.20})$$

### B.3. Deriving the lateral acceleration / Modified Sievers method

The lateral dynamic behaviour is driven by the geometry as the web enters the roller. At the entry of a span the behaviour is defined by the normal entry rule. At the exit of the span the conditions from the previous span are passed on to the next span. For the Timoshenko beam, the lateral position at each roller is required, as well as the cross-sectional rotation of the web. For an Euler-Bernoulli beam ( $a = 1$ ) the cross-sectional rotation is equivalent to the slope of the web. As the dynamic behaviour is determined by the contact points of the web and the roller, the conditions will be evaluated at  $x = 0$  and  $x = L$ . We will now determine the expression for  $\dot{y}_L$  and  $\phi_L$ . From equation 4.4 the following derivatives can be defined:

$$\frac{dy_L}{dx} = (y_0 - y_L) \frac{h_1}{L} + \phi_L h_2 + \phi_0 h_3 \quad (\text{B.21})$$

$$\frac{d^2 y_L}{dx^2} = (y_0 - y_L) \frac{g_1}{L^2} + \phi_L \frac{g_2}{L} + \phi_0 \frac{g_3}{L} \quad (\text{B.22})$$

In these equations the coefficients or shape functions are differentiated with respect to  $x$  and solved for  $x = L$ , which results in:

$$\begin{aligned} g_1 &= L^2 (g_4''(L)) = \frac{K^2 L^2 a (\cosh(KL) - 1)}{a[KLa \sinh(KL) - 2(\cosh(KL) - 1)]} \\ g_2 &= L (g_5''(L)) = \frac{KL(KLa \cosh(KL) - \sinh(KL))}{a[KLa \sinh(KL) - 2(\cosh(KL) - 1)]} \\ g_3 &= L (g_6''(L)) = \frac{KL(\sinh(KL) - KLa)}{a[KLa \sinh(KL) - 2(\cosh(KL) - 1)]} \\ h_1 &= L (g_4'(L)) = \frac{KLa \sinh(KL) - 2(\cosh(KL) - 1)}{KLa \sinh(KL)(1-a)} \\ h_2 &= g_5'(L) = \frac{(a+1)(1-\cosh(KL)) + KLa \sinh(KL)}{a[KLa \sinh(KL) - 2(\cosh(KL) - 1)]} \\ h_3 &= g_6'(L) = \frac{(a-1)(1-\cosh(KL))}{a[KLa \sinh(KL) - 2(\cosh(KL) - 1)]} \end{aligned} \quad (\text{B.23})$$

$$\phi_L = \frac{1}{h_2} \left( \frac{dy_L}{dx} - h_3 \phi_0 - \frac{h_1}{L} (y_0 - y_L) \right) \quad (\text{B.24})$$

$$\frac{d^2 y_L}{dx^2} = (y_0 - y_L) \frac{1}{L^2} \left( g_1 - \frac{g_2 h_1}{h_2} \right) + \frac{g_2}{h_2} \frac{1}{L} \left[ \frac{dy_L}{dx} \right] + \frac{\phi_0}{L} \left( g_3 - \frac{g_2 h_3}{h_2} \right) \quad (\text{B.25})$$

In itself, these spatial derivatives are useful and can be applied in a finite element analysis tool. However, we are looking for the time dependent O.D.E to define our numerical model. To do so, the spatial derivative needs to be transformed into a time dependent equivalent. Both Sievers and Shelton use the same method, although Shelton did this first in his first paper [37]. Shelton used a finite difference method to describe the velocity of two points along the transport direction and allow the spacing of these points to become infinitely small at  $x = L$ . Resulting in:

$$\frac{d^2 y_L}{dt^2} = v_0^2 \frac{d^2 y_L}{dx^2} \quad (\text{B.26})$$

With the derivation we performed so far the final time dependent expression is found. Sievers included the motion of the roller as well, in order to apply the theory discussed so far on steering guides. However, in this thesis no active steering guides will be used. This allows us to reduce the expression. In case the dynamics of the roller with respect to the world is also required, the theory can be expanded to include a steering action as well. Otherwise, we use the following time dependent O.D.E:

$$\frac{d^2 y_L}{dt^2} = (y_0 - y_L) \frac{v_0^2}{L^2} \left( g_1 - \frac{g_2 h_1}{h_2} \right) + \frac{g_2}{h_2} \left[ \frac{v_0}{L} \left( \frac{dz_L}{dt} - \frac{dy_L}{dt} \right) + \frac{v_0^2}{L} \gamma_L \right] + \frac{v_0^2 \phi_0}{L} \left( g_3 - \frac{g_2 h_3}{h_2} \right) + \frac{d^2 z_L}{dt^2} \quad (\text{B.27})$$

In the equation the dynamic behaviour of a web depends on the exit conditions of the web at the upstream roller  $\phi_0$  and  $y_0$ , the web velocity  $v_0$ , roller misalignment  $\gamma$  and the shape factors which are dependent on system parameters such as web tension  $T$ , web material properties and dimensions.

Previously, the Shelton and Sievers method were compared and the main difference in their description was the use of transfer functions or differential equations. In Sievers original equation, the roller actuation  $z$  was also taken into account. However, in the equation proposed in this thesis, the active control on a steering guide is not included. Therefore, the lateral dynamics is once more dependent on a single variable  $y$ . Thus, the equation above can be described as a transfer function.

### B.3.1. Additional derivations for strain

In previous research the definition of the lateral acceleration was the main focus. In this thesis, the beam theory applied in the derivations for the lateral acceleration are more important, as we would like to define the internal deformation in a web span. In this sub-section, the expressions for the moment and shear will be substantiated in order to set up the strain equations for a web span.

Earlier in section B.2 the cross-sectional rotation and shear angle were defined whilst solving the boundary conditions of a web. Both expressions are dependent on the first and third spatial derivative of the lateral position  $y$ , which was also derived and described by equations B.15. These components will be used to determine the bending and shearing which occurs in the web, which will result in the strain equations we are interested in. First the expression for both  $\phi$  and  $\psi$  will be defined, after which they will be used to define the strain equations of a web span. From the strain equations we will conclude that an additional derivation is required to express the curvature of the web  $\frac{d\phi(x)}{dx}$ .

Implementing the first and third derivative  $y'$  and  $y'''$  results into the bending angle  $\phi$  and shear angle  $\psi$  gives the following equations:

$$\begin{aligned}\psi(x) &= -EIa \frac{n}{AG} y''' \\ &= -EIa \frac{n}{AG} K^3 (C_1 \cosh(Kx) + C_2 \sinh(Kx)) \\ &= -\frac{nT}{AG} K (C_1 \cosh(Kx) + C_2 \sinh(Kx))\end{aligned}\quad (\text{B.28})$$

$$\begin{aligned}\phi(x) &= y' + EIa \frac{n}{AG} y''' \\ &= C_3 + (K + EIa \frac{n}{AG} K^3) C_1 \cosh(Kx) + (K + EIa \frac{n}{AG} K^3) C_2 \sinh(Kx) \\ &= C_3 + KaC_1 \cosh(Kx) + KaC_2 \sinh(Kx)\end{aligned}\quad (\text{B.29})$$

In addition to a unique expression for  $\phi(x)$  and  $\psi(x)$ , the spatial derivative  $\frac{\partial\phi}{\partial x}$  also appeared in the strain equations. This expression has not been derived yet, but can easily be formulated from previously introduced equations. In equation B.30 the resulting equation is given. Using equation 4.2 the expression can immediately be simplified by replacing the fourth order derivative to the second order derivative of  $y$ .

$$\frac{d\phi}{dx} = y'' + EIa \frac{n}{AG} y^{iv} \quad (\text{B.30})$$

$$\begin{aligned}\frac{d\phi}{dx} &= y'' + EIa \frac{n}{AG} K^2 y'' \\ &= \left(1 + EIa \frac{n}{AG} K^2\right) y'' \\ &= ay''\end{aligned}\quad (\text{B.31})$$

In this equations  $y''$  is an expression we have not yet used. However, earlier the first and third order derivative were derived from the static web shape in equation 4.4. A similar derivation gives us the

second order derivative:

$$\frac{d^2y(x)}{dx^2} = C_1K^2 \sinh(Kx) + C_2K^2 \cosh(Kx) \quad (\text{B.32})$$

Implementing  $y''$  into  $\frac{d\phi}{dx}$  gives us the desired equation required to complete the strain equations earlier. The physical meaning of  $\phi'(x)$  is the curvature of the web, which is related to the internal moment or bending of the web.

$$\begin{aligned} \frac{d\phi(x)}{dx} &= a \frac{d^2y}{dx^2} \\ &= C_1aK^2 \sinh(Kx) + C_2aK^2 \cosh(Kx) \end{aligned} \quad (\text{B.33})$$

In addition to the strain relations, the explicit expression for  $\phi$  and  $\psi$  can further develop the understanding of deformations in the web by finding an expression for the shear forces or moments in the web. For a Timoshenko beam the moment  $M$  and shear force  $N$  is defined according to equation B.34. In the shear force  $Q$  the constant  $\kappa$  is introduced, which compensates a non-uniformity of the shear force over the web width.  $\kappa$  is dependent on the web geometry and for a rectangular cross-section we can assume  $\kappa = \frac{5}{6}$ .

$$M(x) = -EI \frac{\partial \phi(x)}{\partial x} \quad (\text{B.34})$$

$$Q(x) = \kappa AG (-\phi(x) + \psi(x)) \quad (\text{B.35})$$

Using the equations we derived so far for the strain equations, we can also define a relation for the internal moment and shear forces over the length of the web which are given below. These simple equations make it easier to understand the deformation occurring in the web, and help us in interpreting the more complex expressions such as  $\psi$  and  $\phi'$ .

$$M(x) = -EIaK^2 (C_1 \sinh(Kx) + C_2 \cosh(Kx)) \quad (\text{B.36})$$

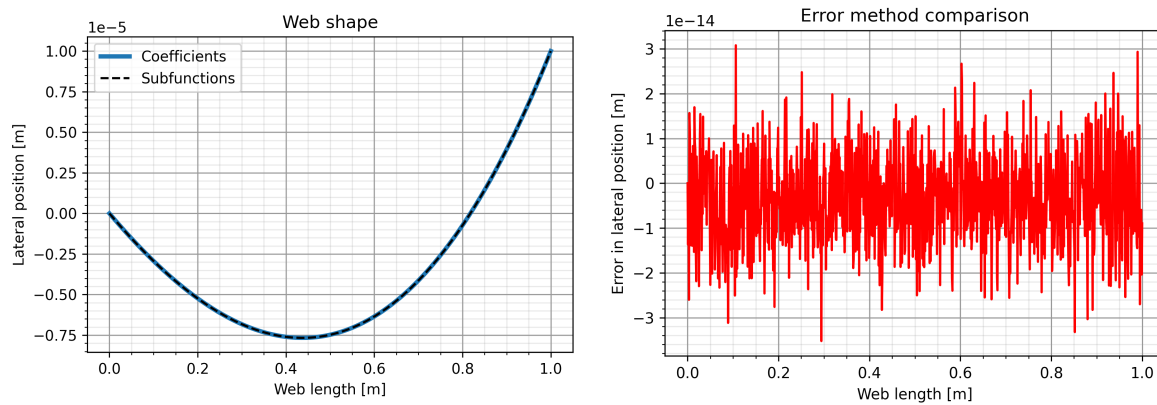
$$\begin{aligned} Q(x) &= \kappa AG (-\phi(x) + \psi(x)) \\ &= -\kappa AG \left( C_3 + \left( 1 + \frac{2nT}{AG} \right) KC_1 \cosh(Kx) \left( 1 + \frac{2nT}{AG} \right) KC_2 \sinh(Kx) \right) \end{aligned} \quad (\text{B.37})$$

### B.3.2. Validation of derived equations

The derivations introduced in this chapter are based on previous work of first Shelton and then Sievers and Brown. In all the documentation of research on web dynamics the analysis refers to subfunctions,  $(f_i, g_i, h_i)$ , in order to describe the web shape. For the strain relations found in this section, the subfunctions do not suffice. Rather, the original coefficient  $(C_1, C_2, C_3, C_4)$  are required in the derivation for  $\phi$ ,  $\psi$  and  $\frac{\partial \phi}{\partial x}$ .

The use of both the shape functions and coefficients is correct, as they are derived from the same system of equations in section B.2. Therefore, the both methods are equivalent and can be rewritten into each other.

To prove the legitimacy of the coefficients, an example can be used. The shape functions are ideally used to describe the web shape  $y(x)$ . Therefore, a web is modelled between two rollers, with web properties:  $L = 1[m]$ ,  $K = 0.07036$ ,  $E = 3.8[GPa]$ ,  $I = 1.62e^{-5}[m^4]$  and  $a = 1.0017$ . Boundary conditions are applied to the web by a misaligned downstream roller with  $\phi_L = 1e^{-5}[rad]$  and  $y_L = 1e^{-4}[m]$ . The resulting shape of the web is analysed by both the shape function and coefficient method is given in figure B.2a.

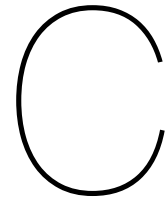


(a) The web shape analysed by Sievers method and the coefficients methods derived in this thesis. (b) The error between the web shapes, derived by the shape functions from Sievers and the coefficients' method from this paper.

Figure B.2: A comparison of the derivations used in this thesis to the expressions used by Sievers and Brown.

At a first glance, the two methods give a similar result. The error between the two methods has been visualized in figure B.2b. In this figure, the order of magnitude for the error is approximately  $10^{-14}$ . The computations performed in each method differ greatly, as the hyperbolic functions have been rewritten to exponential expressions. Therefore, the error can be explained by the arithmetic error in the computation of each method. Aside from this computational error, both methods perform similarly and can both be used in future analysis.





# Lateral web dynamics

## C.1. Case study using an Euler-Bernoulli beam model

### C.1.1. Sine input

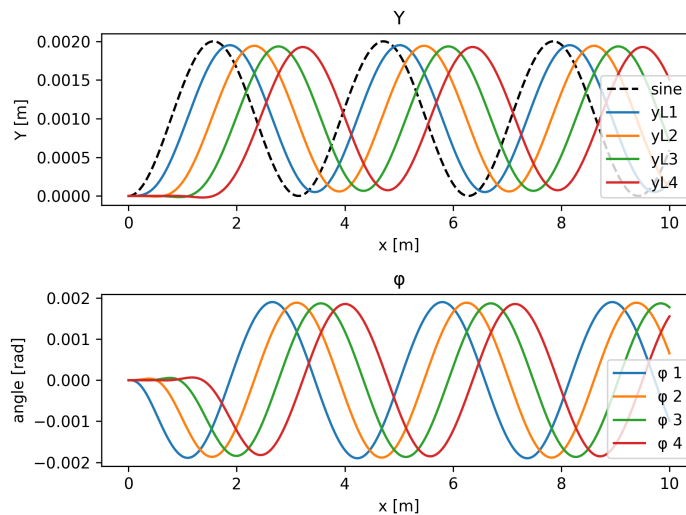


Figure C.1: A sine wave disturbance introduced at the entry of the first roller, with an amplitude of  $1[mm]$  and frequency of  $\frac{2\pi}{6} [rad/s]$ .

### C.1.2. Roller misalignment

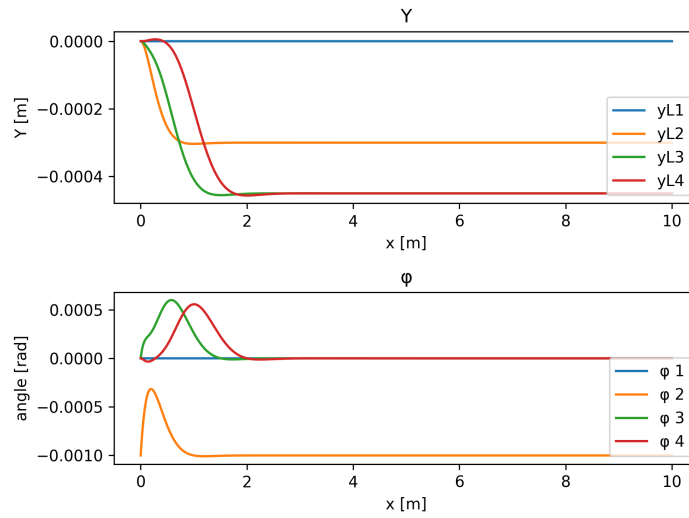


Figure C.2: A web response to an angular misalignment of  $-1[mrad]$  introduced at the second rollers. As a result, the second and downstream rollers move in the lateral direction.

### C.1.3. Eccentricity

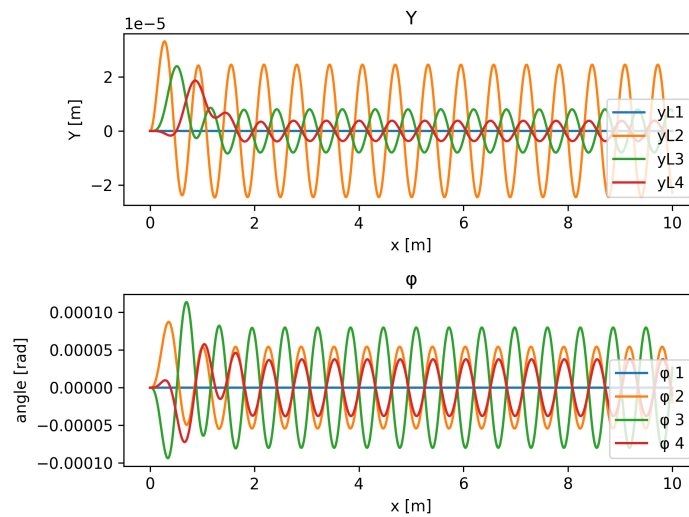
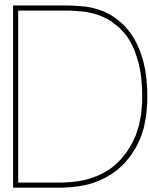


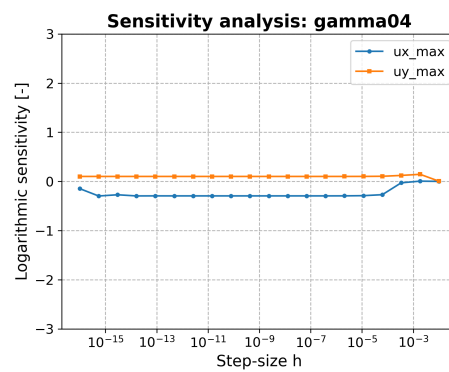
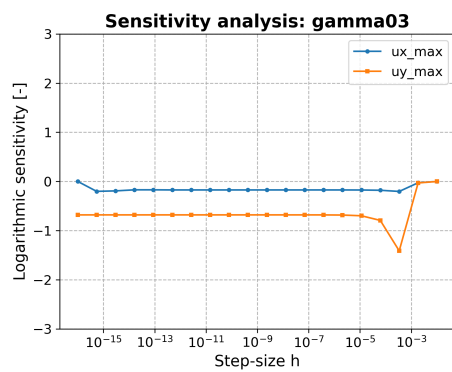
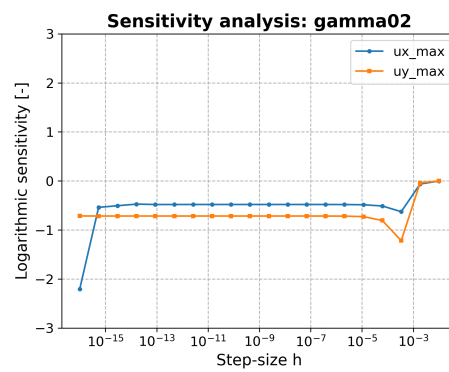
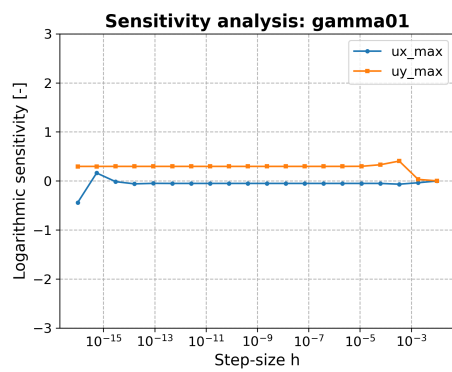
Figure C.3: The effect of roller eccentricity which causes an oscillatory disturbance to the web input.

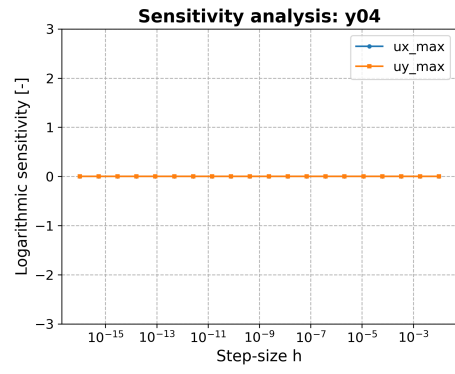
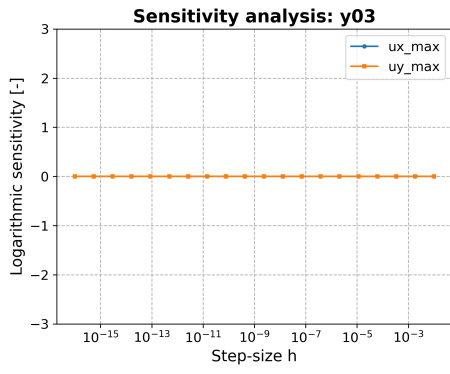
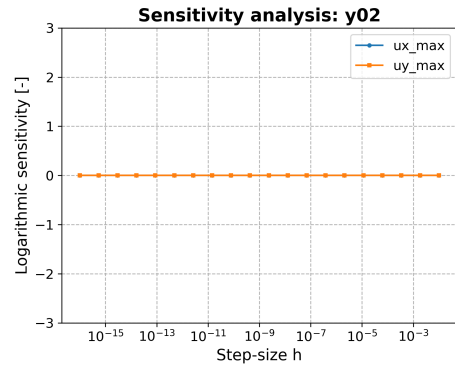
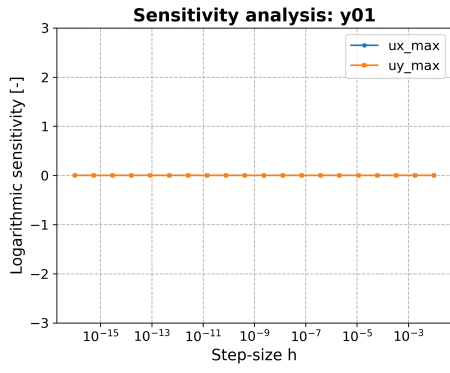




# Sensitivity Analysis

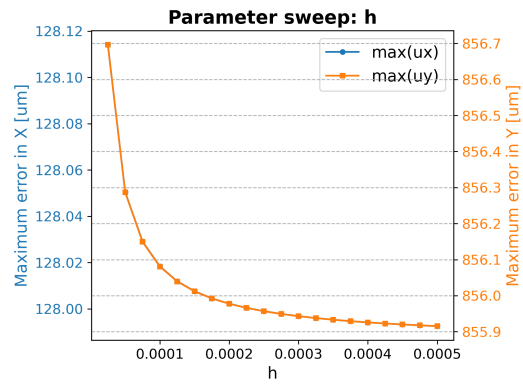
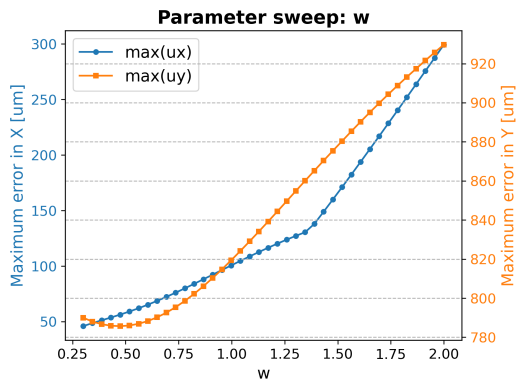
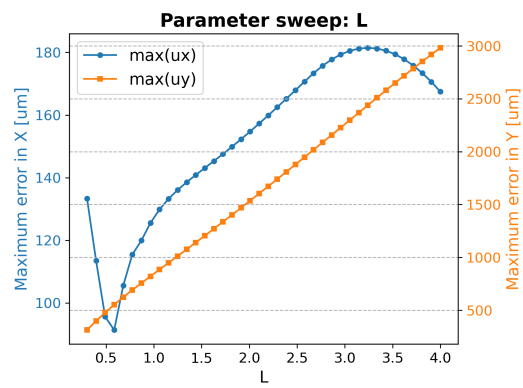
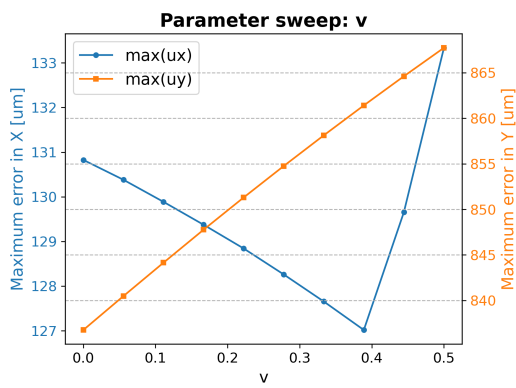
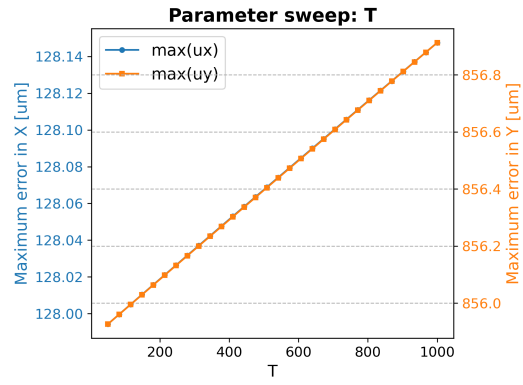
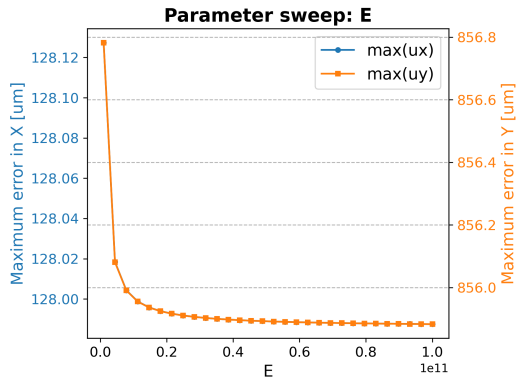
## D.1. Input conditions



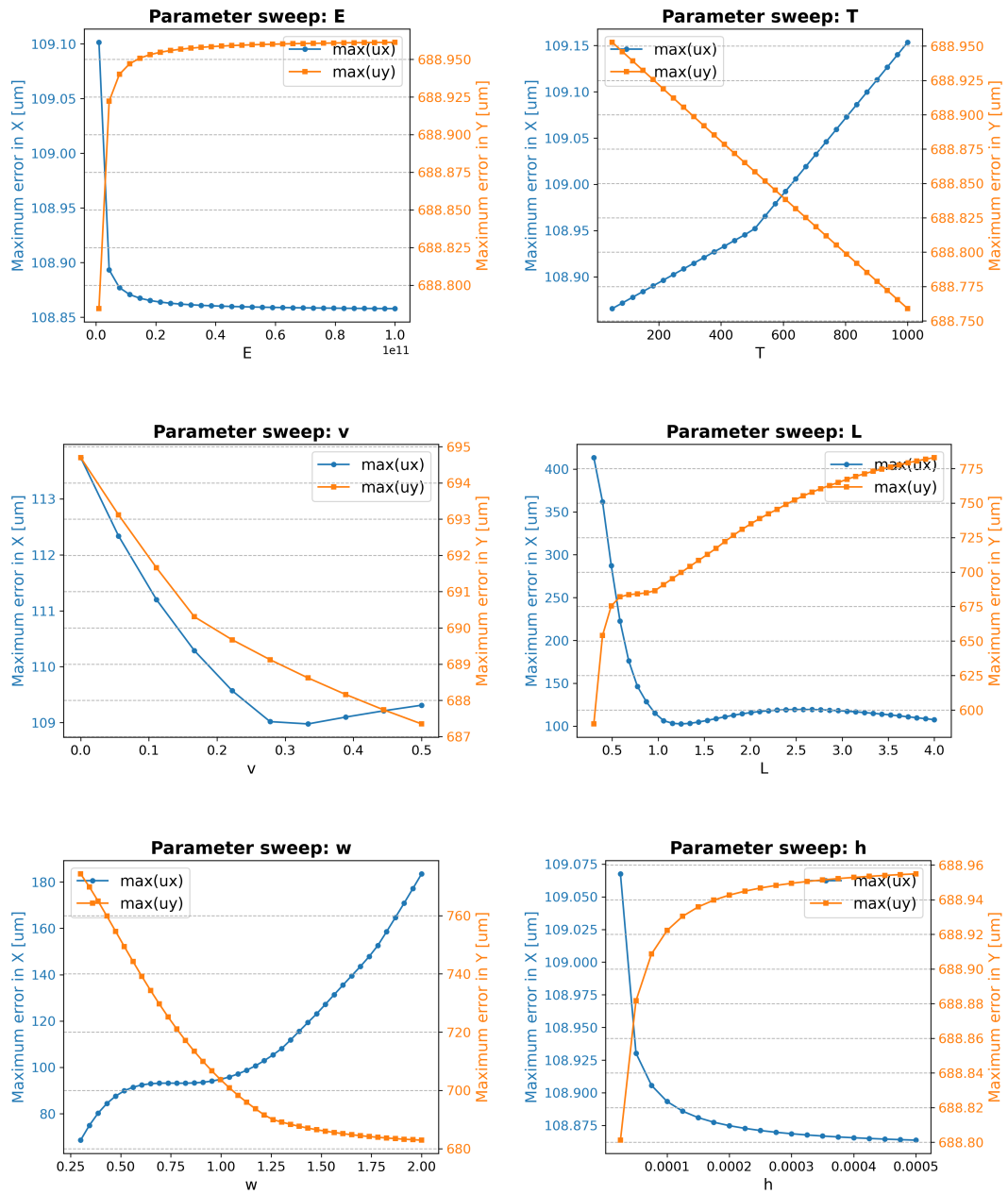


## D.2. Parameter sweep

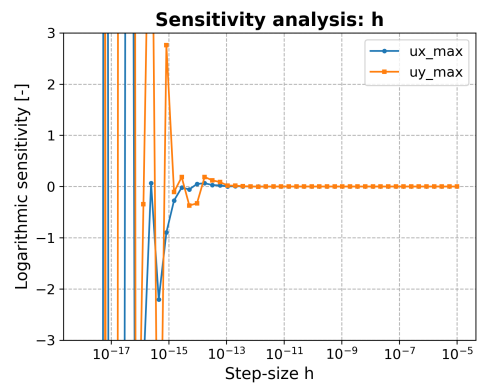
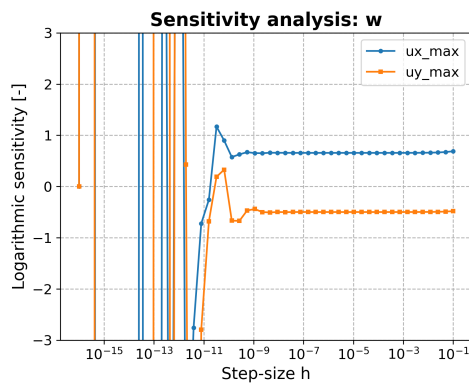
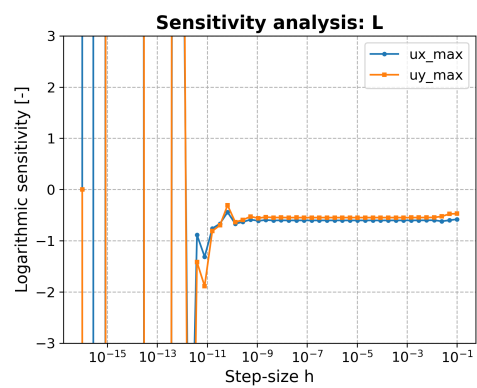
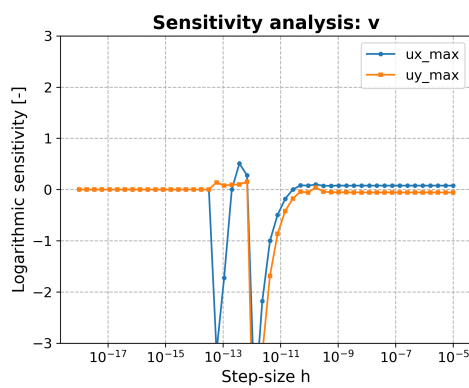
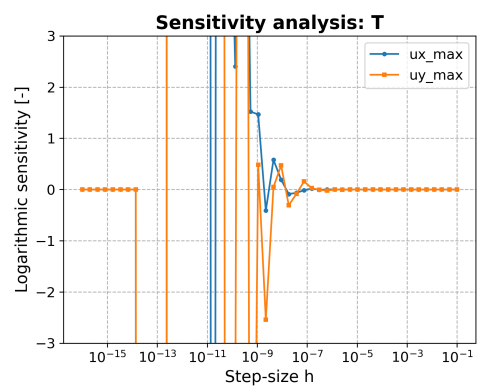
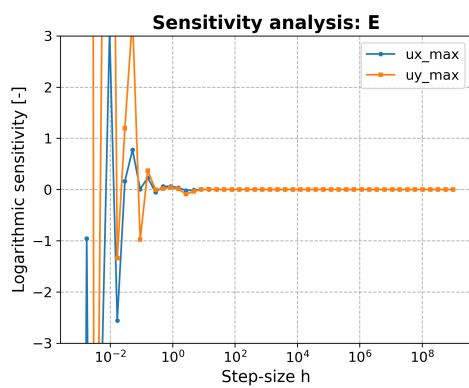
### D.2.1. Angular misalignment



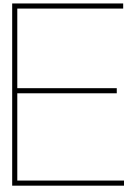
### D.2.2. Lateral displacement



## D.3. Convergence







## Out-of-plane web deformations

The theory introduced by Shelton [37] neglects the out-of-plane deformations and buckling of a web. However, the instability problem of out-of-plane deformations is considered in the beam theory by Timoshenko and Gere [40], which was applied by Shelton. The Timoshenko beam theory states that lateral buckling of a thin beam can only occur if compressive stresses can be sustained within the web. This is not true for a web in which shear forces are neglected. However, in section 4.4 it is stated that the shear stiffness can be quite relevant in the analysis of a web span. Therefore, it is also reasonable to look into the out-of-plane deformations which can occur in a dynamic web span.

The out-of-plane deformations refer to a wave pattern called troughs or wrinkles. Web troughs are a web instability which can occur in between two rollers. Web wrinkling on the other hand is an instability which occurs on the contact area of the web and roller. Wrinkles in a web are creases or fold-overs of the web, which can damage materials or cause failures in production processes. Wrinkles are more severe compared to troughs and seem like two different failures which can occur in webs. However, Beisel and Good have proven that troughs are a premature sign to wrinkle formation, as they indicate compressive stresses in a web span [11] [12] [4].

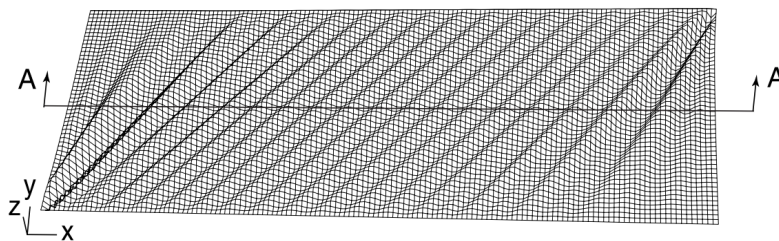


Figure E.1: A visualization of a wrinkled membrane generated in a numerical analysis by Wong [46]

Several causes can be considered in the formation of out-of-plane deformations. In their paper Good and Beisel research the alignment of rollers, taper of rollers and web defects were considered. The effect of roll alignment adds on the theory of chapter 5, in which we looked into the lateral motion of a web. This lateral motion is the result of lateral forces in the contact area of the web with the rollers, and thus can also be linked to compressive stresses in a web. These compressive stresses, when exceeding a relative amount, can result in buckling of the web.

In addition, geometrical defects were also considered in the formation of troughs and wrinkles. Peter Jensen [45] and Brown [16] researched the effect of roller shapes on the formation of compressive stresses. Even the deflection of rollers due to web tension can result in a roller shape which induces compressive stresses, according to Arias [3].

As troughs can be considered as premature signs to wrinkle formation, the focus for the coming sections will be to quantify the initiation of troughs in a web span. If troughs can be prevented during imprinting, the formation of wrinkles will be prevented as well. Still, to verify this assumption a short analysis on the wrinkles will be performed in section E.5.

## E.1. Trough formation

To analyse the instability of free web spans, it is assumed that the web was initially stable but due to compressive stresses in the y-direction troughs have been formed. An isotropic web span, with a width  $b$  and a length  $a$ , is given in figure E.2. The Timoshenko beam theory implies that the deflection equation for an isotropic plate, with a thickness  $h$ , is as follows:

$$D \frac{\partial^4 w}{\partial x^4} + 2D \frac{\partial^4 w}{\partial x^2 \partial y^2} + D \frac{\partial^4 w}{\partial y^4} - \sigma_x h \frac{\partial^2 w}{\partial x^2} - \sigma_y h \frac{\partial^2 w}{\partial y^2} = 0, \quad \text{with } D = \frac{Eh^3}{12(1-\nu^2)} \quad (\text{E.1})$$

A solution which fits the waved out-of-plane deformation  $w$ , in the z-direction, is described by Beisel in the form:

$$w = A_{mn} \sin\left(\frac{m\pi x}{a}\right) \sin\left(\frac{n\pi y}{b}\right) \quad (\text{E.2})$$

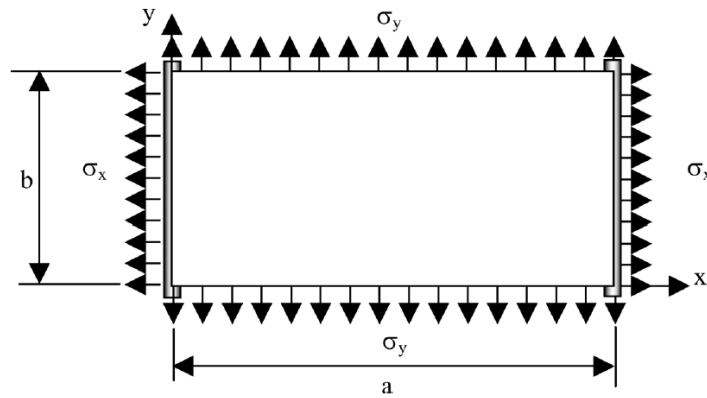


Figure E.2: An isotropic web between two rollers [11].

In equation E.2  $m$  and  $n$  are the half-wave numbers in the x- and y-directions, respectively and  $A_{mn}$  is the maximum amplitude of the out-of-plane deformation. The form of the wave equation implies that the out-of-plane deformation vanishes near the edges. Which is a reasonable assumption as no stresses in the y-direction can be sustained on the edge, according to surface equilibrium. This means that the out-of-plane deformations will dissipate near the edges.

In this analysis, it is assumed that the stress in the x-direction  $\sigma_x$  is positive, as tension is applied on the web. This tensile stress will restrict the half-wave number  $m$  in the x-direction to be unity. If equation E.2 is substituted into equation E.1, and if the equation is solved for  $\sigma_y$ , a relationship for the critical buckling stress will follow:

$$\sigma_{ycr} = -\frac{(b^2 + a^2 n^2)^2 \sigma_e + b^4 \sigma_x}{a^2 b^2 n^2} \quad \text{where } \sigma_e = \frac{\pi^2 D}{a^2 h} \quad (\text{E.3})$$

Equation E.3 defines the critical compressive stress  $\sigma_y$  for a plate for given dimensions and material, which can be determined as a function of the half wave numbers  $n$  in the y-direction and tensile stress in the x-direction. For both variables,  $n$  and  $T$ , increasing the value will result in a higher critical stress and thus stabilizes the web.

Looking back to the static analysis in section 4.2 we see that the web tension is relevant to prevent slack of the web, under misalignment, but now also the formation of troughs and wrinkles are dependent on the tensile stress.



In equation E.3, a dependency on the value of  $n$  and  $\sigma_x$  remains. However, for the half wave numbers  $n$ , we know the values should be fixed integers to comply with boundary conditions that assume zero tension  $\sigma_y$  at the edges. Furthermore, Beisel states that a correct value for  $n$  requires consideration of minimum energy. To introduce this minimum energy, Beisel derivatives equation E.3 and sets it equal to zero. The derivations lead to a new formula, which can be simplified as follows:

$$\sigma_{y_{cr,trough}} \approx -2\sqrt{\sigma_e \sigma_x} = -\frac{\pi h}{a} \sqrt{\frac{E\sigma_x}{3(1-\nu^2)}} \quad (E.4)$$

From this equation it can be concluded that vary little compressive stress may be required to cause instability of a web, depending on the geometry and material. When the stress  $\sigma_y$  becomes more negative than the critical buckling stress the web has buckled and developed troughs.

So far, the theory is applied to isotropic materials. However, in web handling an orthotropic material model is used in many applications and thus quite relevant. The same methods as introduced above can be applied on orthotropic webs as well. Compared to the isotropic equations, we know distinguish material properties per direction, with  $E_x$  and  $E_y$  the moduli of elasticity in the x and y directions,  $G$  the shear modulus,  $\nu$  the Poisson ratio per direction.

Similar to the isotropic case, the equations given above can be implemented to the out-of-plane wave equation E.2. Again, the wave number  $m$  is assumed to be unity due to tensile stress in the x-direction. Also, the concept of minimal energy is applied to derive the critical compressive stress. These derivations with additional simplifications lead to the final formula:

$$\sigma_{y_{cr,trough}} \approx -\frac{\pi h}{a} \sqrt{\frac{\sigma_x E_y}{3(1-\nu_{xy}\nu_{yx})}} \quad (E.5)$$

Comparing the isotropic and orthotropic equations E.4 and E.5 we see that both relations are very similar. The impact of an orthotropic material compared to an isotropic material is the modulus of elasticity in the y-direction.

## E.2. Disturbances which induce web troughs

For a web span to become unstable and produce troughs, compressive stresses  $\sigma_y$  comparable to the critical stresses  $\sigma_{y_{cr}}$  must be applied to the web. Several causes can be considered, such as: roller misalignment, roller taper, roller non-uniform shape, web imperfections/defects etc. For the roll-to-plate application no defects will be considered, as a defect stamp would not be used in a production process. Roller misalignment is a more reasonable cause, which builds upon the lateral dynamics discussed in chapter 5. Roller taper is unexpected in a roll-to-plate process, where high tolerance rollers are used. Still, the taper of rollers will shortly be discussed to compare the maximum taper to typical tolerances applied to rollers and bending due to tension loads.

## E.3. Trough formation by roller misalignment

As discussed in section 4.2, the rollers of a web span can introduce additional shear forces and a moment to the web as a result of roller misalignment. Not only does this cause a lateral motion as discussed in chapter 5, but it can also introduce troughs and wrinkles with the compressive stresses which induce the lateral motion. As both the lateral dynamics and out-of-plane deformation origin from the same concept, the theory will also be very similar.

Beisel and Good applied the same methodology as Shelton in order to analyse the loads in a web span. The web span behaves similarly to a loaded cantilever, provided that the friction forces are sufficient to enforce the boundary conditions. Shelton introduced the 'normal entry rule', which means that the web enters the downstream roller uniformly and perpendicular to the roller axis. Meaning a uniform tension is applied to the web at the downstream roller, and a moment is applied to the web at the upstream roller. In this analysis the shear stiffness of the web is considered, as the shear stiffness is a require-

ment to sustain compressive stresses in the y-direction.

Beisel applies the boundary conditions and assumption, similarly to Shelton. However, for the calculation the Przemieniecki structural stiffness matrix is applied, which incorporates both shear and tension loads for orthotropic materials. From this analogy, the formulas for web shear forces and moment result and can be rewritten in the principle stresses of the web in order to compare the web stress to the critical compressive stresses. The shear force is described by:

$$f_{yj} = \frac{A_s G [240E^2 I^2 + 3T^2 a^4 (1 + \phi) + 8EIT a^2 (13 + 3\phi)]}{240E^2 I^2 + T a^4 (2A_s G + T) (1 + \phi) + 8EI a^2 [15A_s G - T(2 - 3\phi)]} \theta_j \quad (\text{E.6})$$

With:

$$\theta_i = \frac{f_{yj}}{GA_s}, \quad \phi = \frac{12EI}{GA_s a^2}$$

Dividing the shear force  $f_{yj}$  from equation E.6 by the cross-sectional area gives us the shear stress  $\tau_{xy}$  in the web. The second principle stress will be negative (compressive) and can be determined using the tensile stress  $\sigma_x$  and the shear stress  $\tau_{xy}$ :

$$\sigma_2 = \frac{\sigma_x}{2} - \sqrt{\left(\frac{\sigma_x}{2}\right)^2 + \tau_{xy}^2} \quad (\text{E.7})$$

Finally, by comparing the stress in the web to the critical buckling stresses, from equation E.5, a relation for the critical angular misalignment is formed:

$$\theta_{cr, \tau_{avg}} = \frac{6 \left( 5 b^6 E^2 h^2 + a^4 T(5bGh + 3T)(1 + \phi) + a^2 b^3 Eh(25bGh + T(6\phi - 4)) \right)}{5G \left( 5 b^6 E^2 h^2 + 9a^4 T^2(1 + \phi) + 2a^2 b^3 EhT(13 + 3\phi) \right)} \sigma_{ex} \quad (\text{E.8})$$

Where:

$$\sigma_{ex} = \sqrt{\sigma_{ycr} \left( \sigma_{ycr} - \frac{T}{bh} \right)} \quad (\text{E.9})$$

In equation E.9 the variable  $\sigma_{ycr}$  can be substituted from the isotropic expression given in equation E.4 or the orthotropic equation E.5. The angle  $\theta_{cr, \tau_{avg}}$  represents the angle of the downstream roller for which troughs are expected to form over the entire width. Troughs are expected to appear first at the center of the web, where the flexural shear stress is maximum, namely 1.5 times greater than the average value.

## E.4. Trough formation by roller taper

If a roller is not perfectly cylindrical troughs can form as well, due to an additional load applied to the web. The taper of a roller can be described linearly by an average radius and a slope over the width of the roller, as shown in figure E.3. The taper can be described as:  $r(y) = my + R_0$ . As the roller shaft can only have a single rotation, the angular velocity  $\omega$  is uniform. However, the surface velocity scales with the varying roller radius, creating velocity differences according to:  $V(y) = r(y) \cdot \omega = (my + R_0)\omega$ . The average velocity is dependent on the average radius by:  $V_{avg} = R_0\omega$ .

The varying velocity profile over the width of the roll introduces a non-uniform strain profile in the web. Assuming the roller can deliver enough friction, the strain and stress can be described by equations E.10 E.11.

$$\varepsilon_{md}(y) = \frac{V(y) - V_{avg}}{V_{avg}} = \frac{my}{R_0} \quad (\text{E.10})$$

$$\sigma(y) = E\varepsilon_{md}(y) = \frac{Emy}{R_0} \quad (\text{E.11})$$

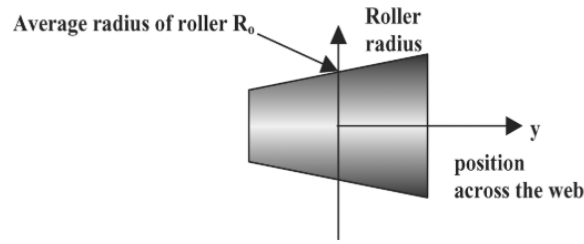


Figure E.3: The enlarged taper in a roller [11].

As a linear slope is assumed for the roller taper, also a linear stress profile will form in the web span. This linear stress profile resembles a moment applied to the web, which can be found by integrating

the stress  $\sigma(y)$  over the width:  $M_j = \int_{-b}^b -\sigma(y)hydy$ .

With the moment  $M_j$  applied to the web the trough formation due to taper has become similar to problem discussed in the previous section for roller misalignment. The moment applied to the web and the web velocity are both known. With these known variables the shear force in the web can be determined, and so also the shear stresses. Beisel and Good found the following relation for the shear force:

$$f_{yj} = \frac{mhb^3E_x}{R_0a} \frac{GA_s [10E_xI + T \cdot a^2(1 + \phi)]}{[60E_xI + Ta^2(1 + \phi)](T + GA_s)} \quad (E.12)$$

This shear force  $f_{yj}$ , can be divided by the cross-sectional area to obtain the shear stress. Similar to the previous section, the shear stress will be used to calculate the second principle stress of the web from equation E.7. With this derivation we have obtained the compressive stresses in a web span as a result of roller taper. Previously, the critical compressive stresses were determined for both isotropic E.4 and orthotropic E.5 materials.

Rewriting the critical stress  $\sigma_{ycr}$  and second principle stress enables us to relate the taper of the roller  $m$  to the point where the second principle stress equals the critical stress value. This results in the following final equation for the maximum acceptable taper:

$$m_{cr} = \frac{2aR_0}{3b^2E_x} \frac{[60E_xI + Ta^2(1 + \phi)](T + GA_s)}{GA_s [10E_xI + Ta^2(1 + \phi)]} \sigma_{ex} \quad (E.13)$$

In this equation the variable  $\sigma_{ex}$  is given by equation E.9.

With the final equation for the roller taper  $m_{cr}$  the tolerances on a roller can be defined, which will be used in the design of roll-to-plate systems.

## E.5. Wrinkle formation

So far, the formation of troughs has been discussed and the critical values for roller misalignment and taper have been quantified. Troughs are instabilities in the web span which occur between two rollers. In that sense, wrinkles are a different phenomenon, as they form on the contact area between the roller and web. A thin web span wrapped around a cylindrical roller can be considered a cylindrical shell, a topic addressed in the field of mechanics by Timoshenko [40].

For the axial buckling of cylindrical shells, Timoshenko developed the following failure criteria for isotropic materials:

$$\sigma_{ycr,wrinkles} = -\frac{Eh}{R\sqrt{3(1-\nu^2)}} \quad (E.14)$$

Beisel derived the same failure criteria for orthotropic webs as well:

$$\sigma_{ycr,wrinkles} = -\frac{h}{R} \sqrt{\frac{E_xE_y}{3(1-\nu_{xy}\nu_{yx})}} \quad (E.15)$$

Comparing the equations for the wrinkle criteria, for both isotropic and orthotropic materials, a clear similarity can be found. The orthotropic relation E.15 also reduces to the isotropic relation E.14 for uniform material properties.

Previously, the wrinkle formation was stated to be more severe, but less likely to occur as higher compressive stresses need to be sustained in order to initiate buckling. This was verified by Beisel, by comparing the buckling criteria for trough and wrinkle formation:

$$\frac{\sigma_{\text{ycr, wrinkle}}}{\sigma_{\text{ycr, trough}}} = \frac{\frac{Eh}{R\sqrt{3(1-\nu^2)}}}{\frac{\pi h}{a} \sqrt{\frac{E\sigma_x}{3(1-\nu^2)}}} = \frac{a}{\pi R} \sqrt{\frac{E}{\sigma_x}} \quad (\text{E.16})$$

From equation E.16, it can be seen how the wrinkles formation relates to troughs in a web span. Substituting common values for the variables:  $R$ ,  $E$ ,  $\sigma_x$  and  $a$ , verify that the stress required to induce wrinkles is 100 to 200 times greater than the stress to introduce web troughs.

As a roll-to-plate system is required to prevent troughs, also wrinkles will be prevented. Therefore, an assumption made at the beginning of this section is valid and a more detailed analysis to wrinkles will not be explained from here on.

## E.6. Relevance of out-of-plane deformations

Troughs form easily and should be prevented. Wrinkling can be neglected if troughs are successfully mitigated.

All the theory is composed of analytical approximations, very limited numerical verification is applied and not numerical models are shown. In practice some researchers do work with finite element models, however these models are not generic and can be complex to build and verify. The analytical models have been verified experimentally and can therefore more easily be applied on a larger range of system parameters.

## E.7. Tension Dynamics

In both roll-to-roll and roll-to-plane nano imprinting, the handling of flexible materials is very important to achieve a repeatable and accurate end-product. As both processes use an elastic material, which is transported through the system, the control of the tension in the span is critical. This tension can vary due to imperfections in machine design or handling of the web, but also by external effects such as humidity or temperature changes.

For roll-to-plate applications, the web is not part of a continuous system with winding- and unwinding-rollers, but fixated between two end-points which actuate the web. This is a result of imprinting on discrete substrates, compared to a continuous web in roll-to-roll imprinting. Therefore, varying lengths should be considered which is dependent on a mass flow in and out of the web span.

A schematic of a web span is given in figure E.4, in which two consecutive rollers are given. Each web span has a tension  $T_i$  and length  $L_i$ , and each roller has a velocity  $v_i$ .

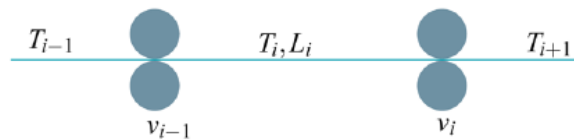


Figure E.4: Schematic of a web span between two rollers and their respective notation [5]

With a unique angular velocity per roller, the mass flow in and out of the web span is inconsistent. According to the mass conservation law the mass of a web span between two rollers can be described as follows [28]:

$$\frac{d}{dt} \frac{L_i \rho_i A_i}{1 + \varepsilon_i} = \frac{\rho_i A_i v_{i-1}}{1 + \varepsilon_{i-1}} - \frac{\rho_i A_i v_i}{1 + \varepsilon_i} \quad (\text{E.17})$$

The mass-conservation law is the basis principle to describe dynamic tension behaviour. For a uniform web the density and cross-sectional area can be assumed as constant. This results in a simplified equation of the mass-conservation law.

In addition, Branca and Reid developed a tension model in which the varying web lengths were taken into account [5]. This property is relevant for roll-to-plate systems, in which varying web lengths are common. The model is described by:

$$\dot{T}_i(t) = \frac{v_i(t) (EA - T_i(t)) - v_{i-1}(t) (EA - T_{i-1}(t)) + (EA - T_i(t)) \dot{L}(t)}{L(t)} \quad (\text{E.18})$$

Equation E.18 is an altered equation for varying web lengths. Likewise, other imperfections in the web handling can be taken into account to describe more accurately the tension in the web.

Other imperfections which can be addressed are roller eccentricity [5], web-slip [34], tension actuators [28] and viscoelastic material models for web tension [27]. Of these different imperfections the roller eccentricity can be neglected as the roll-to-plate process is not as complex as comparable systems. The web-slip will also be neglected as the slip is caused by air entrapment between the web and roller contact surface, which is related to the web transport speed. For imprint applications this transport velocity is very low, and static friction is a reasonable assumption.

### E.7.1. External effects on web tension

Webs handling is also applied to production processes in which a large temperature deviation can be expected. Therefore, a good understanding of the changing mechanical and material behaviour has been developed in the industry [17] [20] [26].

However, even though mathematical models for thermal effects have been developed, it is yet to be determined how these methods apply to a roll-to-plate application. The temperature deviations discussed by Lee [26] involve temperature differences of 50-100 degrees Celsius. The thermal effects discussed include thermal expansion of the web, resulting in a loss of tension. Furthermore, the temperature dependency of material properties are taken into account. For an application with smaller temperature deviations this temperature dependency could be neglected, as material properties would be close to constant.



# Bibliography

- [1] Se Hyun Ahn and L. Jay Guo. "Large-area roll-to-roll and roll-to-plate Nanoimprint Lithography: A step toward high-throughput application of continuous nanoimprinting". In: *ACS Nano* 3.8 (2009), pp. 2304–2310. ISSN: 19360851. DOI: 10.1021/nn9003633.
- [2] Suho Ahn et al. "Continuous ultraviolet roll nanoimprinting process for replicating large-scale nano- and micropatterns". In: *Applied Physics Letters* 89.21 (2006), pp. 1–4. ISSN: 00036951. DOI: 10.1063/1.2392960.
- [3] PEDRO J. ARIAS. "PREDICTION OF WEB WRINKLING INDUCED BY ROLLER DEFLECTION". In: (1998).
- [4] JOSEPH A. BEISEL. "Single Span Web Buckling Due To Roller Imperfections in Web Process Machinery". In: (2000).
- [5] Carlo Branca, Prabhakar R. Pagilla, and Karl N. Reid. "Governing equations for web tension and web velocity in the presence of nonideal rollers". In: *Journal of Dynamic Systems, Measurement and Control, Transactions of the ASME* 135.1 (2013). ISSN: 00220434. DOI: 10.1115/1.4007974.
- [6] Jerald L. Brown. "the Connection Between Longitudinal and Lateral Web Dynamics". In: (2019), pp. 1–13.
- [7] Jerry L. Brown. "A COMPARISON OF MULTI-SPAN LATERAL DYNAMICS MODELS". In: *Journal of Chemical Information and Modeling* 53.9 (2013), pp. 1689–1699. ISSN: 1098-6596.
- [8] P. J. Cegielski et al. "Overlay accuracy limitations of soft stamp UV nanoimprint lithography and circumvention strategies for device applications". In: *arXiv* (2018), pp. 1–15.
- [9] Jaehyuk Chang et al. "Overlay accuracy on a flexible web with a roll printing process based on a roll-to-roll system". In: *Review of Scientific Instruments* 86.5 (2015), pp. 1–9. ISSN: 10897623. DOI: 10.1063/1.4921495.
- [10] Kuo Shen Chena, Kuang Shun Ou, and Yen Ming Liao. "On the influence of roller misalignments on the web behavior during roll-to-roll processing". In: *Journal of the Chinese Institute of Engineers, Transactions of the Chinese Institute of Engineers, Series A* 34.1 (2011), pp. 87–97. ISSN: 21587299. DOI: 10.1080/02533839.2011.552979.
- [11] J K Good, J A Beisel, and H Yurtcu. *INSTABILITY OF WEBS : THE PREDICTION OF TROUGHES AND WRINKLES*. September 2009. 2018, pp. 517–556. ISBN: 4057445900. DOI: 10.15376/frc.2009.1.517. INSTABILITY.
- [12] K Good and A Beisel. "Buckling of Orthotropic Webs in Process Machinery". In: (). URL: <https://shareok.org/handle/11244/321847?show=full>.
- [13] Chin-Chou Kevin Huang et al. "Methodology for overlay mark selection". In: *Metrology, Inspection, and Process Control for Microlithography XXV* 7971 (2011), 79712B. ISSN: 0277786X. DOI: 10.1117/12.879378.
- [14] Chun-Yen Huang et al. "Overlay control methodology comparison: field-by-field and high-order methods". In: *Metrology, Inspection, and Process Control for Microlithography XXVI* 8324.98 (2012), p. 832427. ISSN: 0277786X. DOI: 10.1117/12.916427.
- [15] *Images on web handling*. 2011. URL: <https://pffc-online.com/web-handling/9810-web-handling-top-7-causes-wrinkles-1010>.
- [16] J.L.Brown. "EFFECTS OF CONCA VE ROLLERS, CURVED-AXIS ROLLERS AND WEB CAMBER ON THE DEFORMATION AND TRANSLATION OF A MOVING WEB". In: (), pp. 61–80.
- [17] Kadhim A. Jabbar and Prabhakar R. Pagilla. "Modeling and analysis of web span tension dynamics considering thermal and viscoelastic effects in roll-to-roll manufacturing". In: *Journal of Manufacturing Science and Engineering, Transactions of the ASME* 140.5 (2018), pp. 1–9. ISSN: 15288935. DOI: 10.1115/1.4038888.
- [18] Daniel Kandel et al. "Overlay accuracy fundamentals". In: *Metrology, Inspection, and Process Control for Microlithography XXVI* 8324. April 2012 (2012), p. 832417. ISSN: 0277786X. DOI: 10.1117/12.916369.

- [19] Dongwoo Kang et al. "Distortion mechanism of patterning positions in the soft roller printing process for realizing large-area overlay printing". In: *Journal of Micromechanics and Microengineering* 30.4 (2020). ISSN: 13616439. DOI: 10.1088/1361-6439/ab7323.
- [20] M. Khodjet-Kesba et al. "Effect of moisture absorption on the elastic properties in cracked composite laminates with transient hygrothermal conditions". In: *Procedia Structural Integrity* 13 (2018), pp. 181–186. ISSN: 24523216. DOI: 10.1016/j.prostr.2018.12.030.
- [21] Takuya Kono et al. "Half-pitch 14nm direct patterning with nanoimprint lithography". In: May (2019), p. 16. ISSN: 1996756X. DOI: 10.1117/12.2514685.
- [22] Yasuyuki Kusaka and Nobuko Fukuda. "Decomposition of pattern distortions by the Spread polynomial model in roll-to-sheet reverse offset printing". In: *Journal of Micromechanics and Microengineering* 30.9 (2020). ISSN: 13616439. DOI: 10.1088/1361-6439/ab999c.
- [23] B. Kwon and Jong H. Kim. "Importance of Molds for Nanoimprint Lithography: Hard, Soft, and Hybrid Molds". In: *Journal of Nanoscience* 2016 (2016), pp. 1–12. ISSN: 2356-749X. DOI: 10.1155/2016/6571297.
- [24] L. Sievers. "Modeling of Web Conveyance Systems for Multivariable Control". In: 33.6 (1988), pp. 524–531.
- [25] Hongbo Lan. "Large-Area Nanoimprint Lithography and Applications". In: *Micro/Nanolithography - A Heuristic Aspect on the Enduring Technology* (2018). DOI: 10.5772/intechopen.72860.
- [26] Changwoo Lee, Hyunkyoo Kang, and Keehyun Shin. "A study on tension behavior considering thermal effects in roll-to-roll e-printing". In: *Journal of Mechanical Science and Technology* 24.5 (2010), pp. 1097–1103. ISSN: 1738494X. DOI: 10.1007/s12206-010-0324-5.
- [27] J. O. Lif, S. Östlund, and C. Fellers. "Applicability of Anisotropic Viscoelasticity of Paper at Small Deformations". In: *Mechanics Time-Dependent Materials* 2.3 (1998), pp. 245–267. ISSN: 13852000. DOI: 10.1023/A:1009818022865.
- [28] Yi Liu, Qiang Fang, and Yinglin Ke. "Modeling of Tension Control System with Passive Dancer Roll for Automated Fiber Placement". In: *Mathematical Problems in Engineering* 2020 (2020). ISSN: 15635147. DOI: 10.1155/2020/9839341.
- [29] Yuehao Luo et al. "Boundary layer drag reduction research hypotheses derived from bio-inspired surface and recent advanced applications". In: *Micron* 79 (2015), pp. 59–73. ISSN: 09684328. DOI: 10.1016/j.micron.2015.07.006. URL: <http://dx.doi.org/10.1016/j.micron.2015.07.006>.
- [30] Morphotonics. *Morphotonis R2P NIL*. URL: <https://www.morphotonics.com/roll-to-plate-nanoimprint/>.
- [31] Tetsuro Nakasugi et al. "Multi-field imprint technology: enabling the productivity enhancement of NIL". In: 1161008. February (2021), p. 5. DOI: 10.1117/12.2583385.
- [32] *oksd\_icwh\_2019\_brown2.pdf*.
- [33] *Precision vs. Accuracy*. URL: <https://wp.stolaf.edu/it/gis-precision-accuracy/>.
- [34] Benjamin D. Karl N. Reid Reish. "Modeling Slip Between a Web and a Roller". In: (2019).
- [35] Nilabh Roy et al. "Overlay models for nanoimprint lithography". In: 1161006. March (2021), p. 3. DOI: 10.1117/12.2584742.
- [36] Helmut Schiff and Anders Kristensen. *Nanoimprint lithography*. February 2010. 2017, pp. 113–142. ISBN: 9789533070643. DOI: 10.1007/978-3-662-54357-3{\\_}5.
- [37] J. J. Shelton and K. N. Reid. "Lateral dynamics of a real moving web". In: *Journal of Dynamic Systems, Measurement and Control, Transactions of the ASME* 93.3 (1971), pp. 180–186. ISSN: 15289028. DOI: 10.1115/1.3426494.
- [38] Alexander H Slocum. "Outline .:" in: (1994), pp. 1–35.
- [39] Olga Sorkine and Michael Rabinovich. "Least-squares rigid motion using svd". In: *Technical notes* February (2009), pp. 1–6. URL: [http://www.igl.ethz.ch/projects/ARAP/svd\\_rot.pdf](http://www.igl.ethz.ch/projects/ARAP/svd_rot.pdf).
- [40] James M. Gere Stephen P. Timoshenko. *Theory of elastic stability by S. Timoshenko and J.M. Gere*. 1963.
- [41] Peter R. Krauss Stephen Y. Chou and Preston J. Renstrom. "NanoImprint Lithography". In: *Nano-Lithography* June (1996), pp. 87–168. DOI: 10.1002/9781118622582.ch2.
- [42] Christine Thanner et al. "Nanoimprint lithography for augmented reality waveguide manufacturing". In: February (2020), p. 34. ISSN: 1996756X. DOI: 10.1117/12.2543692.



- [43] Lisa Sievers Thesis and Jerry L Brown. "© 2015 Jerald BrownKooltuin 10, 2645AX, Delfgauw". In: (2015), pp. 1–20.
- [44] Marc A. Verschuuren et al. "Large area nanoimprint by substrate conformal imprint lithography (SCIL)". In: *Advanced Optical Technologies* 6.3-4 (2017), pp. 243–264. ISSN: 21928584. DOI: 10.1515/aot-2017-0022.
- [45] Luc Vinet and Alexei Zhedanov. "A 'missing' family of classical orthogonal polynomials". In: *Journal of Physics A: Mathematical and Theoretical* 44.8 (2011), pp. 1689–1699. ISSN: 17518113. DOI: 10.1088/1751-8113/44/8/085201.
- [46] Y. Wesley Wong and Sergio Pellegrino. "Wrinkled membranes part III: Numerical simulations". In: *Journal of Mechanics of Materials and Structures* 1.1 (2006), pp. 63–95. ISSN: 15593959. DOI: 10.2140/jomms.2006.1.63.
- [47] Dongxu Wu, Nitul S. Rajput, and Xichun Luo. "Nanoimprint Lithography - the Past, the Present and the Future". In: *Current Nanoscience* 12.6 (Oct. 2016), pp. 712–724. ISSN: 15734137. DOI: 10.2174/1573413712666160530120432. URL: <http://www.eurekaselect.com/openurl/content.php?genre=article&issn=1573-4137&volume=12&issue=6&page=712>.
- [48] G. E. Young and K. N. Reid. "Lateral and longitudinal dynamic behavior and control of moving webs". In: *Journal of Dynamic Systems, Measurement and Control, Transactions of the ASME* 115.2B (1993), pp. 309–317. ISSN: 15289028. DOI: 10.1115/1.2899071.
- [49] G. E. Young, J. J. Shelton, and C. Kardamilas. "Modeling and control of multiple web spans using state estimation." In: *Proceedings of the American Control Conference* 88 pt 1-3 (1988), pp. 956–962. ISSN: 07431619. DOI: 10.23919/acc.1988.4789860.
- [50] Cheng Zhang et al. "Printed photonic elements: Nanoimprinting and beyond". In: *Journal of Materials Chemistry C* 4.23 (2016), pp. 5133–5153. ISSN: 20507526. DOI: 10.1039/c6tc01237j. URL: <http://dx.doi.org/10.1039/c6tc01237j>.
- [51] Hao Zhang et al. "Micron-sized feature overlay alignment on large flexible substrates for electronic and display systems". In: *IEEE/OSA Journal of Display Technology* 7.6 (2011), pp. 330–338. ISSN: 1551319X. DOI: 10.1109/JDT.2010.2060312.